6. SITE 752[1]

Shipboard Scientific Party[2]

Hole 752A

Date occupied: 10 May 1988

Date departed: 12 May 1988

Time on hole: 2 days, 12 hr, 15 min

Position: 30°53.475′S, 93°34.652′E

Bottom felt (rig floor; m; drill-pipe measurement): 1097.2

Distance between rig floor and sea level (m): 10.87

Water depth (drill-pipe measurement; corrected m): 1086.3

Total depth (rig floor; corrected m): 1414.8

Penetration (m): 317.6

Number of cores: 34

Total length of cored section (m): 317.6

Total core recovered (m): 217.32

Core recovery (%): 68

Oldest sediment cored:
Depth sub-bottom (m): 308.0
Nature: nannofossil calcareous chalk
Earliest age: early Paleocene
Measured velocity (km/s): 1.90

Hole 752B

Date occupied: 18 May 1988

Date departed: 22 May 1988

Time on hole: 4 days, 3 hr, 30 min

Position: 30°53.483′S, 93°34.652′E

Bottom felt (rig floor; m; drill-pipe measurement): 1097.2

Distance between rig floor and sea level (m): 10.87

Water depth (drill-pipe measurement; corrected m): 1086.3

Total depth (rig floor; corrected m): 1532.8

Penetration (m): 435.6

Number of cores: 19

Total length of cored section (m): 158.0

Total core recovered (m): 112.34

Core recovery (%): 71

Oldest sediment cored:
Depth sub-bottom (m): 435.6
Nature: calcareous chalk and chert
Earliest age: late Maestrichtian
Measured velocity (km/s): 3.3–3.8

Principal results: Ocean Drilling Program (ODP) Site 752 (proposed Site BR-2) is near the crest of Broken Ridge, about 16 km north of the main southward-facing escarpment. The site was positioned to penetrate the dipping reflector sequence midway between proposed Sites BR-1 and BR-3. The coring at Site 752, along with that from Sites 753, 754, and 755 (proposed sites BR-1, BR-3, and BR-4, respectively), is designed to compile a continuous section through the northward-dipping sediments that underlie a prominent truncation surface. A thin (~100-m-thick) cap of subhorizontal pelagic sediments unconformably overlies the dipping units.

The site was picked at shotpoint 945 on line 20 of the seismic reflection survey conducted during *Robert D. Conrad* Cruise 2708 (RC2708). An approach survey of three lines crossing all possible locations for the Broken Ridge sites was made by the *JOIDES Resolution* during the Global Positioning System (GPS) satellite window. Correlation between the two surveys was possible down to the level of subtle features only a few shotpoints across. The observed penetration of the 3.5-kHz echo-sounding system exceeded 0.08 s two-way traveltime (TWT) below the seafloor (bsf) where hard reflectors were present.

Hole 752A was cored with the advanced hydraulic piston corer (APC) and extended core barrel (XCB) systems until refusal at 308 m below seafloor (mbsf) when an XCB cutting shoe sheared off while coring a particularly hard horizon, presumably a chert stringer similar to those cored in the overlying sediments. Average core recovery was 70.6%, with only the first XCB core failing to recover at least one core section (1.5 m). Sites 753 and 754 were drilled before we returned to complete the section at Site 752 by drilling Hole 752B to a depth that overlaps in age with Site 754. Hole 752B was cored with the rotary core barrel (RCB) to a total depth of 436 mbsf, with an average recovery of 71% over the cored intervals.

The following lithologic units were recognized:

Unit I (0–113 mbsf): Pleistocene to uppermost Eocene nannofossil ooze with foraminifers. Sediment color ranges from faint alternations of white and light tan at the top to stark white in the next 40 m, which grades into a rich yellow-brown at the bottom. Oysterlike valves 1 to 3 cm across occur in the lower Miocene. A layer of limestone and chert pebbles, which are up to 6 cm in diameter, is at 94 mbsf. This layer marks a hiatus between the overlying Pleistocene to uppermost Oligocene ooze and the uppermost Eocene ooze at the bottom of the unit. A second pebble layer, which is the only recovery (27 cm) in Core 121-752A-12X, contains reworked material of late Eocene to Campanian/Maestrichtian age.

Unit II (113–436 mbsf): lower Eocene to upper Maestrichtian nannofossil calcareous chalk with a silica-rich section. Unit II is divided into three subunits.

Subunit IIA (113–210 mbsf): lower Eocene to upper Paleocene nannofossil and micritic chalk. The bioturbated chalk is generally light gray to light greenish gray, but darker where the ash content exceeds about 1%. Two major ash layers, over 5 cm thick with more than 50% volcanic debris, and pumice fragments are in this subunit.

Subunit IIB (210–289 mbsf): upper Paleocene to middle Paleocene nannofossil calcareous chalk containing up to 40% radiolarians and diatoms and numerous occurrences of volcanic ash. Chert stringers are common. Subunit IIB is slightly greener in color than Subunit IIA. Fine laminations, some of which exhibit cross laminae and graded bedding, occur in the lower part. This subunit is particularly well defined on the downhole logs.

Subunit IIC (289–436 mbsf): middle Paleocene to upper Maestrichtian hard chalk. The chalk is faintly mottled, greenish gray in color, and characterized by greenish laminae similar to those in Subunit IIB. Ash layers are common between 326 and 422 mbsf. Chert and porcellanite occur sporadically. The Cretaceous/Tertiary boundary is within this subunit, at a depth of about 358 mbsf.

---

[1] Peirce, J., Weissel, J., et al., 1989. *Proc. ODP, Init. Repts.*, 121: College Station, TX (Ocean Drilling Program).

[2] Shipboard Scientific Party is as given in the list of Participants preceding the contents.

The lowermost (upper Maestrichtian) section was deposited in water depths of 200–600 m, based on benthic foraminifers and planktonic/benthic foraminifer ratios. The water depths gradually deepened with time to 500–1000 m by the early Eocene.

The average sedimentation rate throughout the interval spanned by Unit II was about 3.5 cm/1000 yr, which translates into a sediment-accumulation rate of nearly 6 g/cm^2/1000 yr. This is a remarkably high flux rate for pelagic sediment. For comparison, Upper Cretaceous carbonate fluxes on other shallow oceanic plateaus are commonly 1–2 g/cm^2/1000 yr (e.g., Ontong-Java, Shatsky, Manihiki, and Magellan). Only the Hess Rise has similar flux values (3.8 g/cm^2/1000 yr in Campanian-Maestrichtian carbonates and 7.6 g/cm^2/1000 yr in the upper Albian to lower Cenomanian current-deposited carbonates). There is no evidence for significant reworking in Unit II, which indicates that the sediment supply was primarily biogenic and not clastic carbonate material eroded from an uplifted Broken Ridge, as was expected. This and the obvious thinning of the strata to the north suggest that the sedimentation rate was controlled by a high-productivity zone, modified by normal sediment distribution processes in a outer shelf/slope environment.

The lithologic expression of the Cretaceous/Tertiary boundary occurs in Section 121-752B-11R-3 as a dramatic color change from the mottled, cream-colored Maestrichtian chalks below the boundary to a dark green layer that is carbonate poor and ash rich above. This lowermost Paleocene interval is 6 to 6.5 m thick, as defined by clear signatures on the downhole logs. The transition zone between these layers is complex in structure, and it extends for some 60 cm in the recovered core. The diversity of Cretaceous species drops abruptly at 358.75 mbsf, but the first paleontological definition of the Tertiary (the first occurrence of *Biantholithus sparsus*) is 25 cm higher in the section. Sedimentation rates during the earliest Paleocene dropped by a factor of 3 to 5, primarily as a result of the sudden absence of carbonate supply. The bloom in the diversity of Tertiary species occurs at 354.5 mbsf, and normal carbonate levels are restored by 352 mbsf. The recovery from the ecological shock that brought the Cretaceous Epoch to an end lasted 0.5 to 1 m.y.—approximately 10 times longer than the equivalent process documented at lower latitude Cretaceous/Tertiary boundary sites—which is indicative of the relatively slower faunal response time at this high-latitude site to environmental stress.

The ashes in Unit II have Nb/Zr ratios that are consistent with an origin from the Kerguelen/Ninetyeast hot spot. Their primarily basaltic composition suggests a relatively nearby source. At least one relatively silicic ash layer occurs in the unit.

The reasonably complete paleomagnetic reversal stratigraphy defined for Unit II correlates with that at Site 754 and is consistent with the paleontological and seismic stratigraphic constraints. Some uncertainty remains, however, because highly variable sedimentation rates are implied. The assemblages of diatoms, radiolarians, and silicoflagellates found throughout the Paleocene and lower Eocene section allow a unique correlation of Paleocene and Eocene siliceous microfossils with nannofossil and planktonic foraminiferal assemblages. A brief survey of earlier Deep Sea Drilling Project (DSDP)/ODP investigations (especially those from high latitudes) revealed that no similar continuous Paleocene to lower Eocene cores had been recovered. This section will provide an extension to corresponding Neogene to upper Eocene sections drilled on ODP Legs 113, 119, and 120.

Parts of Broken Ridge were apparently uplifted to above sea level between the time the uppermost sediments in Unit II and the lowermost sediments in Unit I were deposited. The pebble layers bracket an upper Eocene section deposited in upper bathyal depths. Substantial amounts of reworked material as old as Campanian support this conclusion. The unconformity marked by the lower pebble layer in Unit I indicates wave-base erosion sometime after the early Eocene (CP10, 54 Ma) and before the late Eocene (CP15, P15–17, 38–41 Ma). Seismic correlation with the drilling results at Site 753 indicates that the unconformity is younger than middle Eocene (CP13c, P10/12, 43–47 Ma). Thus, this unconformity is not much older than the 42 Ma age (magnetic anomaly 18) of when seafloor spreading began between Broken Ridge and Kerguelen Plateau. The upper pebble layer marks a hiatus that appears to be coincident with the mid-Oligocene low eustatic sea-level stand. Estimated past water depths are gradually deeper upsection, from 200–600 m above the unconformity to present depths of about 1000 m.

BACKGROUND AND OBJECTIVES

This section summarizes parts of the detailed discussion of the background and objectives for drilling at Broken Ridge presented in the "Leg 121 Background and Objectives" chapter (this volume). Particular drilling objectives at Site 752 are also presented here.

Background

Previous DSDP drilling at Broken Ridge (Site 255; Fig. 1) terminated at 108 mbsf in an outer shelf/upper slope limestone and chert sequence of Santonian age (Shipboard Scientific Party, 1974). The limestone with chert unit is unconformably overlain by about 20 m of middle to upper Eocene detrital sands and gravels that were deposited in shallow water. A 55-m-thick Neogene pelagic cap disconformably overlies the upper Eocene sediments.

Broken Ridge is noteworthy because the effects of rifting are evident in its seismic stratigraphy (Fig. 2). Because Broken Ridge has remained a fairly shallow-water oceanic platform throughout its history, the stratigraphic section has the potential to provide a clear record of the vertical motions of Broken Ridge as it responded to the rifting process. In particular, rift-related uplift tilted the pre-existing strata gently to the north and exposed parts of Broken Ridge above sea level. A distinctive angular unconformity cut by wave-base erosion across the pre-rift strata (Fig. 2) provided a detrital source for the middle to upper Eocene shallow-water sands and gravels found at Site 255.

Overall Objectives for Drilling at Broken Ridge

We planned the drilling objectives at Broken Ridge in order to extract information on the rifting process—with particular emphasis in learning about the rift flank uplift mechanisms that can produce the 1–2 km of uplift inferred from seismic stratigraphy, gravity anomalies, and previous drilling (Site 255) at Broken Ridge—as follows:

1. To ascertain the age, lithology, and depositional depth of the sediments in the dipping and truncated sedimentary sequence at Broken Ridge.
2. To ascertain the age, lithology, and depositional depth of the sediments comprising the subhorizontal sediments that cap the crest of Broken Ridge.
3. To determine, from these fundamental results, what parts of the total sedimentary section are pre-, syn-, and post-rift deposits.
4. To use the drilling results as constraints on the timing and duration of the rifting event and to determine the magnitude of the vertical motion of Broken Ridge as it responded to the rifting process.

For example, a prolonged precursory shoaling of the section at Broken Ridge prior to the actual rifting event would indicate that extension was initiated by an "active" process (i.e., convective mantle upwelling). However, a pre-rift section that was deepening prior to extension would suggest a "passive" rifting process (i.e., intraplate stress). If the upper part of the dipping and truncated sequence consists of open-ocean biogenic material deposited in water depths of ~1000 m, a middle Eocene rifting event of short duration (~5 m.y.) becomes the probable interpretation. On the other hand, if the downlapping unit in the dipping and truncated sequence is found to be composed of shallow-water clastics, a Maestrichtian rifting event would be indicated.

Drilling Strategy at Broken Ridge

The objectives called for penetration and sampling of the entire dipping and truncated sedimentary sequence, which, on the

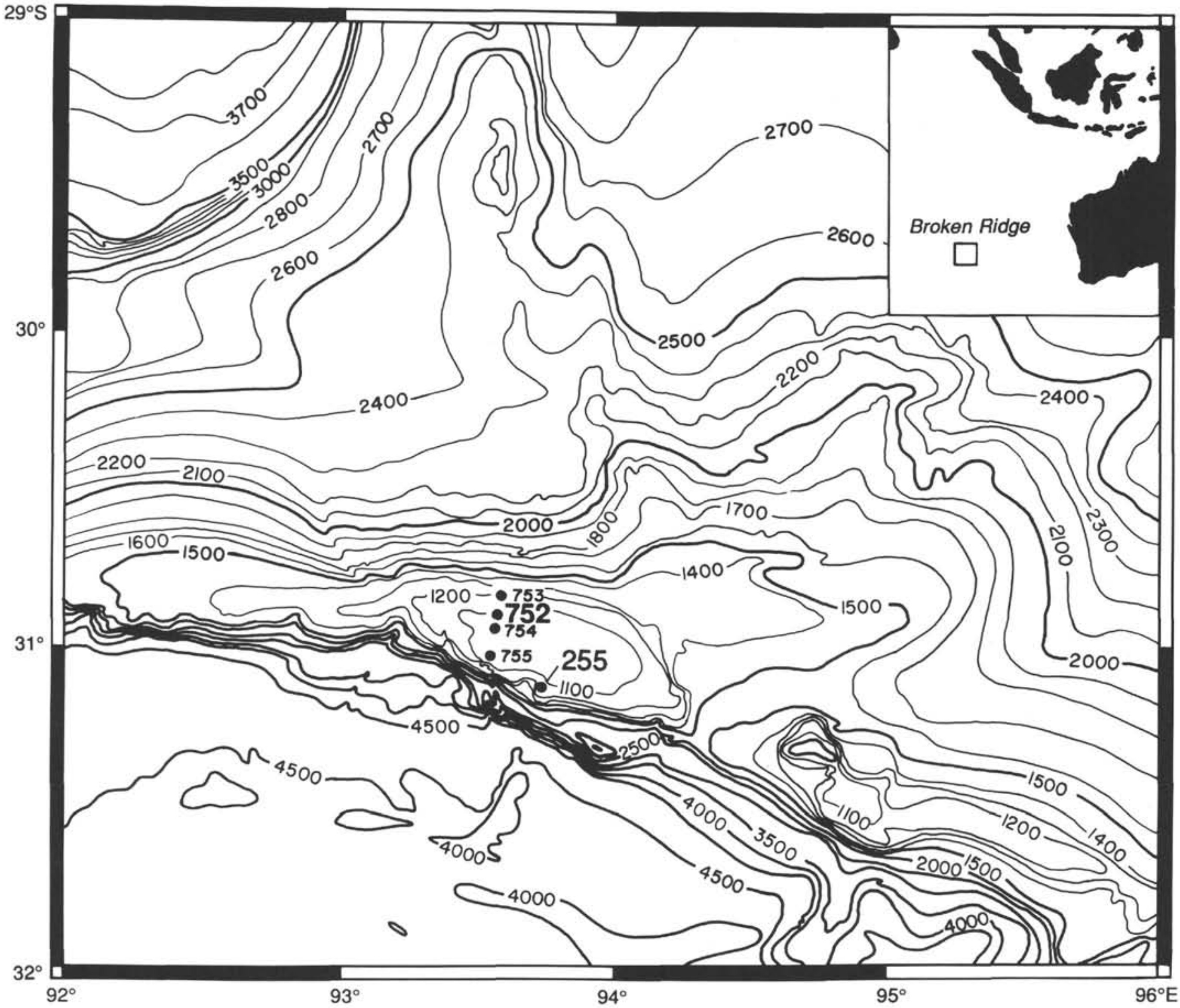

Figure 1. Bathymetric map showing locations of ODP Site 752, DSDP Site 255, and other Leg 121 sites at Broken Ridge. Bathymetry, which is based mainly on RC2708 echo-sounder data, is contoured at 100-m intervals, except along the south-facing escarpment where contours are omitted for clarity.

basis of seismic-refraction velocities, is more than 1500 m thick (see "Broken Ridge Underway Geophysics" chapter, this volume). To have attempted this at one hole would have entailed some risk and would have required setting a reentry cone, a time-consuming operation. We employed an alternative drilling strategy in which the entire dipping and truncated sequence was sampled in a series of four single-bit holes (proposed Sites BR-1 to BR-4; Fig. 2). The proposed sites were located to ensure section overlap between sites by taking advantage of the fact that progressively older strata subcrop beneath the unconformity as the main south-facing escarpment is approached (Fig. 2). However, owing to time constraints and mechanical difficulties, only Sites 752 and 754 (proposed Sites BR-2 and BR-3, respectively) achieved the goal of stratigraphic overlap.

Particular Drilling Objectives at Site 752

Because Site 752 (Fig. 2) was the first site drilled on Broken Ridge during Leg 121, it provided an opportunity to learn about drilling conditions and problems likely to be encountered at other Broken Ridge sites. We selected Site 752 to be drilled first because of the following:

1. The thickness of the capping ooze sequence is approximately 100 m, which is sufficient soft material for burial of the bottom-hole assembly (BHA). We would also have the opportunity to ascertain whether the silty-sand texture of the oozes (Shipboard Scientific Party, 1974) posed a problem for hole stability.
2. We would immediately learn from the age, lithology, and depth of deposition of the uppermost sediment recovered beneath the angular unconformity whether the downlapping strata in the dipping and truncated sequence are syn- to post-rift shallow-water clastics consistent with a Maestrichtian age for rifting and uplift at Broken Ridge or whether the strata are open-ocean pelagic sediments that were deposited in a water depth of about 1000 m before rifting and consequent uplift at Broken Ridge, which is consistent with a middle Eocene age of rifting.

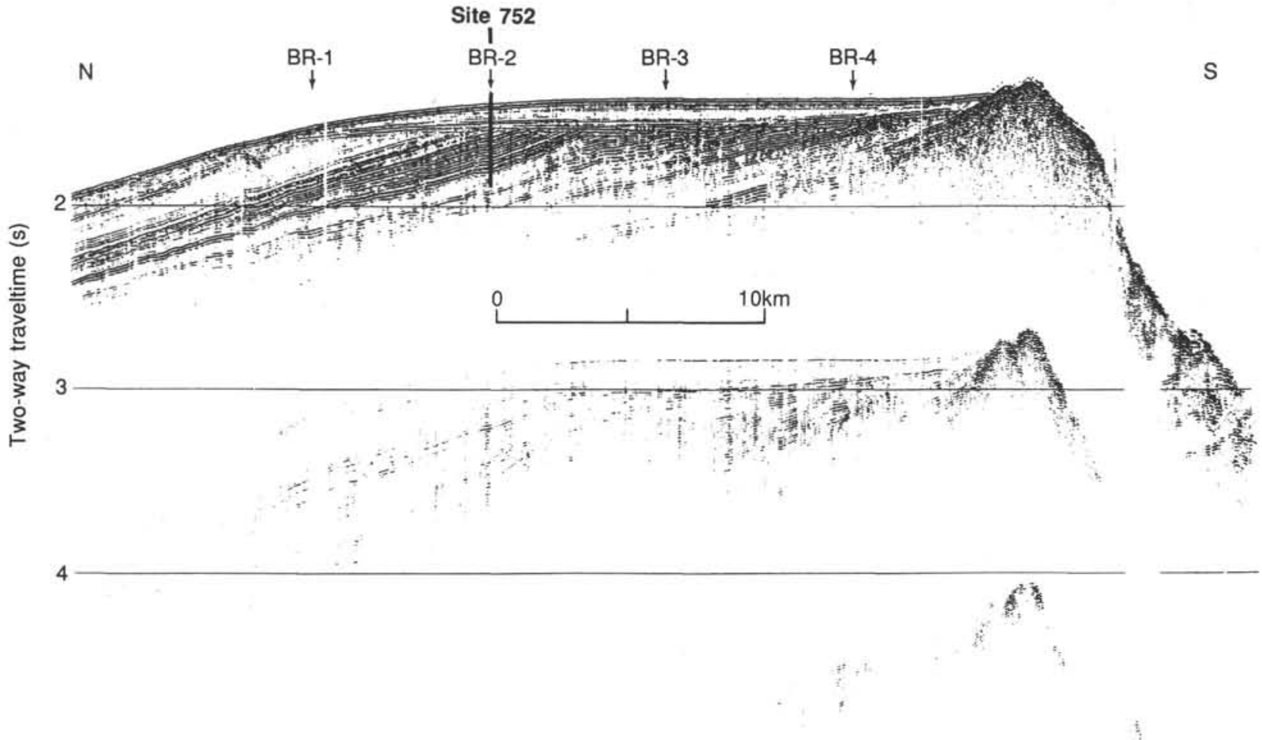

Figure 2. Single-channel seismic-reflection profile (RC2708 line 20) across Broken Ridge showing the location of Site 752 and proposed Sites BR-1 through BR-4.

Drilling operations at Site 752 terminated after penetrating 436 m in Holes 752A and 752B. A full suite of downhole logging runs was made before Hole 752B was abandoned. Although the penetration depth at Site 752 is less than the planned 450 m, the preceding objectives were met in full.

OPERATIONS

Fremantle to Site 752

The transit to Broken Ridge was uneventful, as the vessel made better than 11 kt in comfortable weather. The ship's clocks were retarded 3 hr to UTC + 5 hr during the transit. The ship arrived in the vicinity of the Broken Ridge drill sites at 1055 hr (local time) on 9 May 1988. An extensive predrilling seismic survey, including dropping a sonobuoy, was planned over all of the closely spaced Broken Ridge sites. In order to achieve optimum accuracy of navigation during the survey, the ship waited in drifting dynamic positioning (DP) mode from 1055 to 1408 hr for GPS to come on line with enough satellites in communication to offer accurate position fixes as the possible site locations were crossed.

Our wait for the GPS window was time well spent, however. The weather conditions were calm enough to allow the rig crew to pick up all of the drill collars from their main deck storage locations and make up, to stand in the derrick, both of the BHAs required for operations with the RCB and APC/XCB/Navidrill (NCB). The survey began at 1408 hr and lasted until 0315 hr on 10 May. Although moderate swells were running, the ship's heading during several of the survey pattern legs was well into the oncoming swell, thus producing ship motions mild enough to allow rig floor work to continue. This "bonus" time was used to assemble and check BHA–core barrel spacing on the new version of the XCB system, which was to be used for the first time on Leg 121, and to run a NCB test. The NCB system was assembled and lowered into the BHA, which was, in turn, raised above the rig floor and lowered onto a 55-gal drum of concrete. Sea water was pumped through the top drive/swivel, causing the NCB mud motor to unlatch and rotate according to design. The NCB cut through the cement in less than 3 min and also penetrated the bottom of the steel drum and started to cut into the steel deck plate below before the pump was shut off by the driller. By the time the survey was completed, we had accomplished all of the preliminary checks of the drill rig and coring systems.

The first beacon was dropped near the end of the survey on Site 752 (proposed Site BR-2) at 0135 hr on 10 May. The ship finished the planned survey track and returned to the beacon. The thrusters and hydrophones were lowered and the ship was in DP mode, ready to begin drilling operations at 0400 hr.

Site 752

Proposed Site BR-2 was chosen to be the first drill site, instead of proposed Site BR-1 as originally planned, because it has a thicker ooze section in which to bury the BHA. Proposed Site BR-1 was to be drilled at a location where the Neogene cap was possibly less than 50 m thick. Because previous drilling on Broken Ridge had experienced difficult hole conditions (a BHA was severed at Hole 255), we felt that the "easier" hole should be attempted first to get a feel for the conditions we could encounter during Leg 121 operations.

Hole 752A

The drill string was run in the hole with the APC/XCB/NCB BHA, and the mud line was established at 1097.2 m below the rig floor reference datum with an APC core. Eleven piston cores were taken successfully to a depth of 103.3 mbsf. Successful pore-water sampler and heatflow runs were made after the recovery of Cores 121-752A-4H and 121-752A-8H.

The eleventh APC core barrel penetrated an anticipated unconformity and became stuck in the sandy ooze below the Neogene cap. An overpull of 110,000 lb was used to free the barrel, which, surprisingly, was recovered intact. We then changed coring mode, and Cores 121-752A-12X through 121-752A-33X were cut with the new XCB system. Core recovery was fair; it was quite good in firm chalk, but less satisfactory in sticky calcareous ooze and poor in zones where chert stringers were encountered, after Core 121-752A-18X. Core 121-752A-34X suffered a fatigue-type failure of a threaded connection in the core barrel while attempting to penetrate a very hard chert layer. The broken end of the core barrel flared out slightly below the roller-cone bit and trapped the core barrel in the BHA. Jarring up with the heavy sinker bar's link jars would not dislodge the stuck XCB, necessitating a pipe round trip to handle the problem on deck. At the rig floor it was discovered that the XCB cutter shoe and cutter shoe spacer sub were missing, along with the core catcher; thus, Core 121-752A-34X was not recovered. The bit reached the rig floor at 1355 hr, 12 May, ending Hole 752A. Contrary to expectations, hole stability had been very good. Total penetration in Hole 752A was to 308.0 mbsf, with 68.4% recovery (Table 1).

Hole 752B

Following coring operations at Sites 753 and 754, the ship returned to Site 752 and steadied position on the still-active beacon at 0900 hr, 18 May. Time remaining in the allotment for Broken Ridge operations was to be divided between a logged, RCB single-bit hole at Site 752 cored to the 450-mbsf target depth and a single-bit RCB penetration at proposed Site BR-4 near the crest of the ridge to sample the oldest strata available under the Neogene cap.

The RCB BHA was run to the seafloor and immediately washed without coring to 120 mbsf. Two spot cores were taken to clarify a magnetostratigraphic problem identified while coring Hole 752A. The hole was then washed to a depth of 297 mbsf, where coring began to overlap recovery in Hole 752A by about one core length. Coring proceeded with very good results to 431.6 mbsf, where the last core (estimated to overlap Hole 754A) was to be taken before releasing the bit for logging (Table 1). Core 121-752B-18R came up empty, although it showed signs that the liner had contained a nearly full core at some point. We feared that the limestone core could have fallen out and become lodged in the BHA above the bit. This circumstance was verified by measuring back pressure while pumping without a core barrel in place. About 10 min of flushing with seawater at high flow rate succeeded in dislodging the obstruction, and one more short core was taken to end the hole at a total depth of 435.6 mbsf.

A polymer-gel mud sweep was pumped and a wiper trip to 80 mbsf and back to total depth was made before the bit was released. The hole was then displaced with seawater seven times and filled with KCl-added mud in preparation for logging. With the end of the pipe stationed at 61.3 mbsf the first logging run was started at 0900 hr, 20 May, using the seismic stratigraphic suite (DIT-LSS-CAL-NGT). After obtaining successful logs, the tool would not reenter the drill pipe and parted at the cablehead weak point within minutes after we began to work the partially stuck tool. (One caliper bow spring was subsequently found to have broken, which accounted for the tool's inability to get back into the pipe.)

The logging line was pulled to the deck, where part of the cablehead was found to be still attached to the wireline, which confirmed that the weak point had parted. On the chance that the logging tool had remained partly stuck into the BHA, a "fishing" core barrel was made up with a slip-type core catcher at the bottom large enough to swallow what remained of the Schlumberger cablehead attached to the logging tool. This assembly was run in on the sand line, but it landed in the BHA with the core catcher extending out into open hole, which demonstrated that the logging tool was not in the pipe.

While the fishing core barrel was being retrieved, we decided to try to recover the lost logging tool by dropping a free-fall reentry cone and going after the tool with a commercial overshot fishing tool. The lost tool contained the only LSS instrument aboard ship, and we wanted to obtain a complete series of logs across the Cretaceous/Tertiary boundary at Hole 752B. A mini-cone was assembled around the pipe and dropped. After allowing 25 min for the cone to fall to the seafloor, the pipe was tripped out of the hole. A Bowen overshot with a 3⅜-in. grapple was assembled to the end of the BHA and run back to just above the seafloor. The Colmec underwater TV and Mesotech sonar were lowered down the outside of the drill string with the

Table 1. Coring summary, Site 752.

Core no.	Date (May 1988)	Time (local)	Depth top (mbsf)	Depth bottom (mbsf)	Length cored (m)	Length recovered (m)	Recovery (%)
121-752A-							
1H	10	0850	0.0	8.3	8.3	8.26	99.5
2H	10	1010	8.3	17.8	9.5	8.57	90.2
3H	10	1105	17.8	27.3	9.5	8.61	90.6
4H	10	1150	27.3	36.8	9.5	9.41	99.0
5H	10	1400	36.8	46.4	9.6	9.47	98.6
6H	10	1425	46.4	56.1	9.7	8.13	83.8
7H	10	1455	56.1	65.8	9.7	9.25	95.3
8H	10	1545	65.8	75.4	9.6	9.70	101.0
9H	10	1750	75.4	85.0	9.6	8.73	90.9
10H	10	1810	86.0	94.7	9.7	9.87	102.0
11H	10	1915	94.7	103.3	8.6	8.90	103.0
12X	10	2020	103.3	112.9	9.6	0.27	2.8
13X	10	2105	112.9	122.6	9.7	5.82	60.0
14X	10	2200	122.6	132.3	9.7	6.61	68.1
15X	10	2250	132.3	142.0	9.7	7.49	77.2
16X	11	0020	142.0	151.7	9.7	6.77	69.8
17X	11	0210	151.7	161.4	9.7	5.27	54.3
18X	11	0340	161.4	171.1	9.7	2.76	28.4
19X	11	0545	171.1	180.7	9.6	6.20	64.6
20X	11	0720	180.7	190.4	9.7	2.36	24.3
21X	11	0850	190.4	200.1	9.7	2.96	30.5
22X	11	1105	200.1	209.8	9.7	5.70	58.7
23X	11	1325	209.8	219.5	9.7	2.21	22.8
24X	11	1500	219.5	229.1	9.6	2.38	24.8
25X	11	1640	229.1	238.8	9.7	4.23	43.6
26X	11	1750	238.8	248.4	9.6	9.03	94.0
27X	11	1915	248.4	258.1	9.7	5.58	57.5
28X	11	2040	258.1	267.7	9.6	7.71	80.3
29X	11	2150	267.7	277.4	9.7	9.70	100.0
30X	11	2300	277.4	279.4	2.0	1.50	75.0
31X	12	0025	279.4	288.7	9.3	8.54	91.8
32X	12	0205	288.7	298.4	9.7	9.70	100.0
33X	12	0415	298.4	308.0	9.6	5.63	58.6
34X	12	1400	308.0	317.6	9.6	0.00	0.0
					317.6	217.32	68.4
121-752B-							
1W	18	1530	0.0	120.0	120.0	0.60	(wash core)
2R	18	1600	120.0	129.7	9.7	2.64	27.2
3R	18	1640	129.7	139.4	9.7	9.88	102.0
4W	18	2140	139.4	297.0	157.6	8.97	(wash core)
5R	18	2300	297.0	306.6	9.6	6.79	70.7
6R	19	0110	306.6	316.1	9.5	6.55	68.9
7R	19	0320	316.1	325.8	9.7	8.86	91.3
8R	19	0525	325.8	335.4	9.6	9.96	104.0
9R	19	0800	335.4	345.1	9.7	1.66	17.1
10R	19	1030	345.1	354.8	9.7	9.77	101.0
11R	19	1155	354.8	364.4	9.6	4.99	52.0
12R	19	1315	364.4	374.0	9.6	9.09	94.7
13R	19	1435	374.0	383.6	9.6	8.67	90.3
14R	19	1605	383.6	393.3	9.7	9.49	97.8
15R	19	1730	393.3	403.0	9.7	8.25	85.0
16R	19	1915	403.0	412.6	9.6	4.68	48.7
17R	19	2040	412.6	422.3	9.7	6.97	71.8
18R	19	2235	422.3	431.6	9.3	0.00	0.0
19R	20	0045	431.6	435.6	4.0	4.08	102.0
		Coring			158.0	112.33	71.1
		Washing			277.6	9.57	
					435.6	121.90	

vibration-isolated TV (VIT) frame to search the seafloor for the minicone and its floating glass balls.

First Reentry

The TV search for the hole turned out to be a difficult one because the glass balls were not identifiable on sonar and could not be located visually. Although several large (± 50 ft in diameter) spots of disturbance on the seafloor could be seen, none appeared to contain the minicone. After a box-pattern search of the area where the cone was expected to be found, the pipe was stabbed into the most promising spot, where something resembling one of the missing glass flotation balls appeared to be resting on the seafloor. The pipe immediately reentered the unseen hole without any evidence of contacting the cone at 0430 hr, 21 May. We accepted this bit of luck, recovered the TV frame, and lowered the fishing assembly into the hole with slow rotation in search of the logging tool (the fish). Contact was made with the fish at 408 mbsf; the tool had fallen to the bottom of the hole. A perfect catch of the fish was made by the overshot, as indicated by a sudden increase of pump pressure as the fish sealed off the main flow path through the overshot. With the fish firmly engaged in the overshot assembly, the drill string was tripped out of the hole.

The entire logging tool was recovered by this operation. The bow springs of the caliper were distorted, with one completely broken and twisted sideways. The LSS tool was bent unnaturally in two places. Otherwise, the tool string appeared to be in fair condition.

A reentry/cleanout bit was made up to the BHA in place of the fishing tools, and the drill string was again run to the seafloor.

Second Reentry

The second attempt to reenter the "invisible" minicone was a repeat of the first exercise, except that when the pipe was stabbed into what appeared to be the same spot, the hole was not found and the bit took 10,000 lb of weight on bit immediately. More than a dozen additional stabs were made before the pipe once again found the hole and slipped into it without any evidence of contacting the cone at 1907 hr, 21 May. The second reentry into the hole proved that it had remained open, and the cleanout bit was run in to a depth of 128 mbsf, across the unconformity, to begin the logging operations again.

The lithoporosity suite (LDT-CNT-NGT-DIT) was run in the hole to 339 mbsf, where it hung up. A successful logging run was made above this depth. The pipe was run again to 6 m above the bottom of the hole to knock out bridges, a mud sweep was made, and the geochemical logging suite (GST-ACT-CNT-NGT-GPIT) was run with the pipe at 228 mbsf before we pulled out and abandoned Hole 752B. The cleanout bit was on deck at 1230 hr, 22 May, as the vessel moved in DP mode to the final site of the Broken Ridge campaign, Site 755 (proposed Site BR-4).

LITHOSTRATIGRAPHY AND SEDIMENTOLOGY

A 436-m-long section of Pleistocene through upper Maestrichtian sediments was recovered at Site 752 before drilling was terminated in uppermost Cretaceous chalks (Fig. 3). Two lithologic units were identified: Unit I, 112.9 m of foraminifer and nannofossil ooze of Pleistocene to late Eocene age, and Unit II, a complete, 322.7-m-thick chalk sequence of early Eocene to late Maestrichtian age (Table 2). The Cretaceous/Tertiary boundary occurs within Unit II in Section 121-752B-11R-3, at about 358 mbsf.

Unit I, recovered in Cores 121-752A-1H to 121-752A-12X (0–112.9 mbsf), is a nannofossil/foraminifer ooze. The sediment ranges in color from faint alternations of white (10YR 8/2) and pale brown (10YR 8/3) sediment in the first core to stark white (whiter than 10YR 8/1) through Core 121-752A-5H at 45 mbsf and grades down into a rich yellow-brown (7.5YR 7/6) in Cores 121-752A-9H through 121-752A-11H. The brown ooze in Core 121-752A-11H (94.7–103.3 mbsf) contains rounded, iron-stained quartz grains of medium to coarse sand size.

Shell fragments, including 1–3-cm-diameter oysterlike valves, occur in Cores 121-752A-9H and 121-752A-10H. There are two layers of limestone pebbles in Unit I. The upper layer is in the lower part of Core 121-752A-10H (94 mbsf) and consists of pale yellow (10YR 8/2) limestone pebbles up to 6 cm in diameter that have dark greenish-gray (5G 5/1) coatings (Fig. 4). The larger pebbles are pierced with holes that are either root structures or burrows/borer holes. The lower pebble layer is within Core 121-752A-12X (103.3–112.9 mbsf), for which only 27 cm of material was recovered. These pebbles are a limestone that appears similar to that in the upper layer, and they are found in conjunction with a shell hash. Materials of late Eocene through Campanian/Maestrichtian age are reworked into this layer.

Grain-size information was determined for the bulk unconsolidated sediments of Unit I using the procedures and equipment described in the "Explanatory Notes" chapter (this volume). Grain-size data for Unit I in Hole 752A (Table 3 and Fig. 5) show a fining-upward sequence, beginning with the pebble layer at about 94 mbsf. Subsequent relative size minima occur at 80 (lower Miocene), 50 (middle Miocene), and 15 mbsf (lower Pliocene). Grain-size maxima occur approximately at 60 (upper lower Miocene), 25 (upper Miocene), and 8 mbsf (upper Pliocene).

The oozes of Unit I are Pleistocene to earliest Miocene or latest Oligocene in age above the upper pebble layer and late Eocene in Core 121-752A-11H, between the pebble layers.

Unit II (112.9–317.6 mbsf in Hole 752A and all recovery from Hole 752B, to 435.6 mbsf) is dominated by nannofossil to calcareous chalk with silica-rich sections in Cores 121-752A-23X through 121-752A-31X. Three subunits are identified (Table 2):

1. Subunit IIA: chalks from Cores 121-752A-13X to 121-752A-22X, 112.9–209.8 mbsf, and 121-752B-2R and 121-752B-3R, 120.0–139.4 mbsf;
2. Subunit IIB: the silica-rich section in Cores 121-752A-23X to 121-752A-31X, 209.8–288.7 mbsf (not recovered from Hole 752B);
3. Subunit IIC: hard chalks from Cores 121-752A-32X and 121-752A-33X (no recovery in Core 121-752A-34X), 288.7–317.6 mbsf to total depth, and in Cores 121-752B-5R to 121-752B-19R, 297.0–435.6 mbsf.

The upper nannofossil to calcareous (micritic) chalk subunit is light gray (5Y 7/1) to light greenish gray (5G 7/1) in color and bioturbated. The bioturbation has produced some striking mottles and burrow structures (Fig. 6). Where ash is >1% of the sediment, the cores are noticeably darker in color. Ash layers, over 5 cm thick and consisting of >50% volcanic debris, occur in Cores 121-752A-15X, 121-752A-19X, and 121-752A-26X. Subunit IIA also contains sporadic black pumice fragments, one of which is 3 cm long. Chert has minor occurrences as small centimeter-sized pebbles in Core 121-752A-14X and larger pieces up to 5 cm in diameter in Core 121-752A-19X.

Sediments in siliceous Subunit IIB are similar in composition and color to the overlying and underlying chalks, but contain up to 40% radiolarians and diatoms. The greenish gray coloration is more prominent in this subunit, presumably as a reflection of the observed slight increase in ash content, which, in turn, may enhance silica preservation. Beginning in Core 121-752A-25X at 229.1 mbsf and continuing to the bottom of the hole, faint to prominent millimeter-scale greenish laminae are common. These layers occur in multilaminae bundles that are

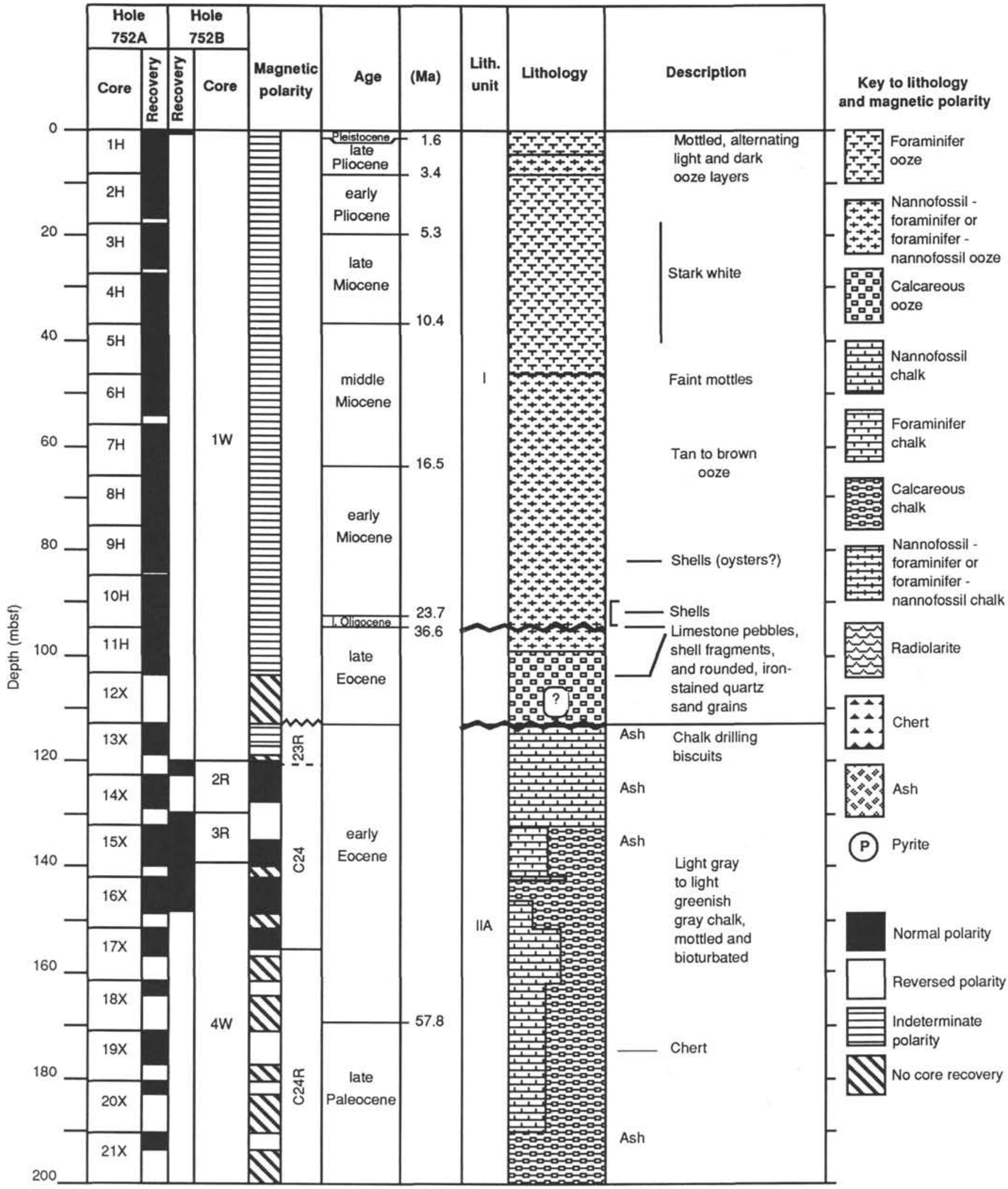

Figure 3. Site 752 summary diagram.

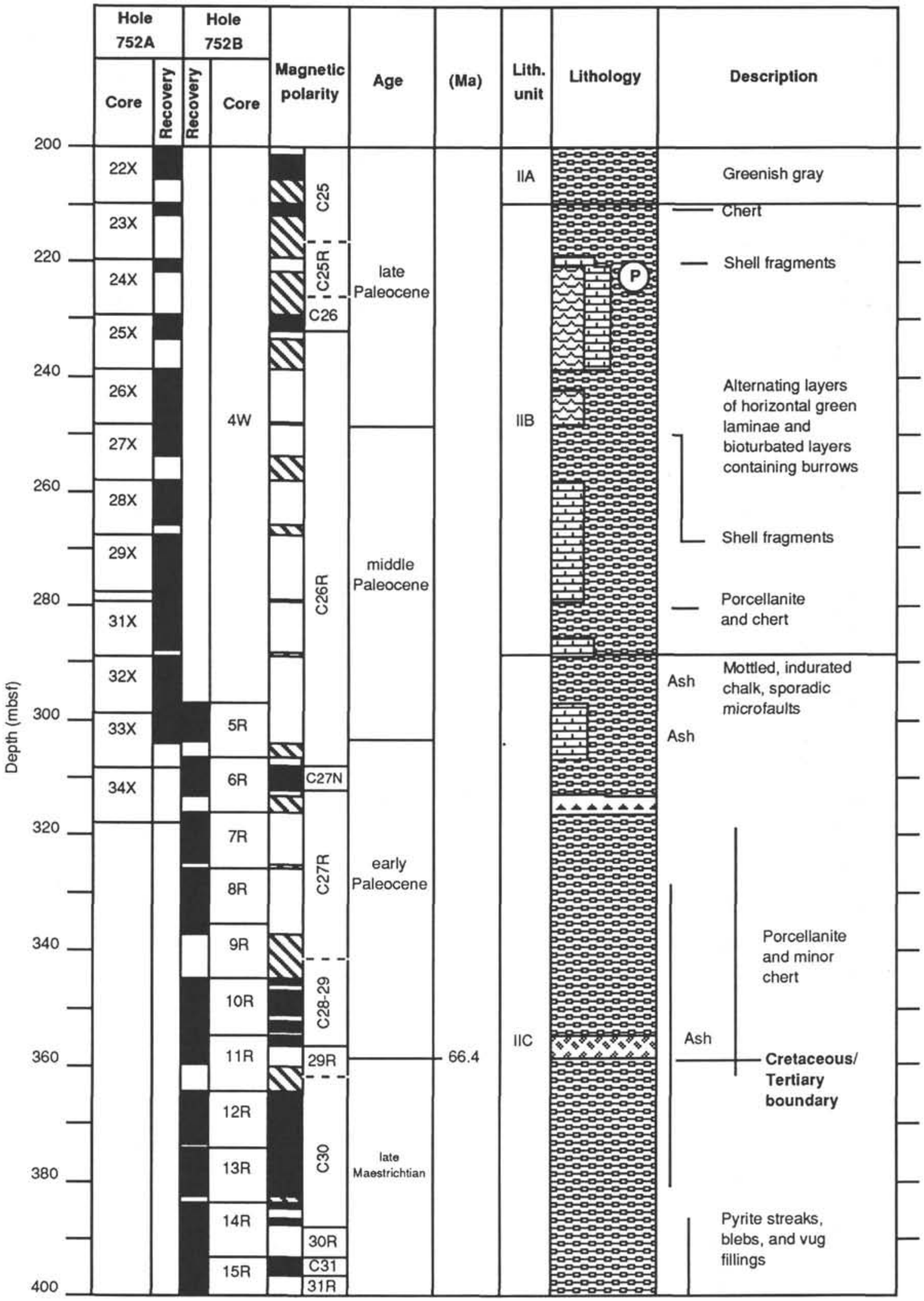

Figure 3 (continued).

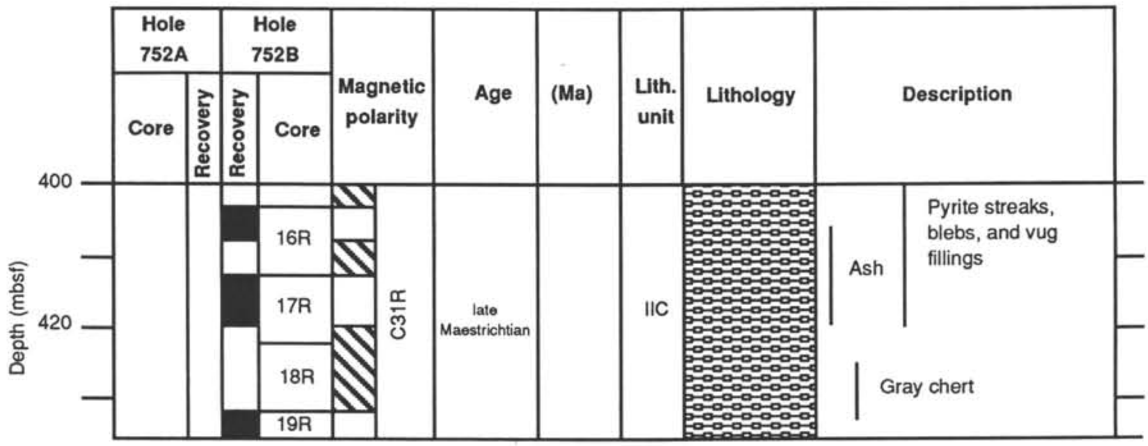

Figure 3 (continued).

Table 2. Lithologic units at Site 752.

Unit	Hole 752A Core interval	Hole 752A Depth (mbsf)	Hole 752B Core interval	Hole 752B Depth (mbsf)	Lithology	Age
I	1H-12X	0-112.9	nr		Foraminifer/nannofossil ooze	Pleistocene to late Eocene
II	13X-34X	112.9-317.6	2R-3R 5R-19R	120.0-139.4 297.0-435.6	Chalk	
IIA	13X-22X	112.9-209.8	2R-3R	120.0-139.4	Nannofossil/calcareous chalk	early Eocene to late Paleocene
IIB	23X-31X	209.8-288.7	nr		Siliceous chalk	late to middle Paleocene
IIC	32X-34X	288.7-317.6	5R-19R	297.0-435.6	Indurated chalk	middle Paleocene to late Maestrichtian

Note: nr = no recovery.

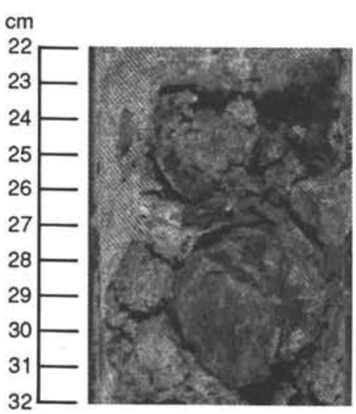

Figure 4. Limestone pebble layer in Section 121-752A-10H-7, 22-32 cm.

Table 3. Grain-size data from the oozes of lithologic Unit I, Hole 752A.

Core, section, interval (cm)	Depth (mbsf)	Mean grain size (μm)	Mean grain size (ϕ)
1H-CC, 1	8.11	54.5	4.20
2H-CC, 1	16.70	41.2	4.60
3H-CC, 1	26.29	57.2	4.13
4H-CC, 1	36.57	50.1	4.32
5H-CC, 1	46.15	40.6	4.62
6H-2, 80	48.70	35.6	4.81
6H-CC, 1	54.37	43.6	4.52
7H-2, 80	58.40	64.0	3.97
8H-CC, 1	65.11	59.6	4.07
8H-CC, 1	75.36	56.8	4.14
9H-2, 80	77.70	39.2	4.67
9H-CC, 1	83.97	47.5	4.40
10H-2, 80	87.30	52.8	4.24
10H-CC, 1	94.65	67.0	3.90

commonly 1 to 2 cm thick, with some cross laminae, sharp and scoured basal contacts, and graded bedding exhibited. Chert is more common in this subunit, occurring as small pebbles in Cores 121-752A-23X and 121-752A-29X, and it impeded the drilling of Core 121-752A-30X, which recovered 1.5 m of chalks with chert and porcellanite layers. A small pyrite bleb is in Core 121-752A-24X, and a shell fragment is in Core 121-752A-26X.

Subunit IIC is a faintly mottled hard chalk, light gray (5GN 7/1) to light greenish gray (5G 6/1) in color, and is characterized by grayish green (5G 5/2) laminae (chalk from 97 to 102 cm, Fig. 7). In this subunit the greenish laminae show indications of being both primary (cross bedding, cut by burrows, curving around shells) and secondary (continuing through mottles). Microfaults, dipping from 45° to 70°, form small normal offsets in both the mottles and laminae from a few millimeters to 2 or 3 cm.

Two minor lithologies are important in Subunit IIC. Ash layers are common in Cores 121-752B-8R through 121-752B-13R (325.8-383.6 mbsf) (ash layer from 60 to 73 cm, Fig. 7), dominate the subunit in Core 121-752B-11R (354.8-364.4 mbsf), and occur again in Cores 121-752B-16R to 121-752B-17R (403.0-

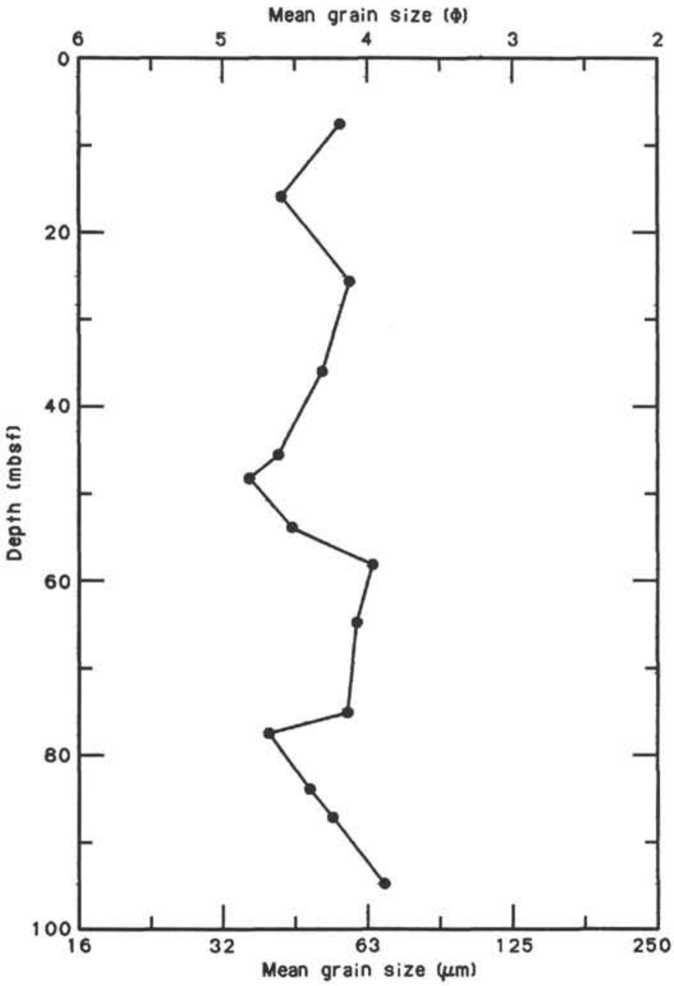

Figure 5. Grain size of the bulk sediment of lithologic Unit I.

422.3 mbsf). Porcellanite with minor chert is common in Cores 121-752B-6R through 121-752B-11R (306.6–364.4 mbsf). Porcellanite may have impeded core recovery in Cores 121-752B-9R and 121-752B-11R. Gray chert occurs in Cores 121-752B-17R and 121-752B-19R (412.56–435.6 mbsf). In addition, pyrite streaks, blebs, and vug fillings occur in Cores 121-752B-14R through 121-752B-17R (383.6–422.3 mbsf).

The lithologic expression of the Cretaceous/Tertiary boundary apparently occurs in Section 121-752B-11R-3, between the bottom of a thick composite ash layer at 37 cm and the top of the normal-appearing greenish gray chalk at 97 cm (Figs. 7 and 8; note that the photographs disagree by as much as 2 cm in the position of the boundaries between the lithologies). The boundary sequence is as follows. The normal light greenish gray chalks of Subunit IIC continue down through Section 121-752B-10R-5. Five centimeters below the top of Section 121-752B-10R-6 the sediments grade into a thick, dark grayish green (5G 4/2 and 5Y 4/1) ash layer that continues down to 37 cm in Core 121-752B-11R-3. This ash layer spans 5.52 m, from 352.65 to 358.17 mbsf. Because of the standard ODP methods for assigning recovery in a core, this value represents a minimum thickness; information from the logging runs suggests that this composite ash layer is 6 to 6.5 m thick. Below the thick ash layer lies 23 cm of chalk with wavy laminations and mottles at 37 to 60 cm, 13 cm of ash with horizontal laminations at 60 to 73 cm, 3 cm of chalk, 8 cm of gray chert and porcellanite at 76 to 84 cm, 7 cm of greenish gray chalk exhibiting soft-sediment deformation structures at 84

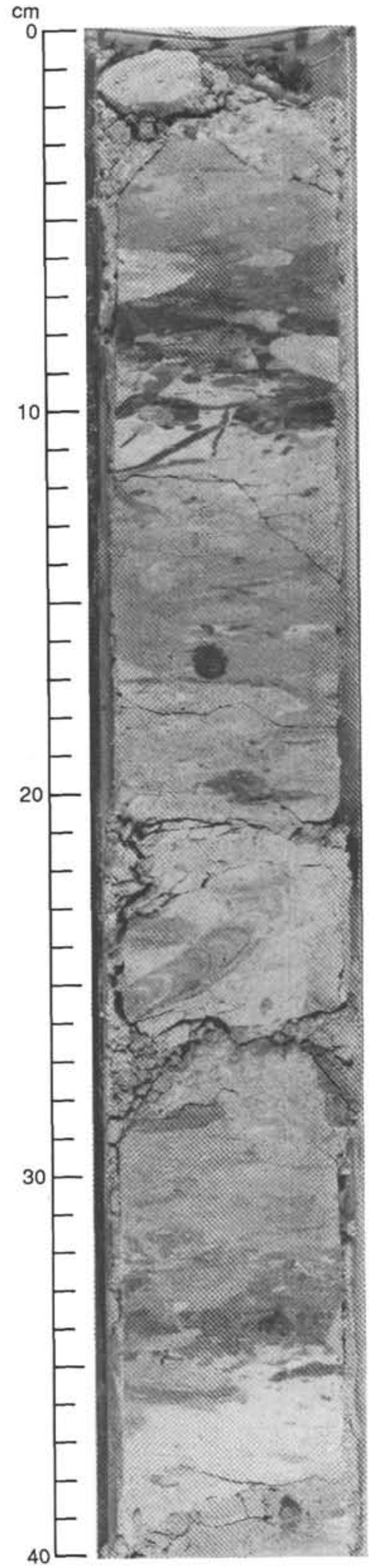

Figure 6. Burrow structures in lithologic Subunit IIA chalks (Section 121-752A-15X-4, 0–40 cm).

Figure 7. Ash, chert, and chalk near the Cretaceous/Tertiary boundary, lithologic Subunit IIC (Section 121-752B-11R-3, 40–102 cm).

to 91 cm, and a dark ash-rich layer overlying a burrow structure at 91 to 97 cm, where the typical mottled and faintly laminated chalks of Subunit IIC resume. Within this sedimentary sequence, the Leg 121 paleontologists have placed the faunal/floral boundary at 73 to 97 cm.

BIOSTRATIGRAPHY

Hole 752A was drilled at Broken Ridge to recover a section of the Neogene cap and sediments from the dipping reflectors below the prominent unconformity on the seismic profiles. The results of this first hole would determine the drilling strategy at other locations on Broken Ridge. Hole 752A was terminated because of XCB bit failure, just above the Cretaceous/Tertiary boundary. Hole 752B was drilled after Sites 753 and 754 were drilled to (1) complete an essential part of the section, (2) recover the Cretaceous/Tertiary boundary, and (3) achieve stratigraphic overlap with Hole 754. All of these goals were met.

A 436-m-long section of Quaternary to Maestrichtian sediments was recovered in Holes 752A and 752B. Lithologic Unit I consists of 112.9 m of Pleistocene through lower Miocene to uppermost Oligocene foraminiferal oozes (Cores 121-752A-1H to 121-752A-10H) underlain by a condensed unit that contains poor assemblages in the late Eocene age (CP15b) pebble layer (Samples 121-752A-10H-CC, 121-752A-11H-CC, and 121-752A-12X-CC). The upper Quaternary to Oligocene section is condensed, but could be stratigraphically complete because the absence of some of the zones (e.g., CN2) might be due to the absence of marker species in these high-latitude areas.

Lithologic Unit II consists of a 322.7-m-thick, probably complete, section of lower Eocene to upper Maestrichtian sediments. The almost complete recovery of an expanded and possibly biostratigraphically complete Cretaceous/Tertiary boundary section in Cores 121-752B-10R through 121-752B-11R was a major feat. We located the boundary between 73 and 95 cm in Section 121-752B-11R-3.

An important paleontologic result of coring Site 752 is the recovery of well-preserved and abundant diatom assemblages in Unit II, from the lower Eocene through the middle Paleocene. This provides the opportunity to tie a detailed diatom zonation with the calcareous nannofossil and planktonic foraminiferal zonations.

In general, planktonic foraminiferal and calcareous nannofossil age determinations are in close agreement (Fig. 9). The top of Unit II, Core 121-752A-13X, is assigned to calcareous nannofossil Zone CP9b and planktonic foraminiferal Zone P8. The base of Hole 752A in Sample 121-752A-32X-CC is assigned to the CP3 and P2-3 Zones. The low diversity of the planktonic foraminiferal assemblages is probably responsible for any minor disagreements.

Hole 752B was terminated in upper Maestrichtian sediments once the overlap with Hole 754B was established. The lowermost Core 121-752B-19R belongs to the planktonic foraminifer *Globotruncana gansseri* and CC24 Zones. The interval from Samples 121-752B-11R-3, 95 cm, to 121-752B-17R-CC was assigned to the topmost Maestrichtian Zones CC25–CC26 and the planktonic foraminifer *Abathomphalus mayaroensis* Zone.

The cool, austral assemblages found throughout the entire section at Site 752 are comparable to assemblages from other austral, temperate areas (Jenkins, 1985; Caron, 1985; Toumarkine and Luterbacher, 1985; Perch-Nielsen, 1985; Herb, 1974). Some low-latitude species were found in intervals (lower Eocene and middle Paleocene).

Water depth estimates from benthic foraminiferal assemblages are middle to lower bathyal for the Neogene and middle to upper bathyal for the Paleogene to Upper Cretaceous sections, with shallower water indicated for the upper Eocene pebble layers. The presence of the calcareous nannofossil *Braarudosphaera*

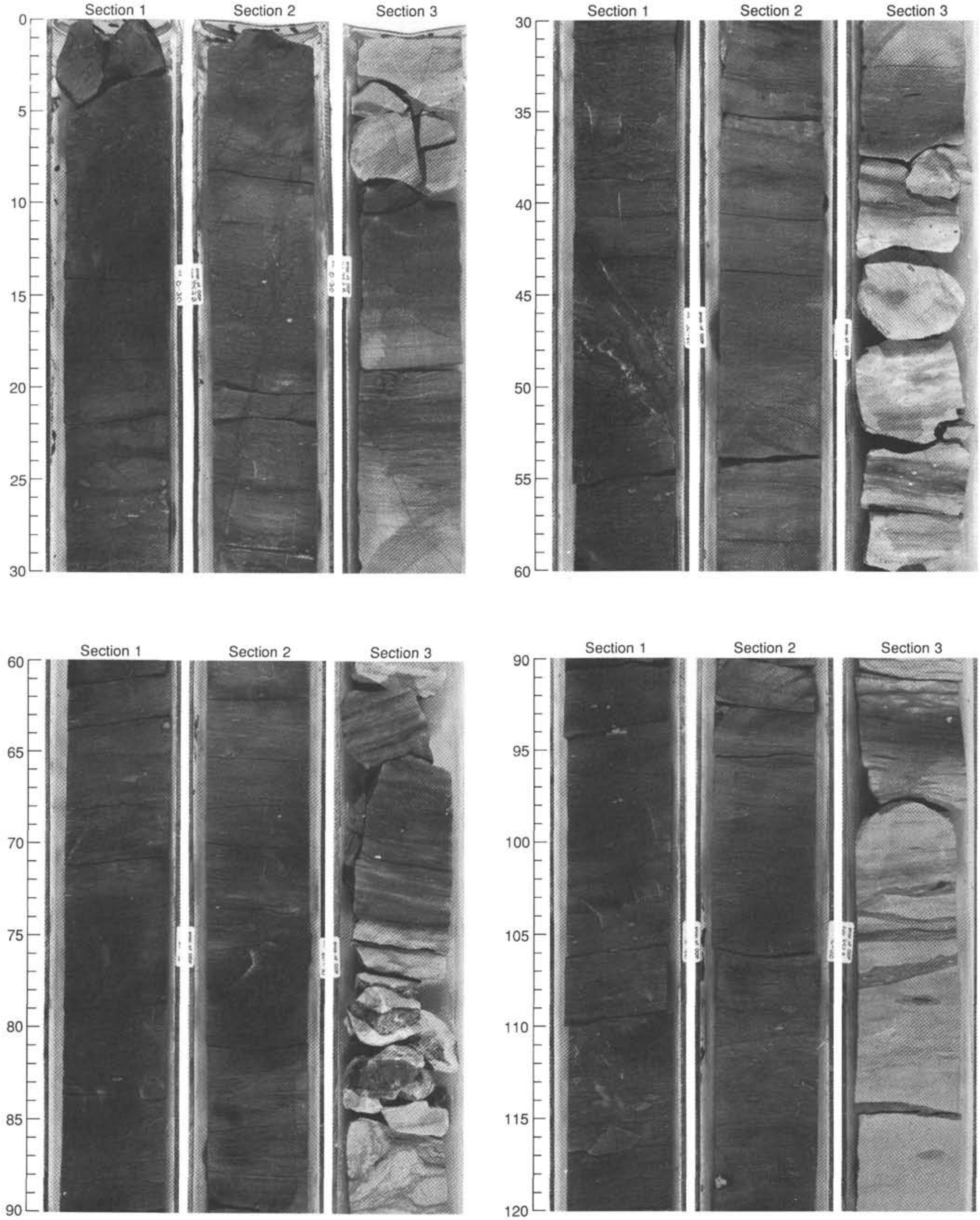

Figure 8. Sequential photographs of the Cretaceous/Tertiary boundary core, Sections 1 through 3 of Core 121-752B-11R.

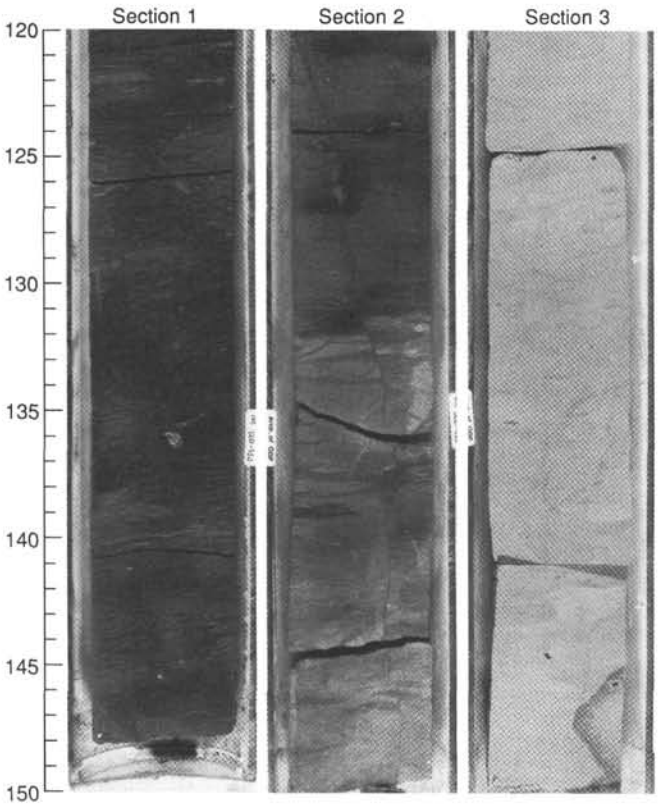

Figure 8 (continued).

and the relatively low planktonic/benthic foraminifer ratio also point to a relatively shallow depth (about 600 m) for Site 752 during the late Eocene. The same upper Eocene interval at Site 754 contains reworked neritic to upper bathyal benthic foraminifers. The uncertainty associated with depth estimates, however, is quite high. On the basis of planktonic/benthic foraminiferal ratios we tentatively see a change uphole from shallow water in the Cretaceous to deeper water environments sometime in the early to middle Paleocene.

Preservation of foraminifers decreases gradually downhole throughout the Paleocene and Maestrichtian, in conjunction with increasing lithification. The absence of well-preserved diatoms is probably also due to increasing diagenesis, because badly preserved radiolarians are present in the Maestrichtian. A noteworthy point is the absence of any detectable reworking throughout lithologic Unit II, the lower Eocene to upper Maestrichtian chalks and limestones. This suggests that Broken Ridge remained a submerged, subhorizontal platform throughout the Cretaceous and early Paleogene. Fauna and especially flora of the Cretaceous are radically different from the Tertiary assemblages and are thus easily detectable, usually appearing in increasing numbers in basal Paleocene strata. We did not detect any Tertiary assemblages until some 6 m above the Cretaceous/Tertiary boundary, which is at 358.75 mbsf.

Sedimentation rates fluctuated from about 1 cm/1000 yr during the Neogene to a high value of 3-4 cm/1000 yr in the Paleogene-Maestrichtian (Fig. 10). Calcareous nannofossil datum levels used for the calculation of sedimentation rates are given in Table 4.

Calcareous Nannofossils

Neogene

Recovery in Hole 752A was generally very good in the Cenozoic sections, with abundant calcareous nannofossils in the foraminifer nannofossil oozes of each core. Nannofossil preservation is good in the Pliocene-Pleistocene sediments but moderate to poor in the Miocene sections. The zonation scheme of Okada and Bukry (1980) was successfully applied to the upper Neogene sequences, but problems were encountered in middle and lower Miocene sediments because of poor nannofossil assemblages and the strong overgrowth of the discoasters. In several cases, it was necessary to combine at least two zones. Comparisons with Miocene sediments from Ninetyeast Ridge Site 756 should aid in obtaining more precise definitions of the zonal assignments for the Broken Ridge material.

The Pliocene/Pleistocene boundary is approximated by the last occurrence of *Discoaster brouweri* in Sample 121-752A-1H-3, 45-46 cm (4.3 mbsf). An apparently complete Pliocene section is present from this sample down to Sample 121-752A-3H-1, 130-131 cm (19.1 mbsf). The first occurrence of *Ceratolithus acutus*, in the latter sample, is used to denote the Miocene/Pliocene boundary. Nannofossils in the Pliocene sediments are diverse, and most marker species are present. The Pliocene assemblages include abundant *Amaurolithus primus, Discoaster pentaradiatus, D. brouweri, Discoaster surculus*, and *Discoaster variabilis*.

Miocene sediments are found down to Sample 121-752A-10H-4, 120-121 cm (91.7 mbsf). The last occurrence of *Reticulofenestra bisecta* and *Zygrhablithus bijugatus* is used to mark the Oligocene/Miocene boundary. The uppermost Miocene sediments are characterized by an increase in diversity in comparison to the middle Miocene sequences. The important age-diagnostic discoasters are absent or rare in the lower units. Strong overgrowths on some discoaster species prevent quick and accurate identification. Lower Miocene sediments contain abundant *Cyclicargolithus floridanus, Sphenolithus* sp., and *Reticulofenestra* sp. Okada and Bukry's (1980) Zone CN2 was not formally recognized in the lower Miocene section, which possibly indicates the presence of a hiatus. Further work on this interval is necessary for confirmation. For a more detailed discussion of Broken Ridge Neogene sections see "Biostratigraphy" section, "Site 754" chapter (this volume).

Paleogene

The lower Paleocene to upper Oligocene sediments recovered from Hole 752A contain abundant, moderately preserved to well-preserved calcareous nannofossils. The highly expanded Paleocene through lower Eocene sequence offers an excellent opportunity for studies in evolution and high-resolution biostratigraphy on an apparently continuous section.

Paleogene sediments were first found in Core 121-752A-10H. The Oligocene/Miocene boundary is approximated in Sample 121-752A-10H-4, 120-121 cm (91.7 mbsf), by the last occurrence of *R. bisecta* and *Z. bijugatus*. The remaining sections of Core 121-752A-10H contain abundant *C. floridanus, Reticulofenestra* sp., and common *R. bisecta* and *Z. bijugatus*. A few specimens of *Cyclicargolithus abisectus* were also noted. Sample 121-752A-10H-7, 10-11 cm, contains a few specimens of *Chiasmolithus altus* and *Reticulofenestra umbilica*, which are reworked. The assemblage is indicative of the upper Oligocene Zone CP19. Examination of Sample 121-752A-10H-CC, however, revealed an early Oligocene age (Zone CP16). The observed assemblage, in this sample, of *Isthmolithus recurvus, Chiasmolithus oamaruensis, Ericsonia formosa*, and *Ericsonia subdisticha* plus the lack of *Discoaster saipanensis* and *Discoaster barbadiensis* indicates that this sample belongs in Subzone CP16a or CP16b. If this assemblage is not entirely reworked, it indicates that a hiatus (missing Zones CP17 and CP18) exists in Section 121-752A-10H-7, but additional work must be done in this area for verification. Sample 121-752A-11H-CC is assigned to the upper Eocene Subzone CP15b. The assemblage includes highly overgrown specimens of *I. recurvus*, few *Coccolithus so-*

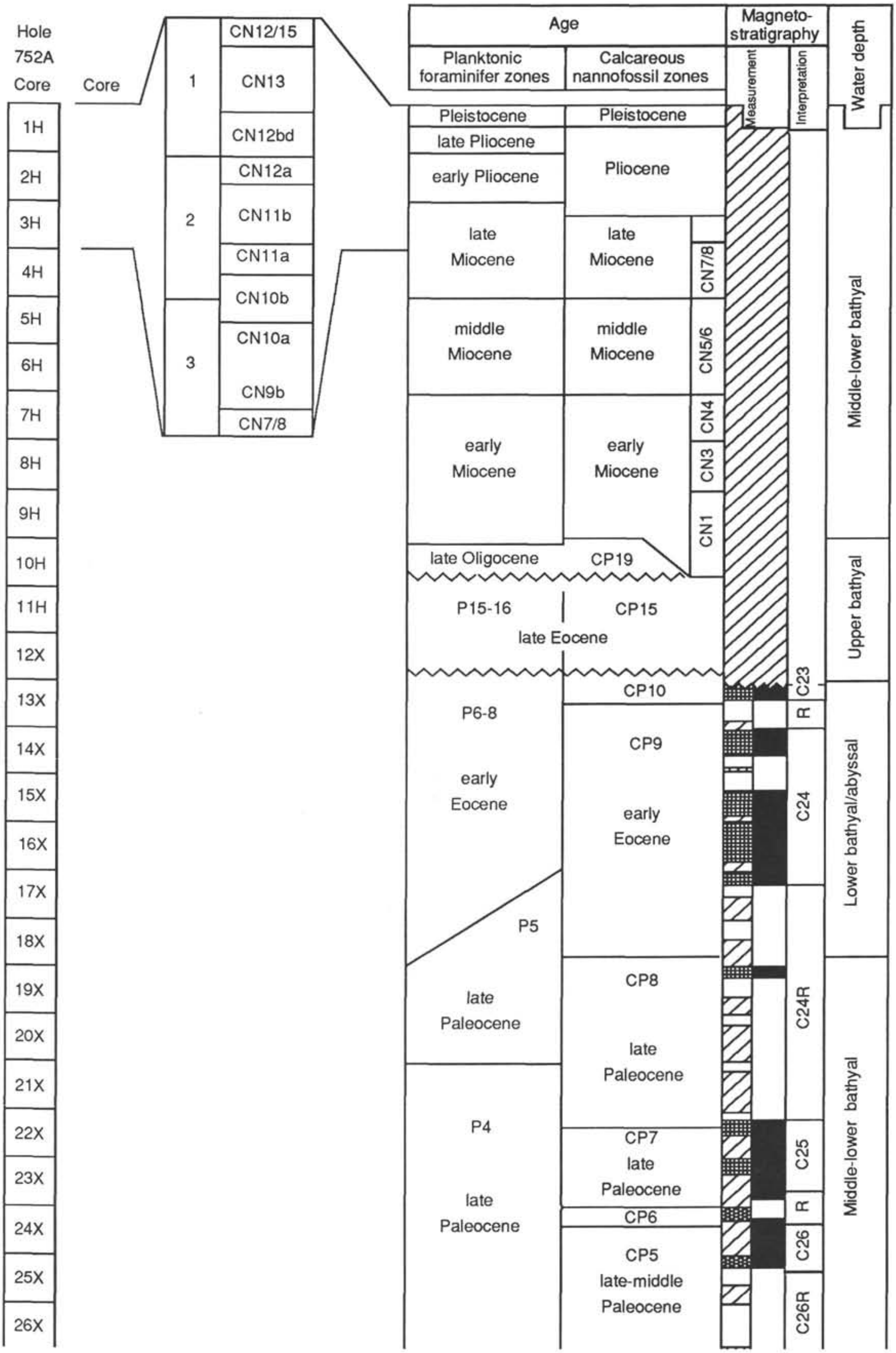

Figure 9. Planktonic foraminifer zones and calcareous nannofossil zones in Holes 752A and 752B.

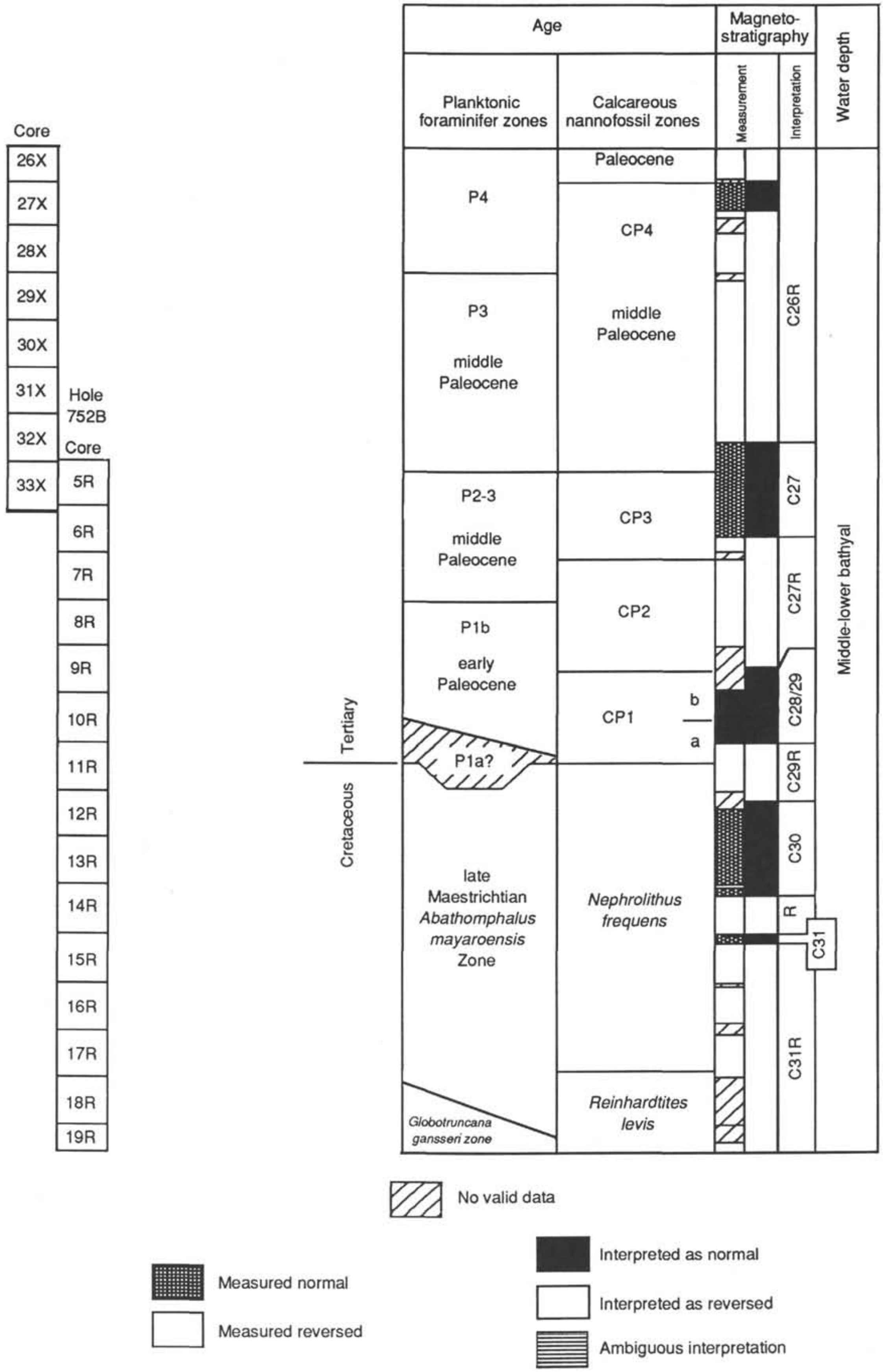

Figure 9 (continued).

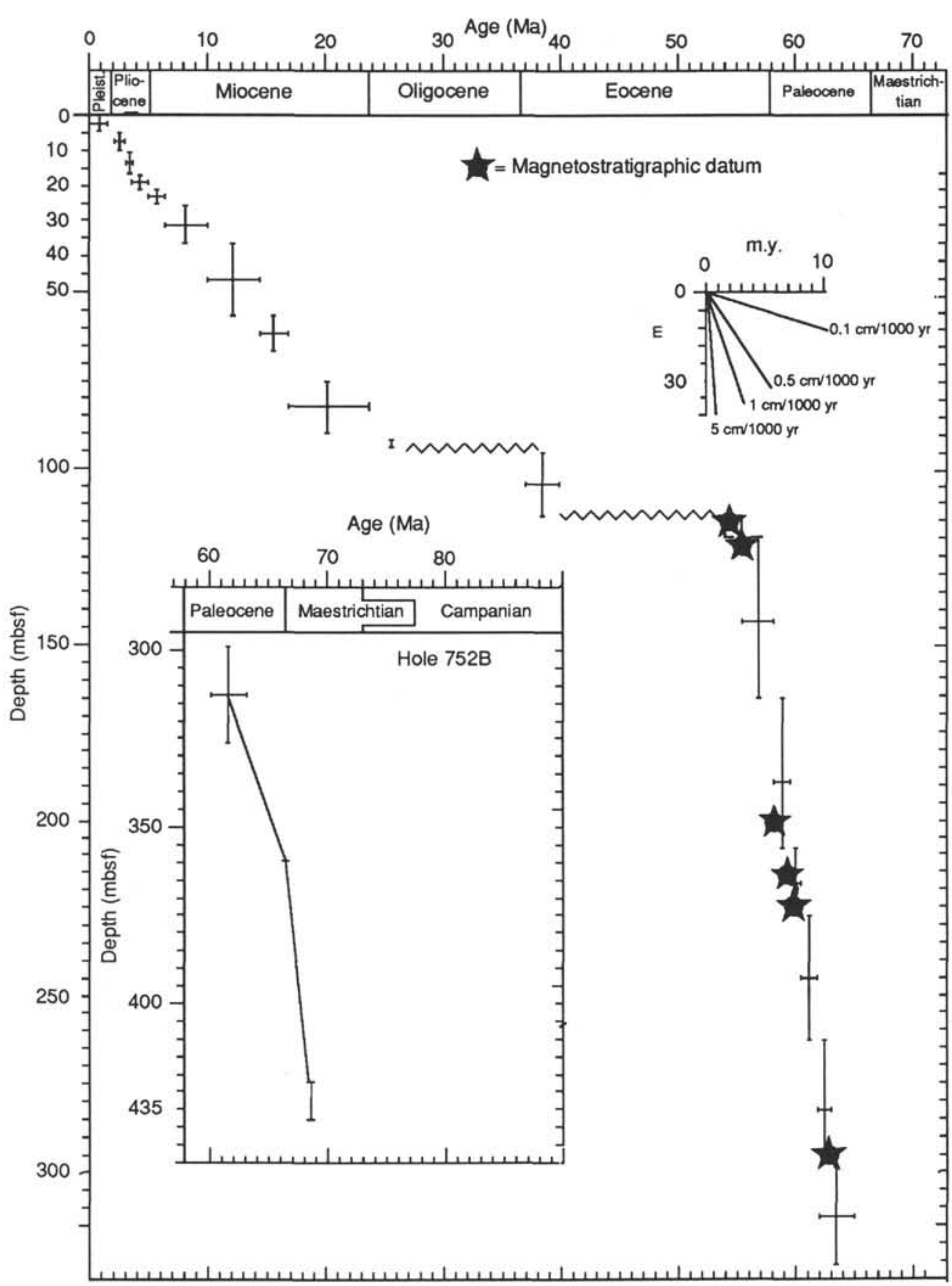

Figure 10. Age vs. depth plot for Site 752, based on calcareous nannofossil datums and augmented with planktonic foraminiferal and magnetostratigraphic datums.

litus, *Coccolithus grandis*, and *R. umbilica*. In addition, *Coccolithus formosus*, *Reticulofenestra hillae*, *Z. bijugatus*, and *Braarudosphaera* are common. The presence of *Braarudosphaera* is consistent with a shallow-water origin for the sediments of this core. Sample 121-752A-12X-CC contains a similar assemblage, but appears to lack the subzonal marker, *I. recurvus*, and thus, is assigned to Subzone CP15a. Because of the very poor nannofossil assemblage and poor recovery in this core, additional work is necessary to confirm this subzonal assignment.

Upper Eocene sediments unconformably overlie nannofossil chalks of late Danian through early Eocene age (112.9–308.0 mbsf). Nannofossil Zones CP11–14 are not present. The underlying sequence, which spans Zones CP3 to CP10, is characterized by moderately preserved to well-preserved nannofossil assemblages of a middle- to high-latitude nature and is remarkably complete. At that time, sedimentation rates were on the order of 3 to 5 cm/1000 yr, thereby producing the thick accumulation of pelagic oozes.

Sample 121-752A-13X-2, 45–46 cm, is assigned to Zone CP10 on the basis of the presence of few *Discoaster lodoensis* and common *Discoaster kuepperi* and *Tribrachiatus orthostylus*. The interval including the remaining sections of Core 121-752A-13X down to Section 121-752A-16X-CC (151.7 mbsf) is placed in Subzone CP9b. *T. orthostylus* is common throughout this interval and is accompanied by abundant chiasmoliths, species of the genus *Toweius*, few *Discoaster* cf. *Discoaster elegans*, and

Table 4. Calcareous nannofossil datums used for calculating sedimentation rates at Site 752 (Fig. 10).

Species[a]	Age (Ma)	Depth (mbsf)
Hole 752A		
LO *Discoaster brouweri*	1.9	4.3
LO *Reticulofenestra pseudoumbilica*	3.4	10.3
FO *Ceratolithus acutus*	5.0	19.1
FO *Amaurolithus primus*	6.4	25.1
LO *Sphenolithus heteromorphus*	14.3	58.1
FO *Sphenolithus heteromorphus*	17.1	73.1
LO *Reticulofenestra bisecta* or *Zygrhablithus bijugatus*	23.7	91.7
LO *Chiasmolithus altus*	28.1	93.4
FO *Isthmolithus recurvus*	37.8	104.3
FO *Discoaster lodoensis*	55.2	114.3
FO *Tribrachiatus bramlettei*	57.8	171.1
FO *Discoaster multiradiatus*	59.1	202.05
FO *Heliolithus riedelii*	59.8	219.5
FO *Heliolithus kleinpellii*	61.6	251.4
FO *Fasciculithus tympaniformis*	62.1	297.7
Hole 752B		
FO *Prinsius martinii* or *Neochiastozygus saepes*	63.7	318.7
FO *Chiasmolithus danicus*	65.0	345.1
FO *Cruciplacolithus tenuis*	65.9	353.46
FO *Biantholithus sparsus*	66.4	358.5
FO *Nephrolithus frequens*	69.0	422.3

[a]FO = first occurrence; LO = last occurrence.

Neococcolithus dubius. A similar assemblage was found in Sample 121-752A-17X-CC, but the additional presence of *Tribrachiatus contortus* places the sample in Subzone CP9a. *Discoaster diastypus*, which is characteristic of this subzone, might be present in the sample, but its precise identification may require the aid of scanning electron microscopy.

The Paleocene/Eocene boundary is tentatively placed in Sample 121-752A-18X-CC, 130–131 cm (171.1 mbsf). Okada and Bukry (1980) use the first occurrence of *D. diastypus* to define this boundary whereas Martini (1971) uses the first occurrence of *Tribrachiatus bramlettei*. Other authors have used the first appearance of *T. contortus*, which occurs slightly higher than the aforementioned markers. For our purposes at Site 752, the boundary is defined by the first occurrence of *T. bramlettei* and the last occurrence of *Fasciculithus* ssp.

The interval including Core 121-752A-17X down to the first occurrence of zonal marker *Discoaster multiradiatus* in Sample 121-752A-22X-2, 45–46 cm (202.05 mbsf), is assigned to the upper Paleocene Zone CP8. Abundant *Toweius* sp., *Fasciculithus tympaniformis*, and *Chiasmolithus bidens*, along with common *D. multiradiatus*, are indicative of this zone. The remainder of Core 121-752A-22X and Core 121-752A-23X are placed in Zone CP7, based on the presence of *Heliolithus reidelii*, which has a first occurrence in Sample 121-752A-23X-CC (219.1 mbsf). *Prinsius bisulcus, F. tympaniformis*, and *Toweius eminens* are abundant and *C. bidens* and *Discoaster mohleri* are common in these cores. Zone CP6 is assigned to the short interval from Sample 121-752A-23X-CC to the first occurrence of *D. mohleri* in Sample 121-752A-24X-2, 45–46 cm. The first occurrence of the CP5 zonal marker *Heliolithus kleinpellii* is noted in Sample 121-752A-27X-2, 148–150 cm (251.4 mbsf). The interval including the remainder of Core 121-752A-27X down to Sample 121-752A-32X-6, 148–150 cm (297.7 mbsf), where the first *Fasciculithus* ssp. appears, is assigned to Zone CP4. *P. bisulcus, Prinsius martinii*, and *C. bidens* are abundant and *Chiasmolithus danicus* and *T. eminens* are common in these sections. Core 121-752A-33X is placed in Zone CP3, based on the presence of abundant *P. martinii* and few smaller forms of *P. bisulcus*. Also present are *C. danicus* and *Prinsius diamorphosus*.

The presence of abundant chiasmoliths and reticulofenestrids attests to the high-latitudinal nature of the Paleogene material recovered from Hole 752A. The nannofossil assemblages compare quite favorably with those of Maud Rise (ODP Leg 113; J. Pospichal and S. W. Wise, Jr., pers. comm., 1988). The sequence on Broken Ridge appears to be more complete and should shed light on many unanswered questions concerning the nannofossil biostratigraphy of Southern Hemisphere, high-latitude Paleocene sediments.

Cretaceous/Tertiary Boundary

Hole 752B was drilled to recover sediments encompassing the Cretaceous/Tertiary boundary and to achieve overlap with the upper Maestrichtian sediments recovered in Hole 754B. A complete Cretaceous/Tertiary boundary was cored to the enjoyment of all involved. After two spot cores containing lower Eocene sediments were retrieved, RCB coring commenced at 297.0 mbsf in Danian ash-rich chalks and continued through sediments of the upper Maestrichtian. Overlap with Hole 754B was achieved, and drilling was terminated at 435.6 mbsf.

The interval consisting of Cores 121-752B-5R and 121-752B-6R down to Sample 121-752B-7R-2, 109–110 cm (297.0–318.7 mbsf), is assigned to Zone CP3, based on the presence of abundant *P. martinii*. The normal marker for Zone CP3, *Ellipsolithus macellus*, is generally absent or very rare in high-latitude sections, but according to Perch-Nielsen (1985), the first occurrence of *P. martinii* or *Neochiastozygus saepes* may be used to define this zone instead. Additional taxa present in this interval include abundant *C. danicus*, common *Cruciplacolithus tenuis, Coccolithus cavus*, and *Thoracosphaera* sp. *N. saepes* and *Cruciplacolithus edwardsii* are present also. The first occurrence of *C. danicus*, defining the CP2/CP1 boundary, was noted in Sample 121-752B-9R-CC (345.1 mbsf). Sediments assigned to this zone contain the austral species *Hornibrookina teuriensis*. Subzone CP1b is defined by the first occurrence of *C. tenuis*, in Sample 121-752B-10R-6, 86–87 cm (353.46 mbsf).

The Cretaceous/Tertiary boundary as defined by calcareous nannofossils is marked by the first occurrence of the usually very rare but distinctive *Biantholithus sparsus*. Two specimens were found in Sample 121-752B-11R-3, 72–73 cm (358.5 mbsf). The results of a quick quantitative study on closely spaced samples taken across the boundary are summarized in the "Biostratigraphy" section of the "Cretaceous/Tertiary Boundary Summary" chapter (this volume).

Cores 121-752B-12R to 121-752B-17R are assigned to Sissingh's (1977) upper Maestrichtian Zones CC25-26. Assemblages consist primarily of *Nephrolithus frequens, Arkhangelskiella cymbiformis, Kamptnerius magnificus*, and *Cribrosphaerella daniae*. Overlap of the upper range of *N. frequens* and the lower range of *Nephrolithus corystus* in Core 121-752B-17R is indicative of the lower part of Zone CC25 (J. Pospichal and S. W. Wise, Jr., pers. comm., 1988).

Cores 121-752B-18R and 121-752B-19R are assigned to Zone CC24. Species additional to those previously listed include *Reinhardtites levis* and *Biscutum magnum*.

The first occurrence of *N. frequens* (Sample 121-752B-17R-CC) corresponds with the last occurrence of *R. levis* in the Broken Ridge sediments. However, Sissingh's (1977) scheme calls for a gap to exist between the ranges of those two forms. This gap has not been found in high-latitude austral sections such as those cored on Maud Rise (J. Pospichal and S. W. Wise, Jr., pers. comm., 1988).

Planktonic Foraminifers

Samples 121-752A-1H-CC to 121-752A-9H-CC contain a condensed Neogene sequence that is almost complete. At the base of this sequence, in Sample 121-752A-9H-CC, a late Oligocene to earliest Miocene age assemblage of planktonic foraminifers occurs above and within the hardground. Below the hardground in Sample 121-752A-10H-CC, a late Eocene age assemblage of planktonic foraminifers extends down to Sample 121-752A-12X-CC.

Neogene

A Neogene assemblage of planktonic foraminifers was recovered down to 92.5 mbsf. Preservation throughout the Neogene is good. In contrast, the late Eocene to late Oligocene age planktonic foraminiferal assemblages within and below the hardground are recrystallized, overgrown with calcite, and contain substantial amounts of reworked Eocene, Paleocene, and Cretaceous faunas.

Dominating the Neogene assemblages are typical midlatitude, temperate faunas and other more cosmopolitan species. The recovered faunas have an affinity with other Neogene faunas at midlatitudes in the Southern Hemisphere, such as southeast Australia (Jenkins, 1960), New Zealand (Jenkins, 1967, 1971), the South Atlantic (Jenkins, 1978), and the South Pacific (Kennett, 1973). Significantly, *Globigerina bulloides*, which is restricted to transitional and cooler waters at the present (Bé and Tolderlund, 1971), is found in abundance throughout.

Because of the lack of low-latitude marker species it is impossible to apply the tropical zonation schemes proposed by Banner and Blow (1965), Blow (1969), or Bolli et al. (1985). Instead, the higher latitude zonal schemes of Srinivasan and Kennett (1981) and Kennett (1973) were applied to sediments of early to middle Miocene and late Miocene to Holocene ages, respectively.

Pleistocene

The upper Pliocene to Pleistocene is present in Sample 121-752A-1H-2, 100–102 cm. Delineation of a planktonic foraminiferal zone is not possible, because the marker species *Globorotalia truncatulinoides* is poorly developed.

Pliocene

A possibly complete Pliocene sequence of sediments was recovered in the interval from Samples 121-752A-1H-CC to 121-752A-2H-CC. Two zones within the Pliocene sediments are delineated, based on the first occurrence of *Globorotalia puncticulata* and *Globorotalia tosaensis*. Temperate species such as *G. bulloides, Globigerina falconensis, Globigerina woodi, Globorotalia conoidea, Globorotalia conomiozea, Globorotalia puncticulata*, and *Globorotalia inflata* dominate the assemblages, alongside the more cosmopolitan species *Orbulina universa, Orbulina suturalis*, and *Globorotalia margaritae*.

Miocene

Miocene sediments were recovered in the interval from Samples 121-752A-3H-CC to 121-752A-10H-CC. The planktonic foraminifer assemblage is dominated by *G. bulloides* and *G. woodi*. The Miocene/Pliocene boundary is tentatively placed at the evolutionary appearance of *G. puncticulata* and *G. margaritae*. Within the upper Miocene assemblages there is an abundance of *Globigerina nepenthes, G. conoidea, Globorotalia miozea, Globorotalia panda*, and *Globoquadrina dehiscens*.

The base of the middle Miocene is not delineated. From Samples 121-752A-7H-CC to 121-752A-10H-1, 150–151 cm, the sediments are of early Miocene age, characterized by *G. dehiscens, Globigerinoides trilobus, Catapsydrax dissimilis, G. bulloides, Globorotalia incognita*, and *Globorotalia zealandica*.

The presence of *Globigerina angulisuturalis* and *Globorotalia kugleri*, along with the absence of *Globigerinoides* sp., *G. dehiscens*, and *Chiloguembelina cubensis*, assigns Sample 121-752A-10H-3, 150–152 cm, to the upper Oligocene.

Paleogene to Cretaceous

Planktonic foraminiferal assemblages in the lower Eocene and upper Paleocene are moderately well preserved. Increasingly harder rocks in the lower Paleocene to Maestrichtian section made the application of ultrasonic treatment necessary, which led to destruction of morphological details on foraminiferal tests. Absent in the assemblages are keeled and ornamented low-latitude species. This is typical for assemblages of the temperate-austral areas (Jenkins, 1985; Caron, 1985). At some intervals (120–160 mbsf, Zones P6-7; 260–300 mbsf, Zone P4; and 386–420 mbsf, *Abathomphalus mayaroensis* Zone) recovered species are more indicative of lower latitudes. Their occurrence may imply incursions of warmer water or changes in climate.

Oligocene to Upper Eocene

Sample 121-752A-10H-CC contains a late Eocene age fauna dominated by *Globigerinatheka index* and *Globigerinatheka luterbacheri*. The youngest Paleogene planktonic foraminifers, which were found in Sample 121-752A-10H-3, 150–152 cm (94.7 mbsf), are of latest Oligocene age and are mixed with forms of late and early Oligocene age. The presence of *Globigerinelloides* sp. and *Acarinina bullbrooki* in these samples indicates reworking from Upper Cretaceous and middle Eocene strata.

Lower Eocene to Paleocene

Cores 121-752A-13X-CC to 121-752A-33X-CC contain austral temperate assemblages of low diversity. The occurrence of *Morozovella marginodentata* and *Morozovella subbotinae* in the lower Eocene (120–160 mbsf) is not mentioned by Jenkins (1985) as typical for temperate, austral areas and may imply a warm-water incursion at Site 752 during the early Eocene. The same holds true for the presence of *Globorotalia angulata*, at 260–300 mbsf in Zone P3. The low-diversity assemblages continue downhole into the upper Maestrichtian and make zonal differentiation difficult. We could not differentiate within the upper and middle Paleocene because of a lack of marker species. Planktonic/benthic ratios are generally high (>90/10), although in Samples 121-752A-32X-CC and 121-752A-33X-CC the ratios drop to about 75/25, suggesting shallowing downsection.

The Cretaceous/Tertiary boundary, defined between 73 and 95 cm in Section 121-752B-11R-3, is probably at 95 cm (358.75 mbsf) because that level marks a large-scale disappearance of Cretaceous foraminiferal specimens and species. In thin sections from 110, 202, and 239 cm above Sample 121-752B-11R-3, 95 cm, planktonic specimens are extremely rare and indeterminable. Therefore, the detailed biostratigraphic zonation at the Cretaceous/Tertiary boundary (Smit, 1982; Smit and Romein, 1985) could not be applied. In a stained slab from Sample 121-752B-10R-CC, rare minute forms were found that are not determinable to generic or species levels. These forms are distinctly different from *Globigerina eugubina*, however, because the specimens from Sample 121-752B-10R-CC have spherical chambers (Smit, 1982).

Cretaceous

A low-diversity fauna was found in the interval from Sample 121-752B-11R-CC to the bottom of Hole 752B. From Samples 121-752B-11R-CC to 121-752B-17R-CC, the assemblages are representative for the *A. mayaroensis* Zone, the uppermost Maestrichtian foraminiferal zone. *A. mayaroensis* is known from temperate, boreal, and austral areas, in contrast to biozones based on low-latitude assemblages; thus, the upper Maestrichtian could be adequately zoned. The stratigraphic overlap with Hole 754B is established by means of the lineage *Globotruncanella citae–Abathomphalus intermedius–Abathomphalus mayaroensis*. The transition of *A. intermedius* to *A. mayaroensis* is between Cores 121-752B-17R and 121-752B-19R. The same transition is found between Cores 121-754B-5R and 121-754B-6R (see "Biostratigraphy" section, "Site 754" chapter).

Benthic Foraminifers

Benthic foraminifers (>125 μm) were examined in all core-catcher samples from Holes 752A and 752B. They are well preserved in the Neogene foraminiferal oozes, but only moderately preserved in the Eocene to Paleocene chalk. In contrast to the abundance of planktonic foraminifers, the benthic foraminifers are generally rare, as indicated by the high planktonic/benthic ratios. In Samples 121-752A-11H-CC to 121-752A-12X-CC, foraminifers are rare and poorly preserved, suggesting downslope transportation.

Pleistocene to Pliocene

Pliocene-Pleistocene faunas are characterized by a diversified benthic fauna represented by *Cibicidoides kullenbergi, Stilostomella lepidula, Planulina wuellerstorfi, Globocassidulina subglobosa, Gyroidina orbicularis, Pullenia bulloides, Oridorsalis umbonatus*, and nodosariid and dentalinid taxa. Compared to the Holocene distribution in the Indian Ocean, these taxa apparently exist in an environment dominated by Indian Bottom Water and Indian Deep Water (Corliss, 1979; Peterson, 1984).

Miocene

Late Miocene age benthic faunas are dominated by *Ehrenbergina carinata, C. kullenbergi, S. lepidula, P. wuellerstorfi, O. umbonatus, P. bulloides*, and *Gyroidina soldani*. Globocassidulinids, stilostomellids (*S. lepidula* and *Stilostomella subspinosa*), and pleurostomellids are also abundant and include many species. Accessory elements in these fauna are *Amphicoryna scalaris, Rectuvigerina striata*, "*Karreriella*" sp., *Heronallenia, Marginulina, Laticarinina pauperata, Bulimina mexicana, Ehrenbergina histrix*, and *Trifarina bradyi*. Although uvigerinids are not dominant, they are consistently observed in the late Miocene age fauna.

Early Miocene age faunas are somewhat similar to the overlying faunas because of the common occurrence of *Stilostomella* and *Cibicidoides*. In Sample 121-752A-9H-CC, *Lenticulina* occur in association with globocassidulinids. These faunas indicate a lower to middle bathyal environment.

Planulina costa and costate uvigerinids are common in the lower Miocene faunas, indicating middle to upper bathyal depths. Agglutinated forms such as *Martinottiella scabra* are also found.

Eocene

The benthic foraminifers obtained from upper Eocene coarse-grained sediments are rare and consist of deep-water genera such as *Hanzawaia, Cibicidoides, Bulimina*, and *Amphicoryna*. Tests of these taxa are usually partially destroyed. Planktonic/benthic ratios of Samples 121-752A-11H-CC and 121-752A-12X-CC are 52/48 and 14/29, respectively. *Amphistegina* and bryozoan fragments were found in Sample 121-752A-11H-CC, suggesting downslope transport to a deep-water region. The occurrence of *Baggina* sp., *Hanzawaia cushmani*, and *Bulimina tuxpomensis* in Sample 121-752A-11H-CC indicates an upper bathyal depth.

Early Eocene age faunas (Sections 121-752B-1W-1 to 121-752B-4W-CC) are characterized by *Nuttalides truempyi, Anomalinoides capitata, Anomalina praeacuta, Alabammina dissonata, O. umbonatus, B. tuxpomensis, Pullenia coryelli*, and other unspecified taxa such as *Lenticulina, Nonion, Bulimina, Gyroidina, Cibicidoides, Vulvulina*, and *Nodosaria*. Similar faunas have been reported from lower bathyal to abyssal water depths in the South Atlantic Ocean (Tjalsma and Lohmann, 1983).

Paleocene

The faunas obtained from Samples 121-752A-18X-CC to 121-752A-33X-CC and 121-752B-5R-CC to 121-752B-9R-CC are represented by *Stensioina beccariiformis, A. capitata, Gyroidinoides globosus, P. coryelli, Cibicidoides velascoensis*, and *Nonion havanensis*. Among these, *S. beccariiformis* is the most characteristic species of the faunas. *N. truempyi*, which occurs in the Eocene sediments, is also commonly observed in Samples 121-752A-22X-CC and 121-752B-10R-CC. *Coryphostoma midwayensis, Neoflabellina semireticulata, Bulimina trinitatensis, Bulimina bradburyi, Allomorphina minuta*, and agglutinated taxa such as *Tritaxia globulifera* and *Spiroplectammina spectabilis* occur sporadically.

The extinction of *S. beccariiformis* near the Eocene/Paleocene boundary at Site 752 corresponds to the "benthic event" proposed by Tjalsma and Lohmann (1983) in the Atlantic Ocean. The depth distributions of these faunas overlap broadly, and many species indicate bathyal to abyssal depths (van Morkhoven et al., 1986).

Cretaceous

The Cretaceous faunas recovered from Site 752 show no significant faunal differences from those of the Paleocene. Generic dominance remains basically unchanged. The characteristic elements found in these faunas are *S. beccariiformis, C. velascoensis, Pullenia* cf. *cretacea, Bolivinoides draco, Osangularia cordieriana, Coryphostoma incrassatus, G. globosus, Praebulimina* spp., *Lenticulina* spp., *Nodosarella* spp., *Astacolus* spp., and *Tritaxia* sp. The water depth suggested by these taxa is middle to lower bathyal.

Inoceramus prisms were noted as additional faunal constituents.

Diatoms

Diatoms are rare to absent in the Pleistocene through upper Eocene sediments, common to abundant in the lower Eocene through middle Paleocene sediments, and absent in the lower Paleocene through Cretaceous sediments.

A major result of Site 752 drilling is the recovery of well-preserved diatom assemblages that occur throughout a long, continuously cored lower Eocene and Paleocene section (180 m).

Our knowledge of early Eocene and Paleocene age diatoms is still limited. Fenner (1985) compiled information on early Eocene age diatoms available from DSDP Sites 94 in the Gulf of Mexico and 339 and 343 in the Norwegian Sea and Hole 390A in the North Atlantic. Late Paleocene age diatoms have been reported in the tropical Indian Ocean from DSDP Site 214 (Bukry, 1974) and Vityaz Core 6744 (Mukhina, 1974, 1976), the South Pacific from DSDP Site 208, the North Atlantic from DSDP Site 384 and Hole 398D, and the South Atlantic from DSDP Hole 327A and Site 524 and ODP Site 700. Early Eocene and Paleocene age diatom deposits are also known in the USSR (Strelnikova, 1987).

Site 752 offers an exceptional opportunity to document the diatom flora of the early Paleogene, to determine evolutionary events through this time interval, and to define biostratigraphic diatom datum levels that can be directly correlated to calcareous nannofossil and planktonic foraminifer zonations.

Because of the lack of zonal markers, Gombos' (1977, 1982) zonations are not applicable here, and Strelnikova's (1987) zonation is useful only for the lower Eocene. Thus, a tentative new zonation is proposed for the Paleocene (see "Explanatory Notes" chapter).

Neogene

Of all the core-catcher samples examined, only upper Miocene Sample 121-752A-3H-CC contains a marine diatom assemblage. The assemblage is poorly preserved and consists of rare specimens of *Thalassiothrix longissima, Denticulopsis* aff. *dimorpha, Rhizosolenia styliformis, Actinocyclus ingens*, and *Thalassiosira* sp.

Paleogene

In the lower Eocene (Cores 121-752A-13X to 121-752A-17X), diatoms are common and moderately to well preserved. Assemblages are similar throughout the section and consist of *Melosira architecturalis, Pyxilla gracilis, Hemiaulus polycystinorum, Hemiaulus* sp., *Arachnoidiscus* sp., *Stephanopyxis turris, Stephanopyxis* sp., *Sceptroneis* sp., *Rhizosolenia* sp., *Trinacria simulacrum, Trinacria excavata* forma *tetragona*, and *Triceratium cellulosum*. Based on the occurrence of *P. gracilis* without the presence of *Pyxilla oligocaenica* var. *tenuis*, this interval is assigned to the *Pyxilla gracilis* Zone.

For the Paleocene (Cores 121-752A-18X to 121-752A-31X), diatoms are abundant and well preserved in Cores 121-752A-18X to 121-752A-27X. Preservation deteriorates below this depth, and diatoms are absent from Core 121-752A-32X to the base of Hole 752A.

The assemblages are similar to those previously described from the upper Paleocene sediments (Gombos, 1977, 1984; Mukhina, 1974, 1976). However, the stratigraphic zonal markers (*Hemiaulus inaequilaterus* and *Odontotropsis klavsenii*) proposed by Gombos (1977) are not present here. The assemblages are dominated by *S. turris, Stephanopyxis* sp., *H. polycystinorum, Hemiaulus incurvus, Hemiaulus* sp., *Rhizosolenia* sp., *Sceptroneis* sp., *Hyalodiscus scoticus* (*sensu* Mukhina 1976), *Hyalodiscus* sp., *Trinacria simulacrum, T. excavata* forma *tetragona, Triceratium* aff. *cellulosum*, and *Triceratium tessellatum*.

Some changes in the diatom assemblages are noted across the Eocene/Paleocene boundary. Species such as *M. architecturalis* and *P. gracilis*, which are common in the Eocene sediments, are not found in the Paleocene sediments. Other species such as *H. incurvus* and *T. tesselatum* are first found in Core 121-752A-18X (uppermost Paleocene). The *Triceratium tesselatum* Zone is between Samples 121-752A-18X-CC and 121-752A-25X-CC, based on the range of *T. tesselatum*. The *Hemiaulus incurvus* Zone is between Samples 121-752A-25X-CC and 121-752A-31X-CC.

Other downsection changes observed in the diatom assemblages might be useful for biostratigraphic determinations. These markers are *Huttonia* sp., which seems to occur only in Core 121-752A-21X, and *Triceratium gracillium*, which is first found in Sample 121-752A-24X-CC.

In order to provide reliable diatom stratigraphic data, further shorebased analyses are required. Additional samples need to be studied, and a more detailed taxonomic documentation of the flora is necessary. In particular, a detailed taxonomic study of the genera *Hemiaulus, Hyalodiscus*, and *Triceratium*, which are diversified in the section, might be of general stratigraphic interest.

Lower Paleocene and Cretaceous

No diatoms were found in the lower Paleocene and Cretaceous core-catcher samples examined from Hole 752B.

Other Siliceous Microfossils

Radiolarians, silicoflagellates, and sponge spicules are present and well preserved in the same samples where diatoms occur (upper middle Paleocene to lower Eocene). In addition, fragments of radiolarians and sponge spicules were found in the Maestrichtian sediments (Samples 121-752B-10R-CC, 121-752B-13R-CC, and 121-752B-19R-CC). These are, however, rare and poorly preserved.

PALEOMAGNETICS

Susceptibility

The susceptibility data for Hole 752A (Fig. 11) reflect the differences between the two lithologic units. Most of the values for Unit I are quite low (around 1×10^{-6} cgs units) and commonly negative. The material is probably dominantly paramagnetic or diamagnetic. Other than a few spikes, which are probably due to contamination by rust flakes, the data are essentially featureless to 70 mbsf (lower Miocene). At this depth in the record, there is a large spike (2.5×10^{-4} cgs units) for which the origin has not been determined. A second and larger spike (4×10^{-4} cgs units) occurs from about 93 to 100 mbsf (upper Eocene) and corresponds to the iron-stained sediments immediately above the Oligocene/Eocene unconformity.

The susceptibilities of lithologic Unit II are generally higher than those of Unit I, with average values around 10^{-5} and spikes as high as 3×10^{-4} cgs units. The strength of the signal is strongly correlated with the amount of volcanic ash present. The ubiquitous presence of this ash throughout Unit II is apparently responsible for the overall increase in susceptibility in comparison with Unit I. The numerous relatively dense, discrete ash layers are also responsible for the large and numerous spikes. The shapes of some of these spikes seem, in many instances, to mimic the observed pattern of ash deposition, which appears to be characterized by a rapid onset in some cases and more gradual influx in others. The pattern of susceptibility highs appears to be periodic, and Fourier analysis seems to show at least one discernable frequency peak. The relationship of susceptibility to ash content and the time behavior of the signal are discussed in the "Tephra" section of the "Broken Ridge Summary" chapter (this volume).

Recovery from Hole 752B (Fig. 12) is entirely within lithologic Unit II and overlaps the bottom of Hole 752A by several meters. The high-frequency susceptibility signal allows precise correlation between the two holes, particularly from the data at about 300 mbsf. Susceptibility values are relatively high, with a base level of 10^{-5} to 10^{-4} cgs units and frequent spikes resulting from ash layers. There is an overall increase in the average susceptibility from the top of the core (5×10^{-5} cgs units) to a maximum at about 350 mbsf (2×10^{-4} cgs units), which is followed by a decrease back to the average level by about 400 mbsf.

Remanence

The intensity of natural remanent magnetization (NRM) of lithologic Unit I (0–112.9 mbsf; Fig. 13) is low at the top of the unit (around 0.1 mA/m). While intensities have a minor increase toward the bottom of Unit I, values rarely exceed 1 mA/m. Although useful measurements can be made at these intensities, the directional data from the archive half of the core appear to be largely random. The problem is compounded by the presence of overprints, probably induced by drilling, which could not be adequately removed by the 9-mT demagnetizer incorporated into the cryogenic magnetometer system. Shorebased work with more sensitive instruments might be able to extract some reliable results, but the data are not interpretable at present.

More reliable results were obtained from Unit II, with NRM magnitudes generally in excess of 1 mA/m and measurable by both the cryogenic and Molspin magnetometers. Overprints are commonly present and commonly not removable by the 9-mT demagnetizer. Multiple-step alternating field (AF) demagnetiza-

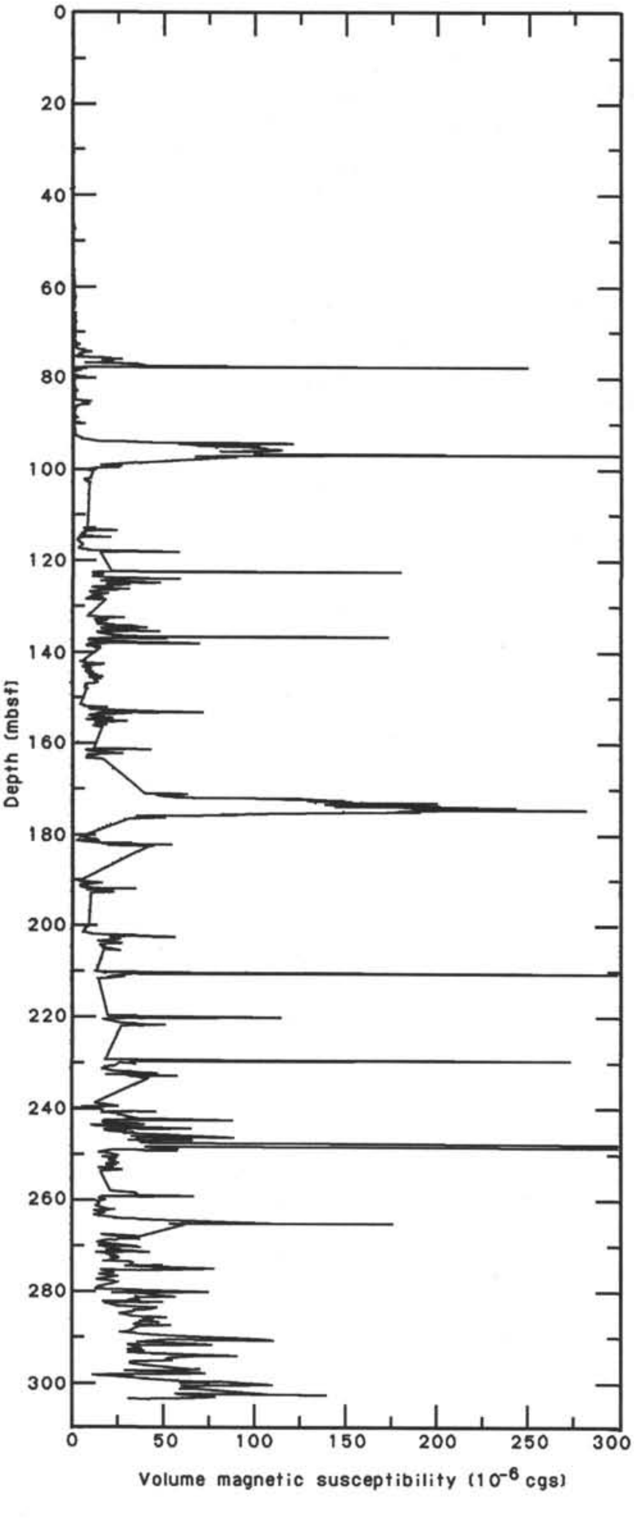

Figure 11. Hole 752A volume magnetic susceptibility plot.

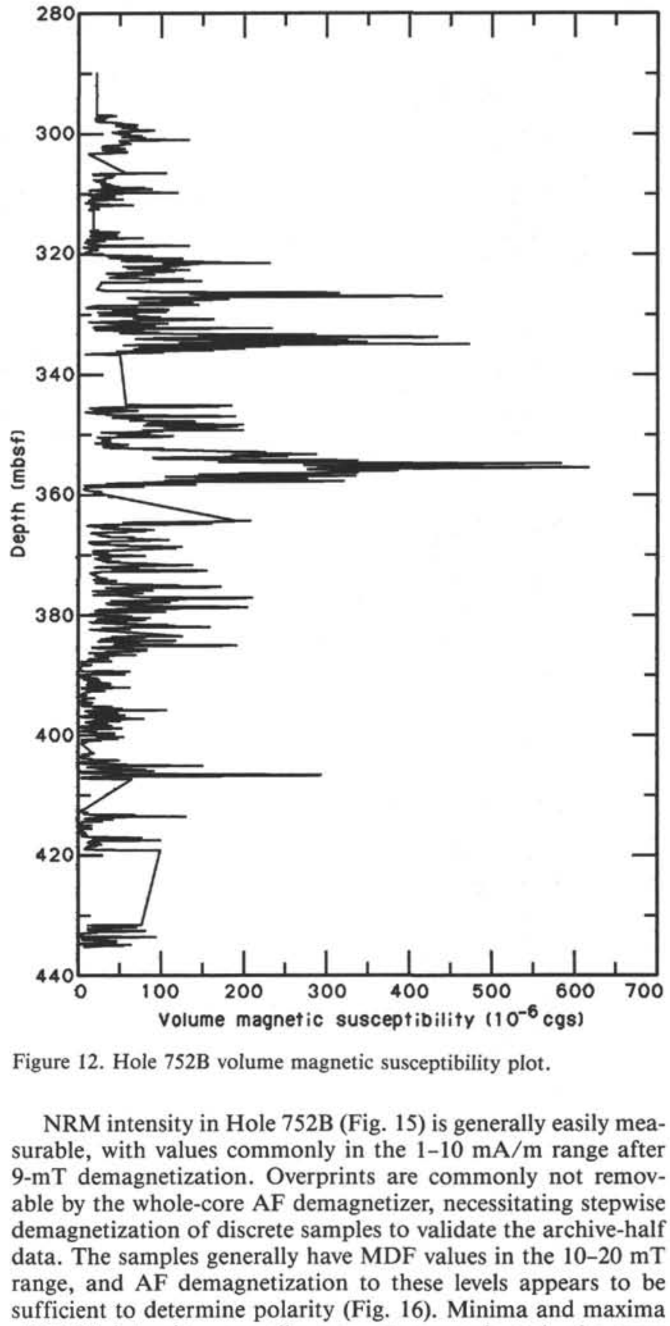

Figure 12. Hole 752B volume magnetic susceptibility plot.

tion of discrete samples was thus necessary to confirm the results of the whole-core data. These samples generally have median demagnetizing fields (MDF) of 10–20 mT and appear to give reliable primary directions (Fig. 14). As discussed in the "Explanatory Notes" chapter, DC-bias problems with the Schonstedt AF demagnetizer limited our interpretation to identification of reversed or normal polarity only. Determination of paleolatitudes awaits shorebased work.

NRM intensity in Hole 752B (Fig. 15) is generally easily measurable, with values commonly in the 1–10 mA/m range after 9-mT demagnetization. Overprints are commonly not removable by the whole-core AF demagnetizer, necessitating stepwise demagnetization of discrete samples to validate the archive-half data. The samples generally have MDF values in the 10–20 mT range, and AF demagnetization to these levels appears to be sufficient to determine polarity (Fig. 16). Minima and maxima of NRM intensity generally occur at approximately the same depth as those of the susceptibility. As the grain-size dependence of NRM intensity is essentially opposite to that of susceptibility, this is a strong indication that both intensities are controlled largely by the amount of magnetic material present (which should be directly related to ash content) and not by intrinsic parameters such as grain size.

Magnetostratigraphy

Whole-core measurements of lithologic Unit I are not of sufficient quality to determine a reliable magnetostratigraphy; none was attempted. Whole-core measurements of lithologic Unit II yield fairly clear polarity intervals after 9-mT demagnetization (Fig. 17). This pattern was checked against discrete samples with a stepwise demagnetization behavior that allows a clear determination of polarity. Where overprints were found, the record was revised accordingly. Correlation of the polarity zones with the geomagnetic reversal time scale (GRTS) was accomplished

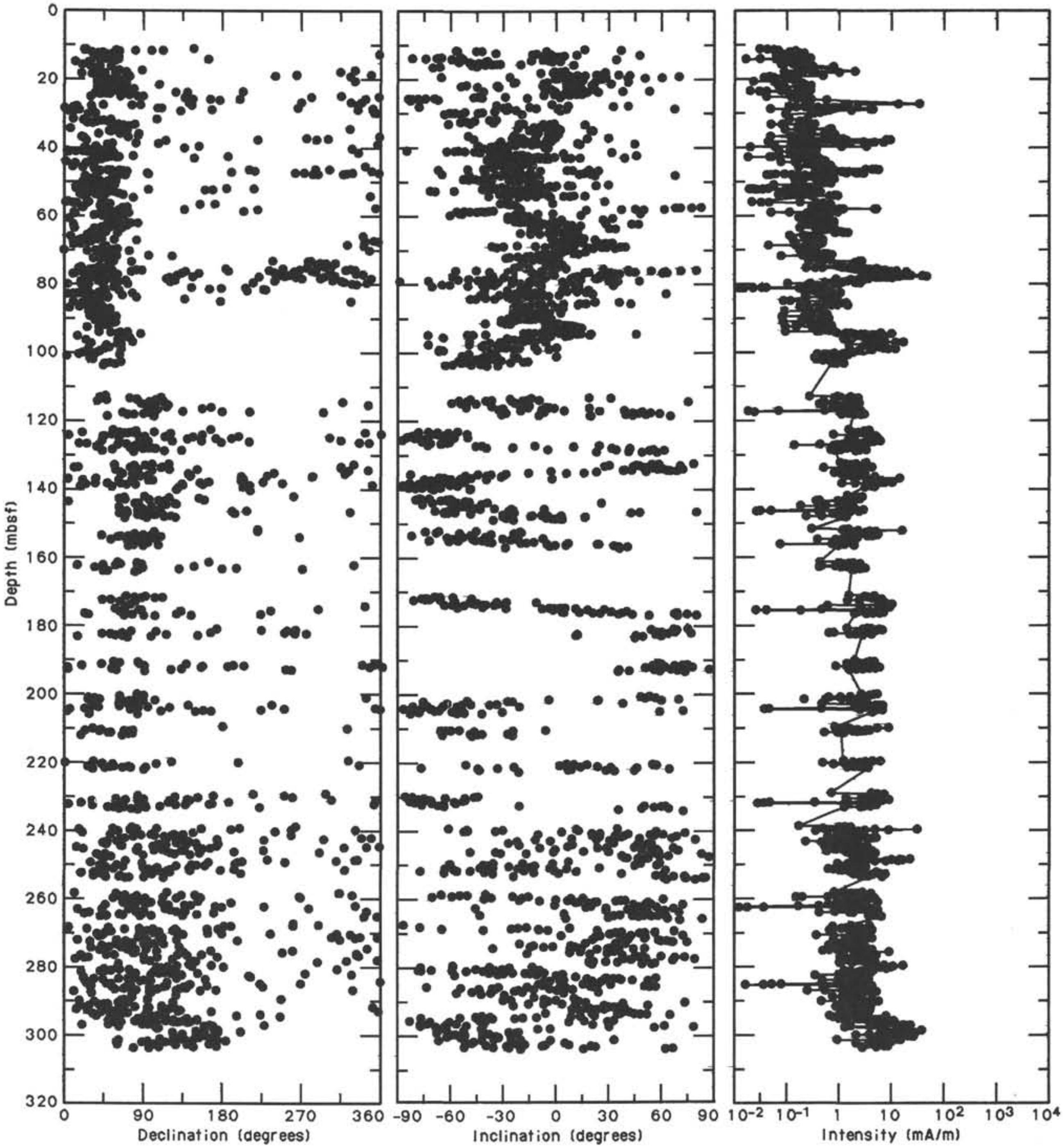

Figure 13. Hole 752A remanence data after 9-mT demagnetization.

with the use of biostratigraphic data combined with a comparison of the lengths of the polarity zones with those of the GRTS (Berggren et al., 1985; Bolli et al., 1985; Kent and Gradstein, 1985).

For Hole 752A, a simple comparison of the GRTS to the polarity stratigraphy, combined with the early Eocene to Paleocene biostratigraphic age of the cores (113-303.5 mbsf), immediately suggests that the two long reversed intervals (123-155.5 and 232-303.5 mbsf) are C24R and C26R, respectively. This identification is confirmed by a detailed comparison of the magnetostratigraphy with calcareous nannofossil first-appearance datums (FAD). The FAD of *Discoaster lodoensis* at 114.3 mbsf requires the reversed interval at the top of the Unit II (113-118.5 mbsf) to be no older than C24N-1. We think, in fact, that it is the lower part of C23R. The FAD of *Tribrachiatus bramlettei* at 171.1 mbsf indicates that the long reversed interval between 155.5 and 201 mbsf must be C24R. Thus, the two overlying normal intervals (123-155.5 mbsf) must be C24N-1 and C24N-2. The relative lengths of the two intervals and the occurrence of a short reversed interval between them are consistent with the

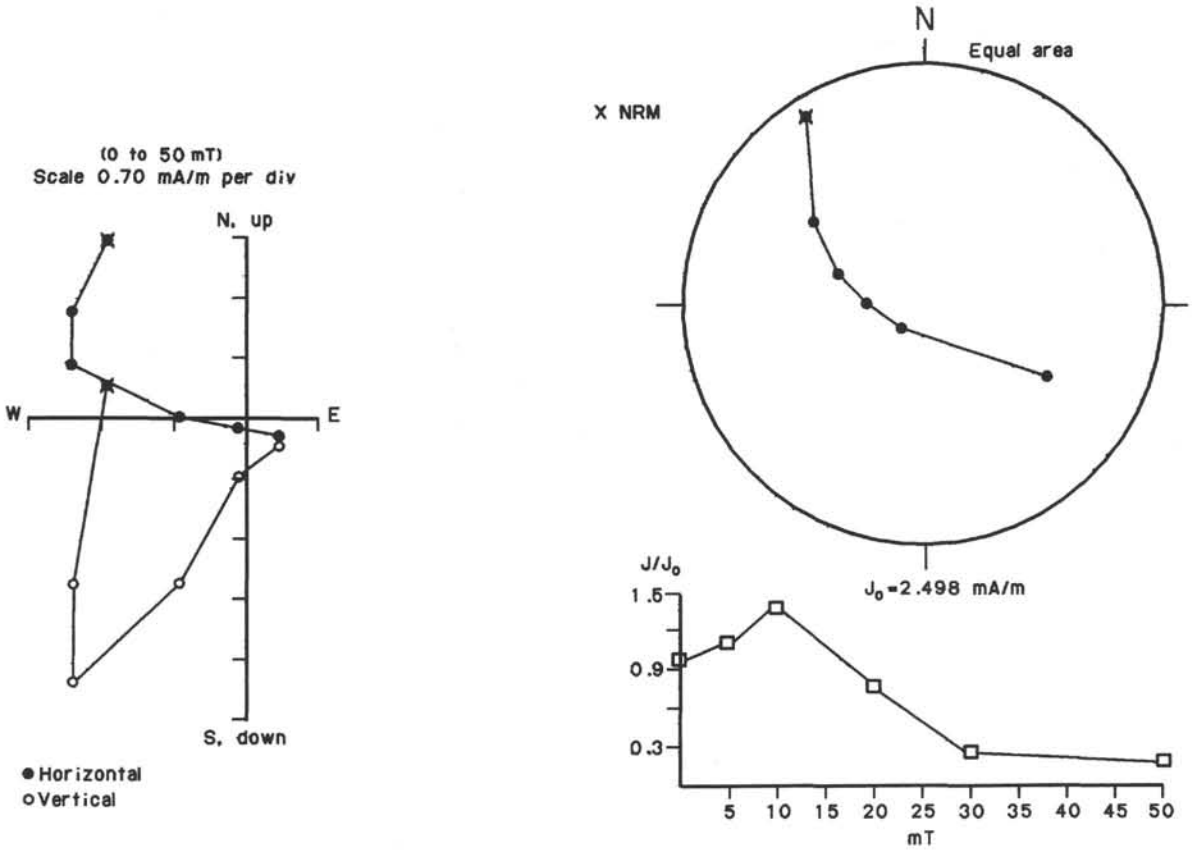

Figure 14. Typical Zijderveld plot of data from lithologic Unit II in Hole 752A showing removal of a normal overprint (Sample 121-752A-33X-1, 137 cm). Failure to converge on the origin is probably due to a y-axis anhysteretic remanent magnetization (ARM).

Berggren et al. (1985) magnetostratigraphy. The boundary between C24N and C23R was not recovered and is hence placed arbitrarily at the midpoint (120 mbsf).

Spot cores that include C24 were taken in Hole 752B to test the possible occurrence of an additional normal interval within the reversed zone. Whole-core data, coupled with discrete sample measurements, suggest that such a zone may be present (Fig. 18). The presence of a normal interval within this reversed zone has been suggested by studies based on magnetic anomalies in the Indian Ocean (Geller et al., 1983), although Liu et al. (1983) did not find an additional normal interval necessary. However, the normal interval we have identified in the core falls very close to the end of the reversed zone—instead of in the middle—and it appears to be much shorter than required by anomaly models. If the normal interval is not an artifact, then either sedimentation has not been constant during this time interval or the normal interval is not the same as that identified by anomaly modeling. We plan to measure the same depth interval in Hole 752A to attempt to determine whether the normal interval is real.

The identification of the next normal interval (201-211.5 mbsf) with C25N is confirmed by the FAD of *Discoaster multiradiatus*, which Berggren et al. (1985) located at the base of C24R and top of C25N. The FADs of *Heliolithus kleinpellii* at 251.4 mbsf and *Fasciculithus tympaniformis* at 297.7 mbsf constrain the long reversed zone at the bottom of Unit II (232-303.5 mbsf) to be C26R. The FAD of *Heliolithus riedelii* (219.5 mbsf) occurs within C25R, consistent with the Berggren et al. (1985) time scale.

The overlap between Holes 752A and 752B is accurately determined from both drilling data and comparison of susceptibility values. This allows us to assign the reversed interval at the top of Hole 752B (297-308 mbsf) to C26R. The occurrence of the Cretaceous/Tertiary boundary at 359 mbsf, within C29R (355-360 mbsf), provides a further constraint on our comparison to the GRTS (Berggren et al., 1985; Lowrie et al., 1982). The details of the sediment magnetization in the vicinity of this boundary are discussed in the "Paleomagnetics" section of the "Cretaceous/Tertiary Boundary Summary" chapter. The assignment of C27 (308-312 mbsf) and C27R (312-335.5 mbsf) follows directly from their position relative to C26R and the fact that their lengths agree reasonably well with the GRTS. These choices are in general agreement with the FAD of *Prinsius martinii* or *Neochiastozygus saepes* at 318.7 mbsf, which Berggren et al. (1985) placed within C27R to C28N. Because C29R is constrained to lie across the Cretaceous/Tertiary boundary, C28N and C28R (340-346.5 mbsf) and C29N (346.5-355 mbsf) must lie between the top of C29R and the lowest observation of C27R. Biostratigraphic and sedimentological data suggest a decrease in the sedimentation rate above the Cretaceous/Tertiary boundary in the lowest Paleocene, which is consistent with the placement of both chronozones within this interval, but the large unrecovered section makes an accurate determination of their boundaries impossible. The FADs of *Chiasmolithus danicus* at 345.1 mbsf, *Cruciplacolithus tenuis* at 353.5, and *Biantholithus sparsus* at 358.5 mbsf are generally consistent with this interpretation.

The long normal interval below C29R (364.5-387.5 mbsf) appears to be C30N, based on its position immediately below C29R and comparison of the lengths of the intervals with the GRTS. We must have an additional short reversed zone within C30N (385-386 mbsf) or a short normal zone in C30R. As the GRTS calls for a very short C30R, we have placed the bottom of C30N below the short normal interval at 387.5 mbsf. We have

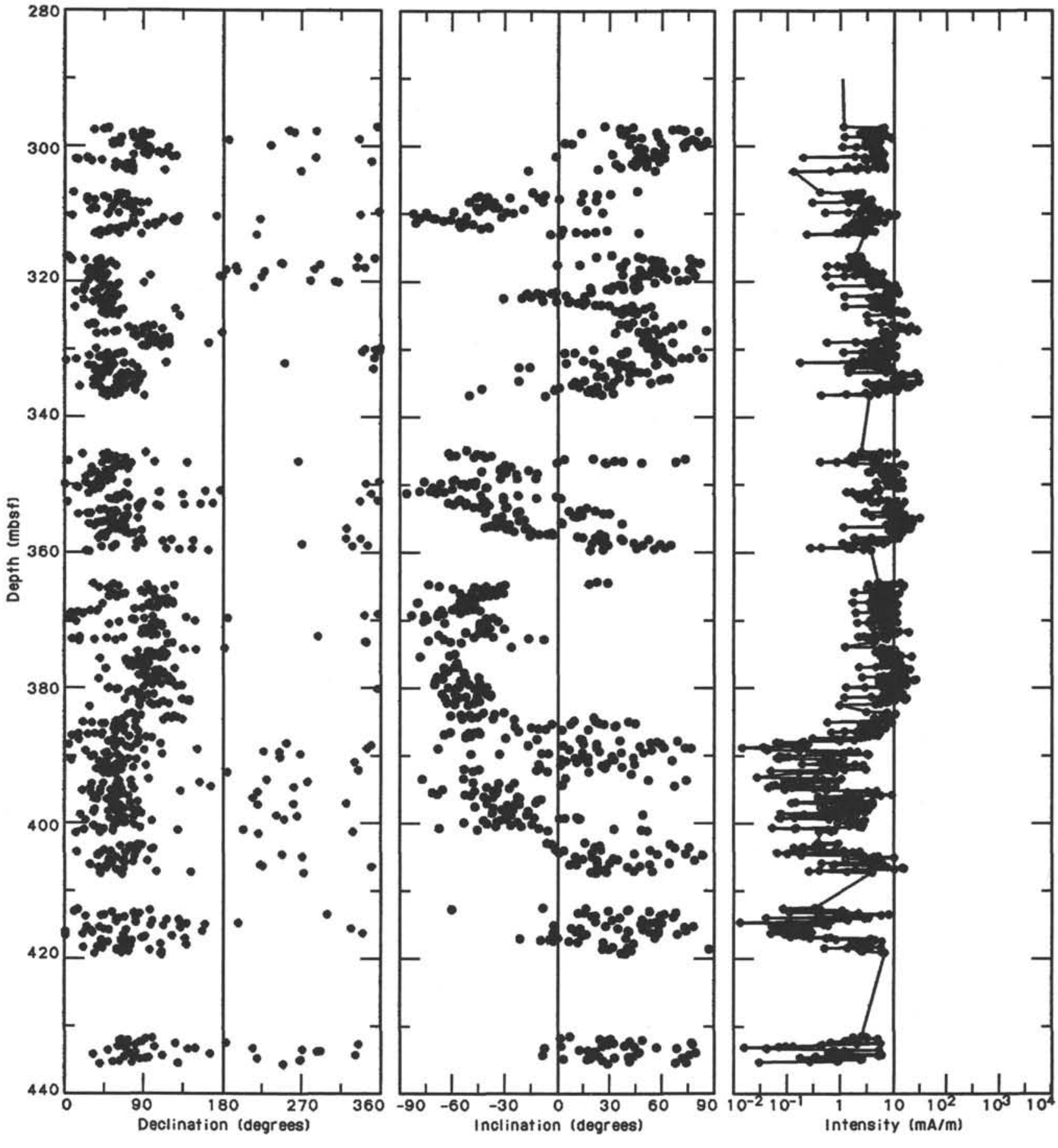

Figure 15. Hole 752B remanence data after 9-mT demagnetization.

assigned the normal interval from 393 to 398 mbsf to C31N, based largely on its position below C30R. This implies some sedimentation rate changes, however, because C31N is much longer than C30R in the GRTS. The remainder of Hole 752B (398–435.5 mbsf) is assigned to C31R because all of the recovered sections are reversely magnetized. Poor recovery makes this assignment somewhat tentative; there may be normally magnetized material that was not sampled. The FAD of *Nephrolithus frequens* within this zone disagrees with Berggren et al. (1985). However, J. Pospichal (pers. comm., 1988) suggests that at high latitudes the first occurrence of this species may in fact be within C31R. Because the datum clearly falls within a reversed interval, we favor this interpretation. The bottom of the hole overlaps with the upper part of the Maestrichtian section cored in Hole 754B. A discussion of the correlation between the two holes can be found in the "Paleomagnetics" section, "Site 754" chapter.

Sedimentation Rates

The identification of reversal boundaries, which are essentially instants in time, allows sedimentation rates to be estimated on a fairly short time scale. The accuracy of these estimates is limited primarily by the accuracy with which the reversal boundaries can be located. In some cases, they can be located to within

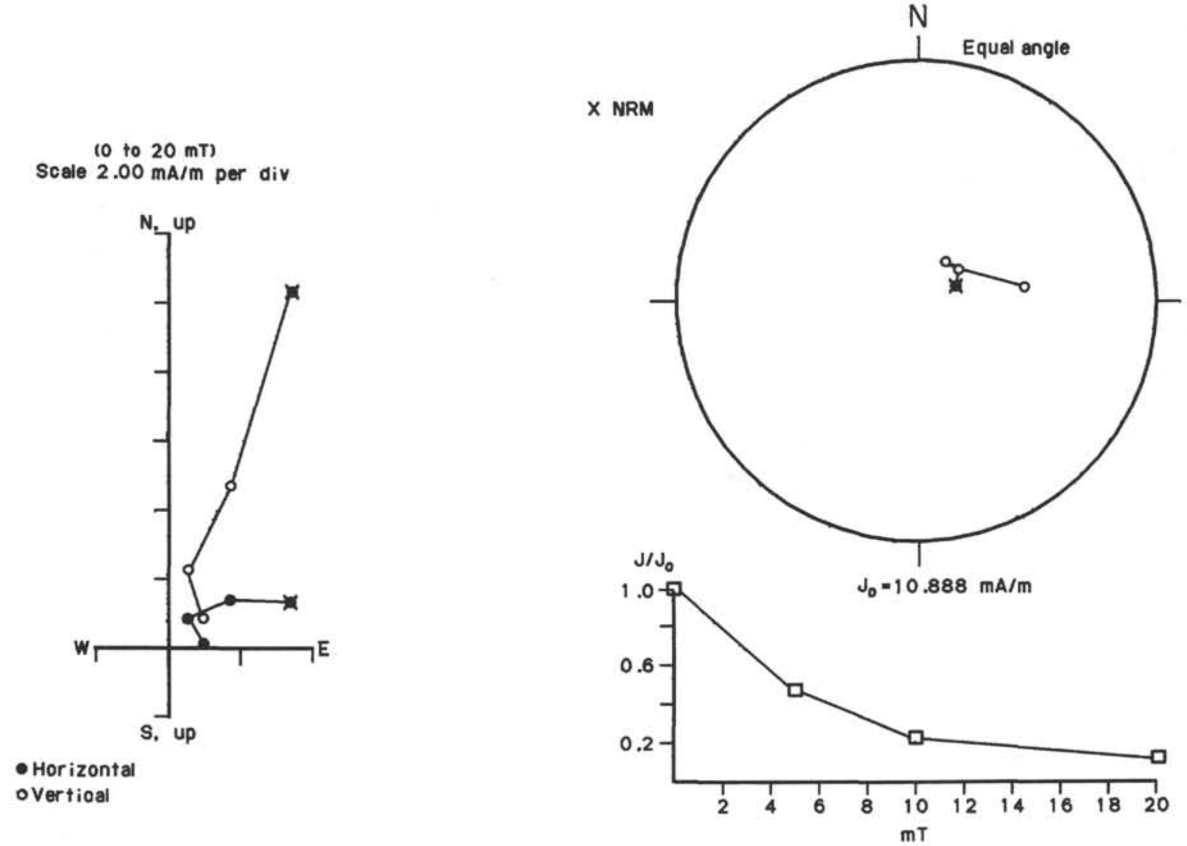

Figure 16. Typical Zijderveld plot of data from lithologic Unit II in Hole 752B (Sample 121-752B-12R-2, 25 cm). Failure to converge on the origin is probably due to a y-axis anhysteretic remanent magnetization.

a few centimeters. In other cores, especially where the boundary was not recovered, uncertainties may reach several meters. The sedimentation rates, as determined from magnetostratigraphy, are given in Table 5. They range from 4.1 to 50 m/m.y., with an average of about 19 m/m.y.

INORGANIC GEOCHEMISTRY

Objectives

A major objective of the chemical measurements on Leg 121 is to determine how uniform chemical gradients in the pore fluids are in a horizontal sense. Traditionally, DSDP and ODP sites have been drilled great distances from one another, or if drilled close together, chemical measurements were made on only one hole. On DSDP Legs 69, 70, and 83, a series of holes were drilled near the Costa Rica Rift in close proximity—only hundreds of meters apart. The chemical gradients showed large differences from hole to hole. These differences, primarily changes in the calcium ion concentration and $^{18}O/^{16}O$ ratios (Mottl et al., 1983), were attributed to alteration in the basaltic basement. The question is whether these spatial changes are limited to environments like the Costa Rica Rift Zone where the sediment cover is currently sealing the oceanic crust. In such an environment, advection of pore waters through the sediments is still occurring. Gradients are absent where advection of fluid through the sediments is rapid and present where no or very low rates of advection occur.

On Leg 121 two different areas of oceanic crust were drilled, Broken Ridge and Ninetyeast Ridge. On Broken Ridge, four sites were drilled on a 20-km-long north-south line perpendicular to the strike of the ridge. Thin Neogene sediments overlie an angular unconformity of Late Cretaceous to early Tertiary age. The sediments underneath are more lithified than the overlying Neogene sediments, with induration increasing to the south as older sediments are recovered.

Because of the differences in stratigraphy, tectonics, and topography, differences in chemical gradients from site to site may occur. On Broken Ridge, the underlying lithologies differ and the degree of induration also varies. Because the chemical signatures in the pore waters, particularly the calcium ion and oxygen isotope signatures, are the result of the alteration of volcanic material (Lawrence and Gieskes, 1981), a variation in the percentage of volcanic material from one site to another in the underlying tilted sediments could change the intensity of the pore-water chemical signatures. Furthermore, differences in the degree of induration of the underlying sediments could influence the chemical signature coming from the deeper basaltic basement. In summary, chemical and isotopic measurements of pore fluids help to define patterns of alteration and water transport in the oceanic crust, which, in turn, aids in defining the physical and thermal structure of the oceanic crust.

Discussion of Results

There are three major groups of chemical changes in deep-sea pore waters (Gieskes, 1975, 1983). The changes in calcium and magnesium ions are usually related to the alteration of volcanic material in the sediments or in basaltic basement below. The changes in sulfate, alkalinity, and ammonia are related to sulfate reduction and oxidation of organic material by bacteria in the sediments. The changes in silica and strontium ion concentration are related to the diagenesis of biogenic silica and carbonate, respectively.

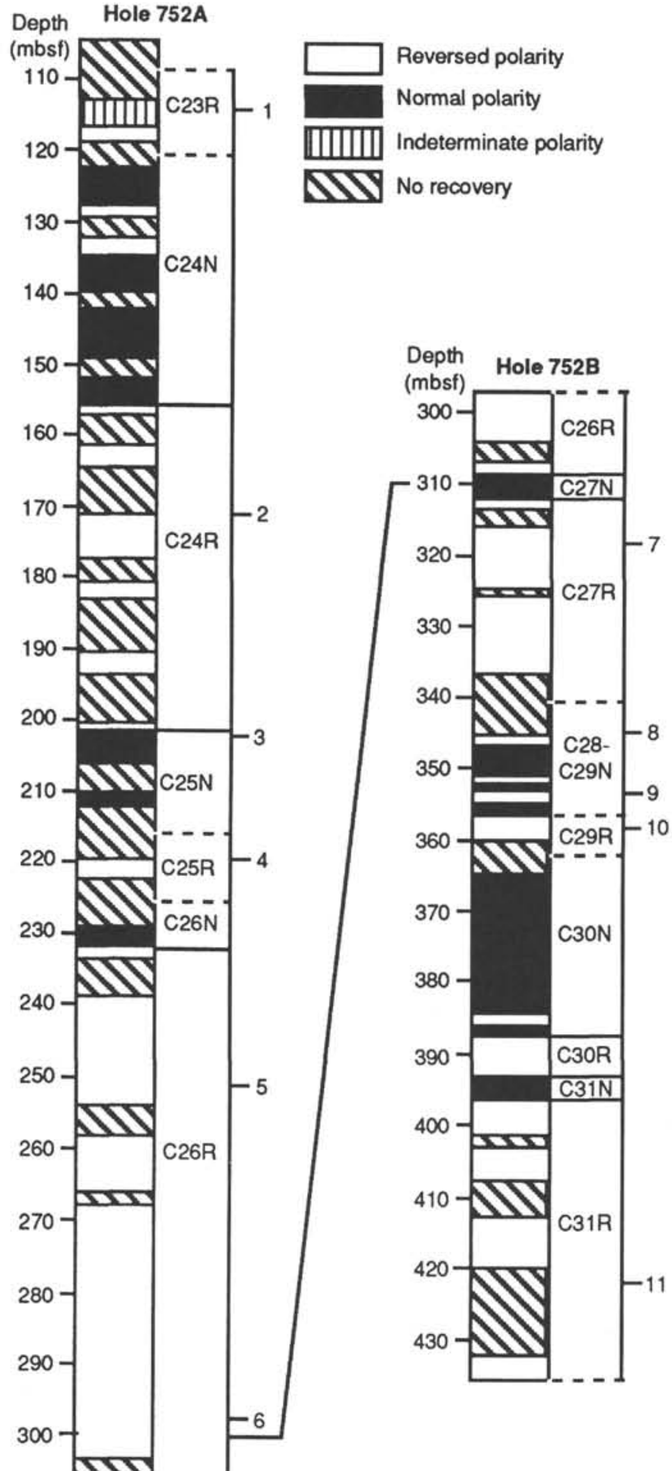

Figure 17. Site 752 remanence data for lithologic Unit II. Interpretation in terms of the GRTS is given to the right of the polarity zones. Dashed lines indicated boundaries inferred to occur within an unrecovered zone. Numbered tick marks to the right of the interpretation indicate nannofossil first-appearance datums: 1 = *Discoaster lodoensis*, 2 = *Tribrachiatus bramlettei*, 3 = *Discoaster multiradiatus*, 4 = *Heliolithus riedelii*, 5 = *Heliolithus kleinpellii*, 6 = *Fasciculithus tympaniformus*, 7 = *Prinsius martinii* or *Neochiastozygus saepes*, 8 = *Chiasmolithus danicus*, 9 = *Cruciplacolithus tenuis*, 10 = *Biantholithus sparsus*, 11 = *Nephrolithus frequens*.

Results of the interstitial-water chemical analyses are listed in Table 6. Plots of calcium and magnesium ion concentrations are shown in Figure 19. The increase in calcium and the decrease in magnesium with depth at Site 752 are moderately high for deep-sea sediment pore waters (see Lawrence and Gieskes, 1981). These changes reflect the alteration of volcanic material in the sediments and possibly basaltic basement below. Ash occurs at this site at depths ranging from 90 mbsf to the bottom of the hole at 436 mbsf (see "Lithostratigraphy and Sedimentology" section, this chapter). The bulk sediments are composed mostly of carbonate, but the noncarbonate fraction is composed mostly of fine-grained smectitic clay (see Fig. 20 and Table 7) and volcanic ash, from which the clay was probably derived. The noncarbonate fraction of the sediment in the interval from 120 to 300 mbsf averages 25% ± 12% for 68 samples (see "Organic Geochemistry" section, this chapter). Overall, it would appear that alteration of ash in the sediments is the major factor causing the observed changes in the calcium and magnesium gradients in the pore waters. Quantitative estimates of the amount of alteration of volcanic material (see Lawrence and Gieskes, 1981) at this site await oxygen isotope measurements of pore waters on shore. The marked increase in the calcium ion concentration and decrease in magnesium ion concentration in the interval from 260 to 300 mbsf probably reflect a decrease in the permeability of the sediments (see "Lithostratigraphy and Sedimentology" section).

The chemical analyses of sulfate ion concentration and alkalinity do not show any evidence of a significant degree of sulfate reduction and oxidation of organic matter at Site 752 (Fig. 19). Sulfate changes little with depth, and alkalinity does not show the characteristic increase followed by a decrease with depth over the first few hundred meters. The decrease in alkalinity with depth probably reflects supersaturation with respect to calcium carbonate. (Note that the calcium ion concentrations increase with depth; Fig. 19.) The step in the chemical values at 150 mbsf is a result of the misassignment of the correct depth to Core 121-752B-4W. The sediments from this core are probably from a greater depth.

ORGANIC GEOCHEMISTRY

Methods

At Site 752, measurements of (1) hydrocarbon gases, (2) total carbon and carbonate carbon, and (3) hydrogen and oxygen in organic matter were performed. Details of the methods used are described in the "Explanatory Notes" chapter.

Amounts of hydrocarbon gases were determined on headspace samples. Samples (5 cm^3) were taken from every third core, usually at the top of Section 5, immediately after cutting the core into sections and before it was contaminated by acetone. Samples were closed gas-tight and kept for 1-3 hr in an oven at 60°C. Concentrations of methane, ethane, and propane were analyzed on a Carle AGC Series 1000 gas chromatograph.

Carbonate carbon measurements were performed on physical-property samples, on selected interstitial-water samples, and on samples taken specifically for organic geochemical analyses. The latter samples are from Section 4 of each core, between 50 and 51 cm. If Section 4 was not available, the same interval from one of the first three sections was sampled. Total carbon was additionally measured on the organic geochemistry samples. Both carbonate carbon and organic carbon were analyzed by a coulometric method.

The amount of hydrogen and oxygen in the organic matter was indirectly determined using a Rock-Eval III instrument. At Site 752, only the few samples in which organic carbon values exceed 0.3% were selected for Rock-Eval pyrolysis.

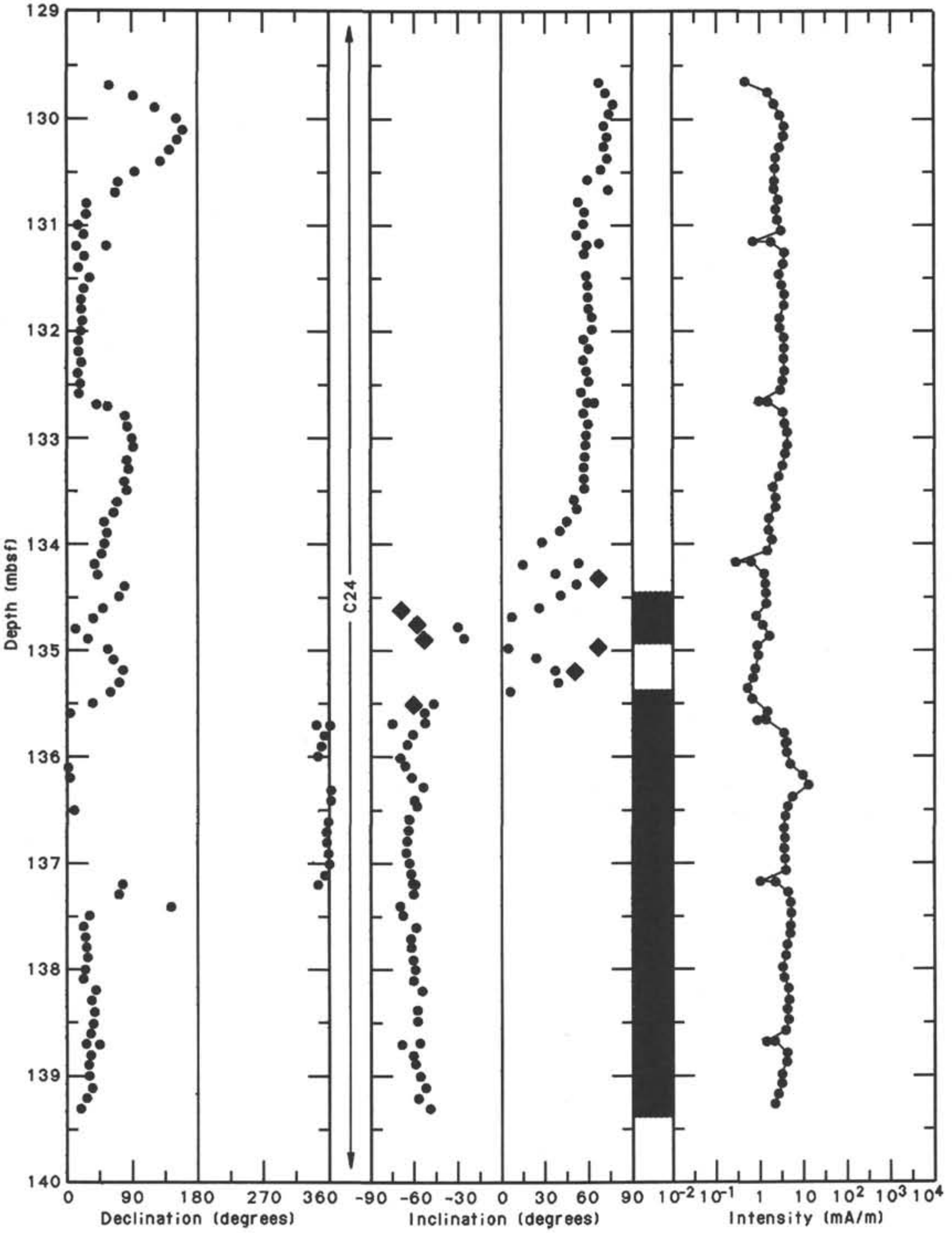

Figure 18. Remanence data from Core 121-752B-3R after 9-mT demagnetization. Diamonds indicate discrete sample data. The reversed interval at the top of the core is between the two normal intervals of C24, and the normal interval at the bottom of the core is the lower of the two normal intervals in C24. The short normal interval above 135 mbsf has not been previously described.

Hydrocarbon Gases

The headspace gases contained no measurable ethane and propane. Methane concentrations did not exceed 50 ppm and were usually between 10 and 20 ppm (Table 8 and Fig. 21). These values are equivalent to concentrations of about 30–60 μL methane/L rock. They are low in comparison to values of other sediments and indicate that very little thermal gas was generated in the sediments or migrated into the pore space from external sources.

Organic Carbon Content and Character

Total amounts of organic carbon (C_{org}) were obtained from the equation

$$C_{org} = TC - CC,$$

where TC is total carbon and CC is carbonate carbon. In the cored sequence at Site 752, organic carbon contents are low (Table 9 and Fig. 22), which is typical for open-ocean sedimenta-

Table 5. Sedimentation rates inferred from magnetostratigraphy, Site 752.

Anomaly[a]	Depth[b] (mbsf)	Age range[c] (Ma)	Sedimentation rate (m/m.y.)
C24N-2	135-157	55.66-56.14	46
C24R	157-201	56.14-58.64	17.5
C25N	201-(212-218)	58.64-59.24	18.5-28.5
C25R	(212-218)-(222-229)	59.24-60.21	4-11.5
C26N	(222-229)-233	60.21-60.75	7.5-20.5
C26R	233-308	60.75-63.03	11
C27N	308-312	63.03-63.54	8
C27R	312-(336-349)	63.54-64.29	32-49.5
C29R	355-(360-364)	66.17-66.74	9-16
C30N	(360-364)-388	66.74-68.42	14.5-16.5
C30R	388-393	68.42-68.52	50
C31N	393-398	68.52-69.40	5.5

[a] Intervals that could not be reasonably well located are omitted (C28N, C28R, and C29N).
[b] Parentheses denote the possible depth ranges for boundaries located in unrecovered parts of the cores.
[c] Dates from Berggren et al. (1985).

tion. The upper Eocene, Oligocene, and Neogene sediments have, on average, slightly higher amounts of organic carbon than the sediments drilled between 120 and 180 mbsf (lower Eocene to upper Paleocene). The remaining Paleocene rocks consistently contain 0.3% organic carbon. Sediments drilled in Hole 752B above and below the Cretaceous/Tertiary boundary (358 mbsf) are practically free of organic matter, as are the upper Maestrichtian rocks at Site 754.

The hydrocarbon generation potential of all sampled sediments is poor, as revealed by the low S2 and hydrogen index values documented in Table 10 and Figure 23. The hydrogen-poor character of the organic matter points toward deposition of terrestrial, instead of marine, organic matter. The latter can only be preserved under favorable conditions, for example, in stagnant basins with anoxic bottom waters. At Broken Ridge, the organic part of the biomass was almost completely destroyed prior to deposition and burial.

Carbonate Carbon Content

The Pleistocene to Paleocene sequence at Site 752 on Broken Ridge is rich in carbonate. The original carbonate carbon values are here transferred into calcium carbonate (calcite) percentages ($CaCO_3$ = CC × 8.33) and plotted vs. depth in Figure 22. There is an obvious change in the chemical composition of the sediments between 90 and 100 mbsf (i.e., near the hiatus between the Oligocene and Eocene). All of the overlying Neogene sediments contain more than 90% calcite, whereas values in the underlying strata vary between 30% and 90%. Low carbonate percentages of about 60% were found in the brown sands and gravels at 100 mbsf. The wide variation of calcite contents in the lower Eocene and Paleocene section is due to the mixing of marine fossils and volcanic ash. The average content of volcanic ash decreases by about 20% from the lower Paleocene to the lower Eocene.

PHYSICAL PROPERTIES

The sediments cored at Site 752 consist of a Pleistocene to upper Oligocene cap composed primarily of carbonate ooze. Two hiatuses, represented by limestone pebble layers at about 94 and 104–113 mbsf, separate Oligocene from upper Eocene ooze and upper Eocene ooze from lower Eocene to upper Maestrichtian chalk, respectively. An interval marked by the appearance of biogenic silica occurs in lithologic Subunit IIB, from 209.8 to 288.7 mbsf (see "Lithostratigraphy and Sedimentology" section). Porcellanite, chert, and ash constitute minor lithologies in the lower Eocene to Paleocene section, and ash is increasingly predominant downhole in the Maestrichtian section.

Hole 752A was cored with the APC and XCB systems to 308 mbsf, and Hole 752B was rotary cored to 434.6 mbsf. Although the first two coring modes induce much less sedimentary disturbance than rotary coring, the coring effects on sediments, particularly carbonate oozes, can be significant in terms of the physical properties (Walton et al., 1983). Samples were selected from sections with minimum disturbance, generally avoiding the first section in the cores. The objectives of the physical-properties measurements were to study the consolidation of this

Table 6. Site 752 interstitial-water geochemistry data.

Core, section, interval (cm)	Depth (mbsf)	Volume (mL)	pH	Alkalinity (mmol/L)	Salinity (g/kg)	Magnesium (mmol/L)	Calcium (mmol/L)	Chloride (mmol/L)	Sulfate (mmol/L)	Mg^{2+}/Ca^{2+}
121-752A-										
1H-4, 145-150	5.95	27	7.70	2.670	35.0	53.00	10.70	559.00	29.60	4.95
3H-4, 120-125	23.50	32	7.70	2.700	36.0	53.40	11.80	584.00	29.90	4.53
5H-1, 0-1	36.80	14	7.90	2.340	36.2	51.40	13.20	569.00	30.40	3.89
6H-4, 145-150	52.35	30	7.50	2.380	35.5	49.10	14.40	542.00	28.10	3.41
9H-1, 0-1	75.40	12	8.10	2.260	36.5	48.60	16.20	571.00	32.10	3.00
9H-4, 145-150	81.35	32	7.50	2.340	36.0	47.30	16.40	574.00	29.10	2.88
10H-4, 148-150	90.98	5			36.2	46.70	17.20	559.00	29.60	2.72
11H-4, 148-150	100.68	7			36.0	45.80	17.60	569.00	30.00	2.60
13X-3, 145-150	117.35	25	7.50	2.110	36.0	44.30	18.30	571.00	28.50	2.42
14X-3, 148-150	127.08	3			35.0	43.20	18.60	541.00	29.30	2.32
15X-3, 0-1	135.30	1				44.30	18.60			2.38
16X-3, 140-150	146.40	27	7.60	1.630	36.0	43.60	20.40	563.00	27.80	2.14
19X-3, 140-150	175.50	39	8.00	0.730	36.2	39.70	22.80	576.00	28.50	1.74
22X-3, 140-150	204.50	30	7.80	0.920	36.2	35.60	27.40	576.00	28.70	1.30
25X-2, 140-150	232.00	25	7.70	0.840	36.0	32.80	30.60	562.00	28.40	1.07
28X-2, 139-142	260.99	3			36.0			570.00	27.80	
28X-3, 140-150	262.50	6			36.0	32.30	31.40	570.00	28.40	1.03
31X-4, 140-150	285.30	28	7.70	0.770	36.2	29.10	34.80	588.00	28.10	0.84
32X-5, 142-144	296.12	2				26.60	37.30			0.71
121-752B-										
2R-1, 140-150	121.40	15	7.60	1.740	36.0	43.30	18.50	563.00	27.60	2.34
4W-1, 140-150	145.40	25	7.60	1.330	36.5	42.90	18.80	563.00	27.00	2.28
5R-3, 140-150	301.40	15	8.00	0.840	36.5	25.90	36.50	570.00	25.10	0.71

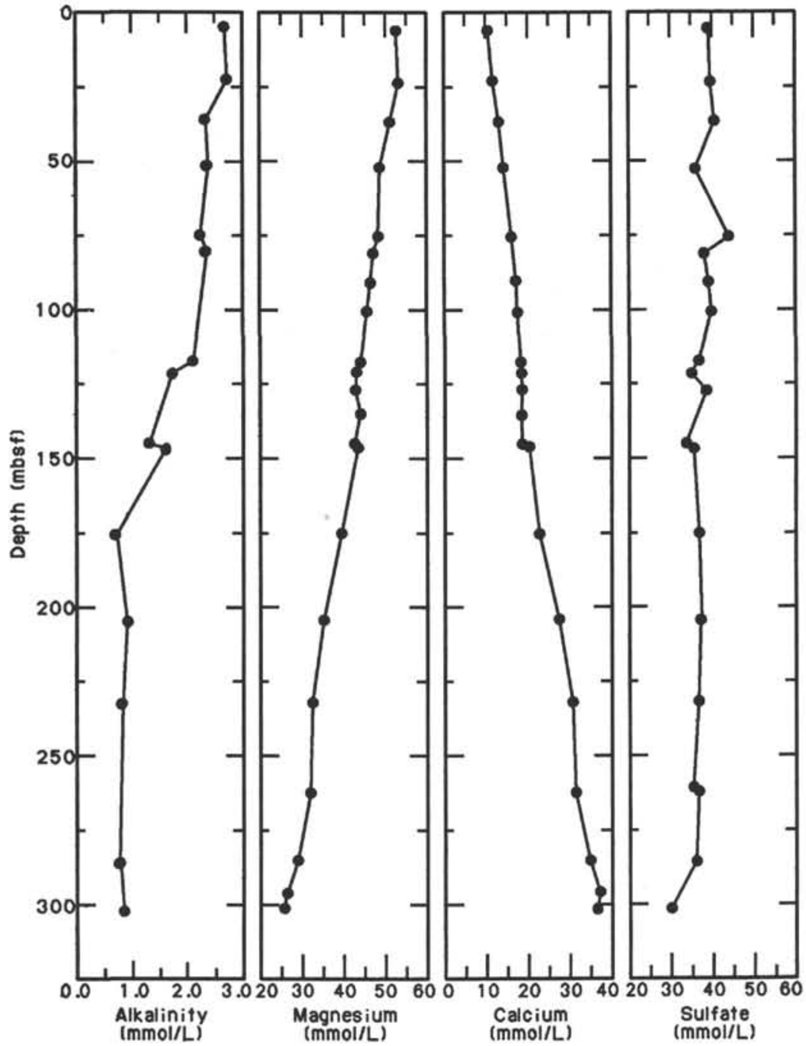

Figure 19. Interstitial-water alkalinity, magnesium, calcium, and sulfate profiles, Site 752.

calcareous section, to provide ties between cored lithologies and seismic survey reflection profiles, and to relate these properties to the regional geologic history.

Methods

The physical properties recorded for the Site 752 sediments are index properties using the pycnometer and balance and GRAPE, compressional-wave velocity using the *P*-wave logger and Hamilton Frame, vane shear strength, formation factor, and thermal conductivity. These methods are described in the "Explanatory Notes" chapter.

Results

Index Properties

Porosity, bulk density, water content (expressed as water weight relative to wet sample weight), grain (or matrix) density, and dry-bulk density of the Site 752 sediments are listed in Table 11 and plotted relative to depth in Figure 24. Three physical-properties units characterize the cored section. Unit A, from 0 to 112.9 mbsf, corresponds to lithologic Unit I. Within this unit, index properties exhibit little variation. Water contents are nearly constant at 40% below the upper 5 m of the section. Monotonic values for bulk density, porosity, grain density, and dry-bulk density characterize physical-properties unit A. The exception to this trend is a zone between 63 and 83 mbsf (lower Miocene), in which bulk densities increase to between 1.7 and 1.9 g/cm^3, possibly in relation to a sand-rich zone at this level. Because of procedural errors in the laboratory, dry weight/volume relationships are not available for the 63–103 mbsf interval.

Physical-properties unit B (112.9–295 mbsf) extends from the upper Eocene to lower Eocene hiatus, which was poorly recovered in Core 121-752A-12X, to slightly deeper than the base of lithologic Subunit IIB. This unit is marked by a shift to higher bulk densities and corresponding lower porosities, reflecting the lithologic shift from calcareous oozes to chalks. Sediments in unit B have a bulk density near 1.8 g/cm^3 and a porosity and water content of about 50% and 30%, respectively. A subtle decrease in bulk and grain densities, with corresponding increases of porosity and water content, occurs at 175 mbsf. An ash-rich zone at this depth may account for these changes. Water contents exhibit a sharp shift from 15%–20% above 220 mbsf to >40% at 221 mbsf, marking the boundary between physical-properties subunits B1 and B2. This abrupt shift corresponds to the presence of biogenic silica in the calcareous sediments. The effect of silica is also noted in other index properties, including a slight decrease in grain density to values near 2.50 g/cm^3.

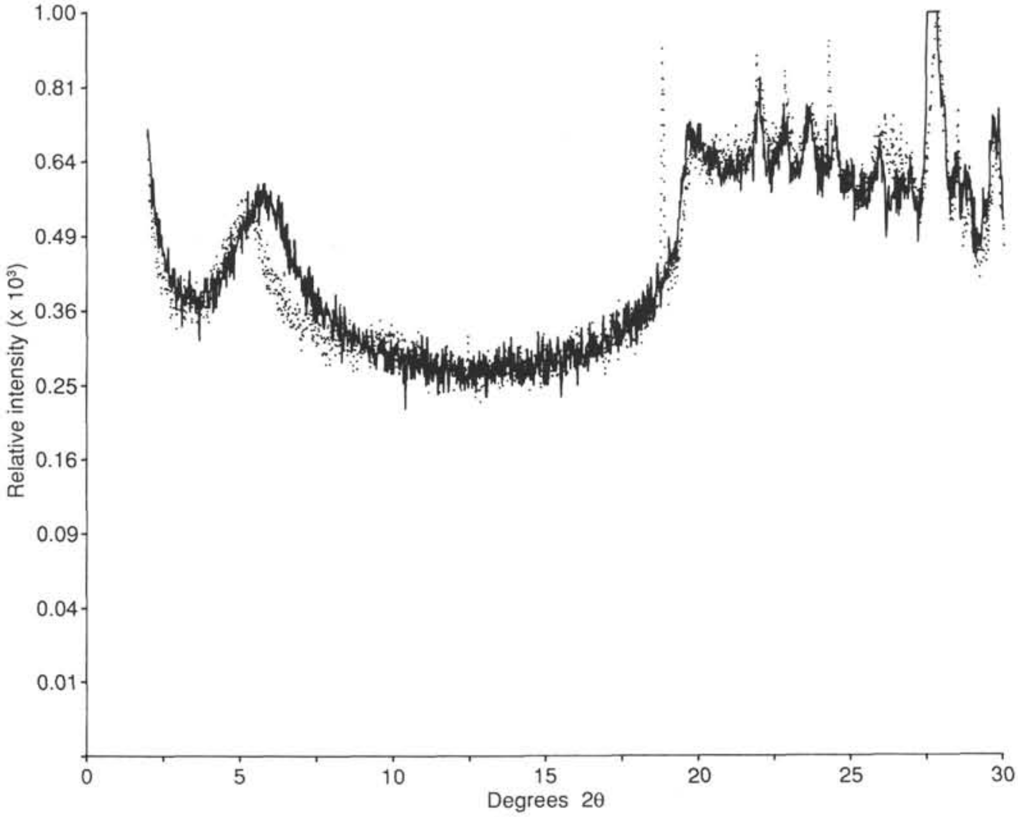

Figure 20. X-ray-diffraction patterns of acid-treated carbonate-free sediments from Sample 121-752A-15X-3, 0-1 cm. The dotted pattern was made after glycolation.

Table 7. Site 752 X-ray-diffraction patterns.

Core, section interval (cm)	Shipboard database file number	Minerals identified
121-752A-		
13X-3, 145-150	038UBN.RD	Smectite, feldspar
	072UBG.RD	(carbonate removed by 1N HCl)
14X-3, 148-150	037UBN.RD	Smectite, feldspar
	071UBG.RD	(carbonate removed by 1N HCl)
15X-3, 0-1	036UBN.RD	Smectite, plagioclase
	070UBG.RD	(carbonate removed by 1N HCl)
16X-3, 140-150	032UBN.RD	Smectite
	066UBG.RD	(carbonate removed by 1N HCl)
19X-3, 140-150	034UBN.RD	Smectite, feldspar, calcite
	068UBG.RD	(carbonate removed by 1N HCl)
22X-3, 140-150	039UBN.RD	Smectite, calcite
	073UBG.RD	(carbonate removed by 1N HCl)
25X-2, 140-150	033UBN.RD	Smectite, plagioclase
	074UBG.RD	(carbonate removed by 1N HCl)
28X-2, 139-142	030UBN.RD	Smectite, plagioclase
	064UBG.RD	(carbonate removed by 1N HCl)
28X-3, 140-150	035UBN.RD	Smectite, plagioclase
	069UBG.RD	(carbonate removed by 1N HCl)
31X-4, 140-150	031UBN.RD	Smectite, plagioclase, quartz
	065UBG.RD	(carbonate removed by 1N HCl)
121-752B-		
7R-4, 100-102	009UBN.RD	Calcite, smectite, feldspar
	013UBG.RD	
8R-2, 124-126	011UBN.RD	Smectite, calcite, plagioclase
	062UBG.RD	Heulandite
8R-3, 148-150	012UBN.RD	Calcite, heulandite, unknown
	063UBG.RD	(peaks at 4.05-4.09 Å)
16R-3, 83-85	010UBN.RD	Smectite, calcite
	014UBG.RD	

Table 8. Methane (C_1) content in headspace gases of samples from Site 752. The ratio of headspace to sediments in the 20-μL glass cylinders is about 0.3. Thus, methane concentrations of 10 ppm are equivalent to 30-40 μL methane/L sediment. No ethane or propane was detected in the gases.

Core, section, interval (cm)	Depth (mbsf)	C_1 (ppm)
121-752A-		
3H-5, 0-1	23.80	25
6H-5, 0-1	52.40	5
9H-5, 0-1	81.40	11
13X-4, 0-1	117.40	4
15X-5, 0-1	138.30	9
16X-4, 0-1	146.50	45
19X-5, 0-1	176.82	10
22X-4, 0-1	204.60	9
25X-3, 0-1	232.10	11
28X-4, 0-1	262.60	34
29X-5, 149-150	275.19	5
30X-1, 149-150	278.89	7
31X-5, 0-1	285.40	9
31X-5, 143-144	286.83	6
121-752B-		
2R-1, 148-150	121.48	40
6R-4, 0-1	311.10	10
8R-6, 0-1	331.90	11
11R-2, 0-1	356.30	5
14R-4, 149-150	389.59	9
19R-2, 149-150	433.09	7

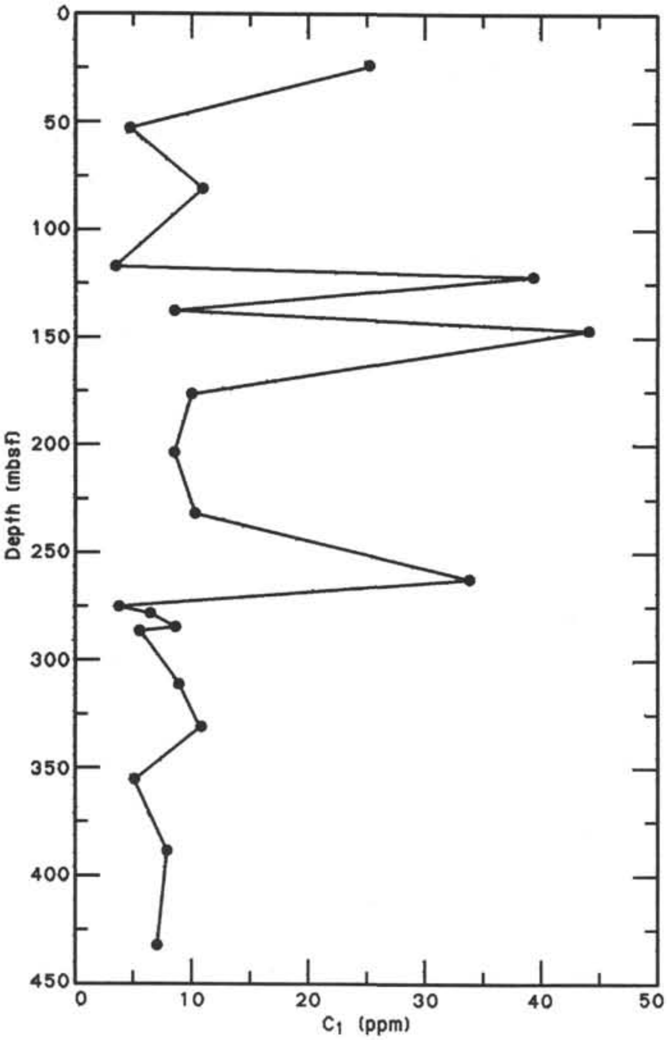

Figure 21. Methane concentrations in headspace gases from Site 752.

Below 295 mbsf, physical-properties unit C corresponds to the highly indurated chalks of lithologic Subunit IIC. The shift from bulk-density values of 1.8 g/cm^3 in the overlying unit B to 2 g/cm^3 and greater in unit C, along with water content and porosity changes, clearly marks a transition in the indurated character of these chalks. The chalks are easily distinguished by their physical-properties values. The wet- and dry-bulk densities exhibit a gradual increase with depth in unit C, from 2.0 to 2.4 g/cm^3 and 1.8 to 2.0 g/cm^3, respectively. Grain density also increases within this interval, possibly reflecting a subtle downhole compositional change.

Compressional-Wave Velocity

Velocity data collected from laboratory samples are listed in Table 12 and displayed in Figures 24 and 25. *P*-wave-logger velocities were the only measurements made of the soft oozes of lithologic Unit I, and they range from <1500 to 1600 m/s (Fig. 24). This slight velocity increase is sharply offset across the physical-properties units A/B boundary, below which velocities range from 1700 to 2200 m/s. A local, high-velocity layer between 200 and 215 mbsf corresponds to the base of lithologic Subunit IIA, immediately overlying siliceous Subunit IIB.

Physical-properties unit C is marked by a distinct velocity increase from 2000 to over 2500 m/s below 310 mbsf. Velocities in unit C also show a continuous increase to values near 3500 m/s at the base of Hole 752B. The samples from this lower unit were

Table 9. Percentages of total carbon, organic carbon, carbonate carbon, and calcium carbonate in samples from Site 752.

Core, section, interval (cm)	Depth (mbsf)	Total carbon (%)	Inorganic carbon (%)	Organic carbon (%)	Calcium carbonate (%)
121-752A-					
1H-1, 50–52	0.50		11.45		95.4
1H-3, 50–52	3.50		11.59		96.5
1H-4, 50–51	5.00	11.62	11.52	0.10	96.0
1H-5, 50–52	6.50		11.71		97.5
2H-2, 89–91	10.69		11.71		97.5
2H-4, 50–51	13.30	11.53	11.36	0.17	94.6
2H-4, 89–91	13.69		11.69		97.4
3H-2, 80–82	20.10		11.65		97.0
3H-4, 80–82	23.10		11.51		95.9
3H-5, 50–51	24.30	11.55	11.00	0.55	91.6
3H-6, 80–82	26.10		11.58		96.5
4H-2, 90–92	29.70		11.52		96.0
4H-4, 50–51	32.30	11.57	10.90	0.67	90.8
4H-4, 80–82	32.60		11.52		96.0
5H-2, 80–82	39.10		11.64		97.0
5H-4, 50–51	41.80	11.53	11.38	0.15	94.8
5H-4, 80–82	42.10		11.65		97.0
5H-6, 80–82	45.10		11.62		96.8
6H-2, 90–92	48.80		11.53		96.0
6H-4, 50–51	51.40	11.65	11.53	0.12	96.0
6H-5, 90–92	53.30		11.63		96.9
7H-2, 90–92	58.50		11.54		96.1
7H-4, 50–51	61.10	12.20	11.41	0.79	95.1
7H-4, 80–82	61.40		11.43		95.2
7H-6, 80–82	64.40		11.52		96.0
8H-2, 80–82	68.10		11.60		96.6
8H-4, 50–51	70.80	11.46	11.36	0.10	94.6
8H-6, 80–82	74.10		11.37		94.7
9H-2, 80–82	77.70		11.51		95.9
9H-4, 50–51	80.40	11.46	11.53	0.00	96.0
9H-4, 80–82	80.70		11.59		96.5
10H-2, 80–82	87.30		11.51		95.9
10H-4, 50–51	90.00	11.29	11.00	0.29	91.6
10H-4, 70–72	90.20		11.45		95.4
10H-6, 70–72	93.20		10.79		89.9
11H-2, 80–82	97.00		3.95		32.9
11H-4, 80–82	100.00		5.90		49.2
11H-4, 148–150	100.68	8.00	7.50	0.50	62.5
12X-1, 6–7	104.36	8.18	7.78	0.40	64.8
13X-2, 80–82	115.20		11.29		94.1
13X-4, 50–51	117.90	10.90	10.60	0.30	88.3
14X-2, 9–10	124.19	8.87	8.77	0.10	73.1
14X-2, 80–82	124.90		9.87		82.2
14X-3, 10–11	125.70	9.77	9.54	0.23	79.5
14X-4, 50–51	127.60	9.74	9.60	0.14	80.0
14X-4, 80–82	127.90		9.73		81.1
15X-2, 73–75	134.53		9.01		75.1
15X-4, 8–9	136.88	4.42	4.33	0.09	36.1
15X-4, 50–51	137.30	10.60	10.60	0.00	88.3
15X-4, 84–86	137.64		10.12		84.3
16X-2, 120–122	144.70		10.45		87.1
16X-4, 50–51	147.00	9.47	9.50	0.00	79.1
16X-4, 85–87	147.35		10.49		87.4
17X-1, 35–37	152.05		10.18		84.8
17X-3, 141–143	156.11		10.09		84.1
17X-4, 37–38	156.57	10.14	10.20	0.00	85.0
18X-1, 50–51	161.90	10.59	10.73	0.00	89.4
18X-1, 91–93	162.31		10.04		83.6
18X-CC, 19–21	163.97		10.06		83.8
19X-1, 60–62	171.70		8.62		71.8
19X-3, 63–65	174.73		4.66		38.8
19X-4, 42–43	176.02	8.70	8.69	0.01	72.4
19X-4, 60–62	176.20		7.50		62.5
20X-1, 50–51	181.20	10.04	9.60	0.44	80.0
20X-1, 60–62	181.30		9.69		80.7
21X-1, 50–51	190.90	10.05	10.04	0.01	83.6
21X-1, 81–83	191.21		10.46		87.1
21X-2, 57–59	192.47		7.69		64.1
22X-1, 90–92	201.00		10.67		88.9
22X-4, 40–42	205.00		10.17		84.7
22X-4, 50–51	205.10	9.64	9.49	0.15	79.1
23X-1, 80–81	210.60	9.71	9.34	0.37	77.8
23X-1, 91–92	210.71		9.65		80.4
23X-CC, 7–9	211.63		10.28		85.6
24X-1, 30–32	219.80		8.26		68.8

Table 9 (continued).

Core, section, interval (cm)	Depth (mbsf)	Total carbon (%)	Inorganic carbon (%)	Organic carbon (%)	Calcium carbonate (%)
121-752A- (Cont.)					
24X-1, 50-51	220.00	7.98	7.77	0.21	64.7
24X-2, 90-92	221.42		6.99		58.2
25X-1, 142-143	230.52		8.70		72.5
25X-2, 92-93	231.52		9.45		78.7
25X-3, 50-51	232.60	7.61	7.37	0.24	61.4
26X-2, 38-40	240.88		7.17		59.7
26X-4, 50-51	243.80	8.34	8.13	0.21	67.7
26X-4, 77-79	244.07		9.10		75.8
26X-6, 74-76	247.04		7.73		64.4
27X-1, 41-42	248.81		6.99		58.2
27X-2, 41-42	250.31		9.75		81.2
27X-4, 50-51	253.40	9.53	9.20	0.33	76.6
28X-3, 12-14	261.22		9.65		80.4
28X-4, 12-14	262.72		8.02		66.8
28X-4, 50-51	263.10	10.06	9.86	0.20	82.1
29X-2, 106-108	270.26		11.28		94.0
29X-4, 11-13	272.31		9.49		79.1
29X-4, 50-51	272.70	9.49	9.09	0.40	75.7
29X-6, 147-149	276.67		10.28		85.6
30X-1, 123-125	278.63		9.38		78.1
31X-2, 90-92	281.80		9.00		75.0
31X-4, 2-4	283.92		8.24		68.6
31X-4, 50-51	284.40	8.66	8.36	0.30	69.6
31X-6, 12-14	287.02		8.00		66.6
32X-2, 19-21	290.39		4.98		41.5
32X-3,105-107	292.75		8.44		70.3
32X-5, 50-51	295.20	6.55	6.33	0.22	52.7
32X-6, 78-80	296.98		9.11		75.9
33X-1, 94-96	299.34		9.41		78.4
33X-2, 37-39	300.27		9.38		78.1
33X-3, 94-96	302.34		5.97		49.7
33X-4, 19-21	303.09		9.13		76.1
121-752B-					
2R-1, 78-80	120.78	10.21	10.18	0.03	84.8
2R-2, 23-25	121.73	9.93	9.97	0.00	83.1
3R-2, 79-81	131.99		9.75		81.2
3R-4, 140-142	135.60	10.05	10.04	0.01	83.6
3R-6, 87-89	138.07		10.47		87.2
4W-2, 90-91	141.80		9.98		83.1
4W-4, 100-102	144.90	10.69	10.61	0.08	88.4
4W-6, 89-91	147.79		10.90		90.8
5R-2, 79-81	299.29	8.93	8.94	0.00	74.5
5R-4, 79-81	302.29	10.10	10.12	0.00	84.3
6R-2, 89-91	308.99		9.80		81.6
6R-4, 89-91	311.99	9.14	9.12	0.02	76.0
7R-2, 89-91	318.49	10.75	10.73	0.02	89.4
7R-4, 89-91	321.49	7.10	6.99	0.11	58.2
7R-6, 89-91	324.49		7.73		64.4
8R-2, 89-91	326.83		6.89		57.4
8R-4, 89-91	329.79	7.70	7.64	0.06	63.6
8R-6, 89-91	332.79		7.29		60.7
9R-1, 100-101	336.40	8.37	8.37	0.00	69.7
10R-2, 90-92	347.50		8.21		68.4
10R-4, 69-71	350.29	8.85	8.90	0.00	74.1
10R-6, 72-74	353.32	3.85	3.73	0.12	31.1
12R-3, 78-80	368.18	9.94	9.96	0.00	83.0
12R-6, 87-89	372.77		6.44		53.7
13R-1, 119-122	375.19	5.87	5.72	0.15	47.7
13R-3, 100-102	378.00		8.17		68.1
13R-5, 77-79	380.77	10.25	10.25	0.00	85.4
14R-1, 91-93	384.51		10.59		88.2
14R-3, 90-92	387.50	10.56	10.51	0.05	87.6
14R-5, 82-84	390.42		10.91		90.9
15R-2, 88-90	395.68		10.09		84.1
15R-4, 89-91	398.69	11.12	11.42	0.00	95.1
16R-2, 89-91	405.39	11.24	11.19	0.05	93.2
17R-2, 89-91	414.99		10.43		86.9
17R-4, 90-91	418.00	9.84	9.99	0.00	83.2
19R-2, 89-90	433.99	10.37	9.79	0.58	81.6

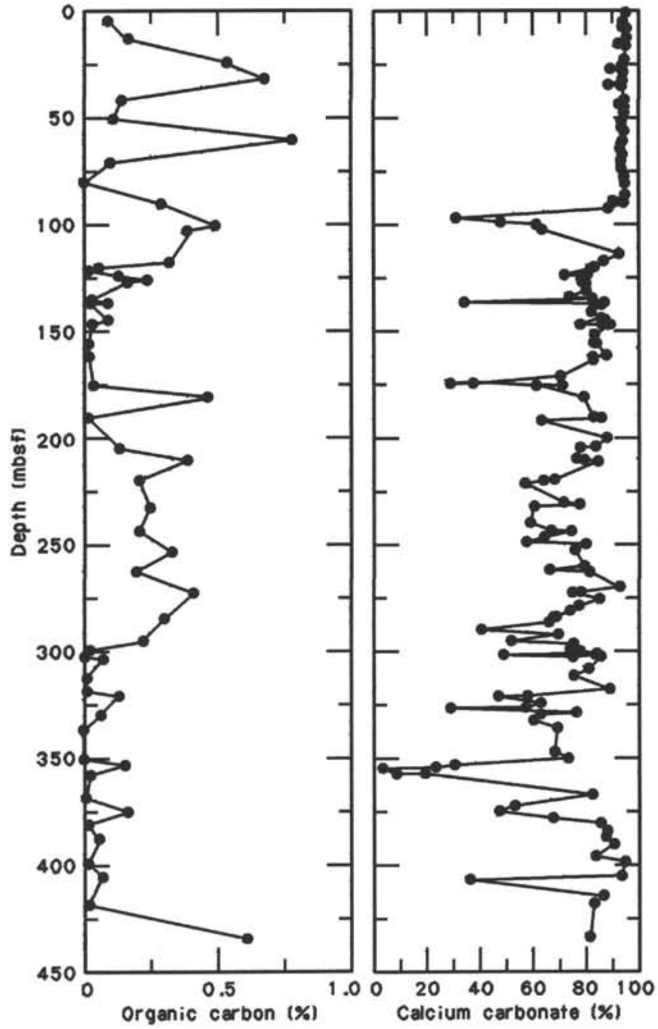

Figure 22. Organic carbon content and calcium carbonate content in samples from Site 752.

tested by propagating a compressional wave through three mutually perpendicular directions to obtain measures of velocity anisotropy (Table 13 and Fig. 25). Horizontal vs. vertical velocity anisotropy in this basal unit is calculated as

(average horizontal velocity − vertical velocity)/vertical velocity.

This anisotropy ranges from −2.2% to 19.7% in unit C, with an average of 8.3%. Velocities in the vertical direction are significantly lower than those measured horizontally, a fact that must be considered when comparing laboratory velocities to seismic-derived velocities. The sediments in this lower unit commonly have a laminated structure that is expected to enhance the anisotropy of physical characteristics.

The impedance log, computed from GRAPE and *P*-wave-logger data in the section recovered with the APC and from laboratory measurements in the remaining cores (below 104 mbsf), shows strong contrasts at 104–112, 200–220, 275–295, and 350–375 mbsf (Fig. 24). These impedance contrasts account for the sources of strong reflectors in the seismic record (see "Seismic Stratigraphy" section, this chapter). Most of these impedance contrasts are expressions of different degrees of lithification in the calcareous section. The contrast at 355 mbsf, however, represents a low-velocity zone associated with a thick ash horizon im-

Table 10. Results of Rock-Eval pyrolysis of samples from Site 752.

Core, section, interval (cm)	Depth (mbsf)	Weight (mg)	T_{max} (°C)	S1 (mg HC/g rock)	S2 (mg HC/g rock)	S3 (mg CO_2/g rock)	Productivity index (S1/[S1 + S2])	S2/S3	Pyrolysized carbon (0.083[S1 + S2])	Total organic carbon (wt%)	Hydrogen index (mg HC/g C_{org})	Oxygen index (mg CO_2/g C_{org})
121-752A-												
3H-4, 50-51	3.50	106.4	368	0.25	0.11	0.96	0.69	0.11	0.03	0.50	22	192
4H-4, 50-51	32.30	97.0	299	0.12	0.06	0.95	0.67	0.06	0.01	0.70	8	135
7H-4, 50-51	61.10	98.4	389	0.21	0.12	0.97	0.66	0.12	0.02	0.80	15	121
12X-1, 6-7	104.36	100.9	496	0.03	0.19	0.27	0.14	0.70	0.01	0.40	47	67
20X-1, 50-51	181.20	97.8	550	0.07	0.98	1.26	0.07	0.77	0.08	0.50	196	252
23X-1, 80-81	210.60	98.9	370	0.09	0.38	0.55	0.20	0.69	0.03	0.37	102	148
27X-4, 50-51	253.40	98.9	428	0.07	0.23	0.60	0.23	0.38	0.02	0.33	69	181
29X-4, 50-51	272.70	98.2	368	0.12	0.13	1.19	0.50	0.10	0.02	0.40	32	297
31X-4, 50-51	284.40	103.0	429	0.03	0.30	0.68	0.09	0.60	0.01	0.44	100	226
121-752B-												
19R-2, 89-90	433.99	103.8	441	0.04	0.14	0.23	0.22	0.60	0.01	0.58	24	39

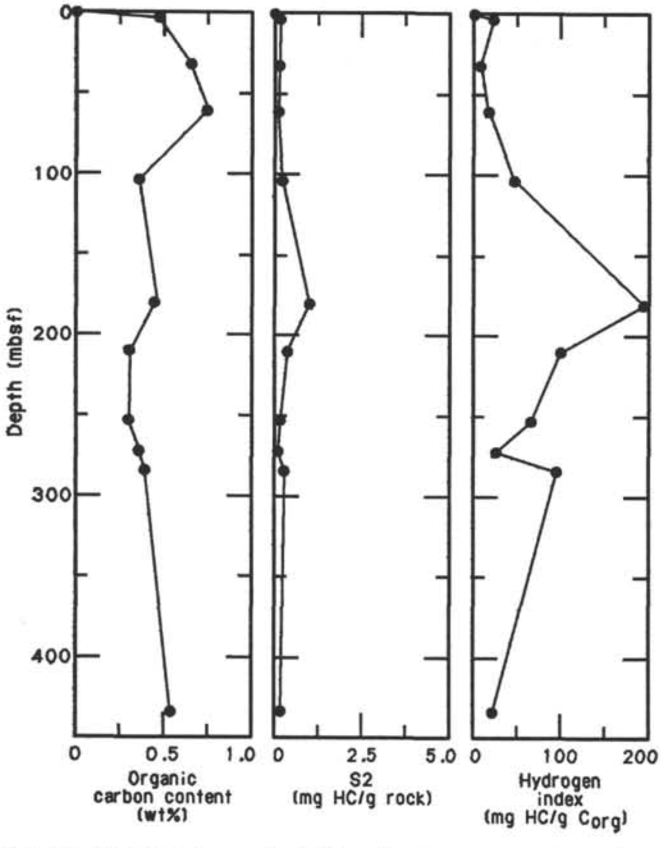

Figure 23. Organic carbon content, S2, and hydrogen index values of selected samples from Site 752.

mediately overlying the Cretaceous/Tertiary boundary. Other subtle impedance contrasts near 80 and 180 mbsf are also considered as possible sources for the reflection of seismic energy, although these have not been interpreted as such ("Seismic Stratigraphy" section). Several reflectors that are not associated with clear impedance contrasts seem to match lithologic changes, such as increases in mean grain size, that were not detected in the physical-properties measurements.

The laboratory-derived velocities compare quite favorably with those obtained from logging (see "Geophysical Well Logging" section, this chapter), and are discussed in the "Physical Properties" section of the "Broken Ridge Summary" chapter.

Vane Shear Strength

Records of torque vs. vane rotation were obtained from the APC-recovered section in Hole 752A. The silty nature of the noncohesive calcareous sediments resulted in extremely low strength values, as indicated in Table 14 and Figure 26. The sediments gain some strength in the lowermost part of the section, where the calcareous component is finer grained, but residual shear strength is clearly lacking throughout the 100 m of burial. The diagenetic shift to indurated chalks is only apparent in the lowermost sample.

Formation Factor

The formation factors measured in the upper 100 m of Hole 752A (Table 14 and Fig. 27) vary from 1.52 to 2.78. This relative range, however, is generally low and reflects an open and continuous porosity. The relative variations downhole are not related to any lithologic changes, with the possible exception of the low values found near 70 and 90 mbsf, which match slightly sandier horizons in lithologic Unit I. The lack of a developing trend of increasing formation factor with greater depth is a function of the almost homogenous physical properties of unit A. A comparison of formation factor and porosity, however, shows the expected relationship between these two parameters (Fig. 28).

Thermal Conductivity and Heat Flow

Thermal-conductivity values are reported in Table 15 and displayed in Figure 29. Conductivities range from approximately 1.2 to 2.2 W/m°C in physical-properties unit A, with a mean value of 1.36 W/m°C. Below the upper/lower Eocene unconformity, thermal conductivities range from 1.3 to 2.23 W/m°C. Unit C exhibits a clear increase to higher thermal conductivities, from values near 1.6 to 2.4 W/m°C. The relatively higher values of thermal conductivity in subunit B1 at 112-145 mbsf and in unit C below 360 mbsf correspond to sections in which ash is more predominant in the sediments.

Four deployments of the WSTP (water sampler-temperature-pressure) tool yielded *in-situ* temperatures in Holes 752A and 753A. Data from both holes are reported here to consolidate these results. The 4-km distance between Sites 752 and 753 is not expected to significantly effect an estimate of the regional downhole temperature gradient calculated by combining the downhole temperature measurements at these two sites. Figure 30 presents the complete test records obtained from each deployment of the tool. The Uyeda probe thermistors used in the WSTP tool were calibrated in a temperature-controlled bath at 1°C increments prior to arrival at Site 752 (see "Explanatory

Table 11. Index properties of Site 752 sediments.

Sample (interval in cm)	Depth (mbsf)	Water content (%)	Porosity (%)	Density: Wet bulk (g/cm^3)	Density: Dry bulk (g/cm^3)	Density: Grain (g/cm^3)
752A-1H-1, 50	0.50	53.40	75.81	1.76	0.82	2.76
752A-1H-3, 50	3.50	43.84	67.65	1.61	0.90	2.71
752A-1H-5, 50	6.50	37.65	61.56	1.70	1.06	2.69
752A-2H-2, 90	10.70	40.92	65.02	1.63	0.96	2.72
752A-2H-4, 90	13.70	37.02	61.61	1.72	1.08	2.77
752A-3H-2, 80	20.10	43.56	67.02	1.59	0.90	2.66
752A-3H-4, 80	23.10	43.15	66.76	1.60	0.91	2.68
752A-3H-6, 80	26.10	40.55	64.28	1.65	0.98	2.67
752A-4H-2, 90	29.70	42.40	66.27	1.63	0.94	2.70
752A-4H-4, 80	32.60	44.55	68.31	1.58	0.87	2.71
752A-5H-2, 80	39.10	42.72	66.71	1.62	0.93	2.72
752A-5H-4, 80	42.10	43.65	67.17	1.59	0.90	2.67
752A-5H-6, 80	45.10	39.71	63.59	1.65	1.00	2.68
752A-6H-2, 90	48.80	36.70	60.67	1.71	1.08	2.69
752A-6H-5, 90	53.30	38.08	62.73	1.69	1.05	2.77
752A-7H-2, 90	58.50	39.44	63.76	1.67	1.01	2.73
752A-7H-4, 80	61.40	45.69	69.14	1.57	0.85	2.69
752A-7H-6, 80	64.40	—	—	1.93	—	2.74
752A-8H-6, 80	74.10	—	—	1.64	—	2.71
752A-9H-2, 80	77.70	—	—	1.86	—	2.69
752A-9H-4, 80	80.70	—	—	1.71	—	2.79
752A-10H-4, 70	90.20	—	—	1.57	—	2.84
752A-10H-6, 70	93.20	—	—	1.64	—	2.78
752A-11H-2, 80	97.00	—	—	1.61	—	2.81
752A-11H-4, 80	100.00	—	—	1.73	—	2.68
752A-11H-6, 80	103.00	—	—	1.80	—	2.68
752A-13X-2, 80	115.20	30.31	53.08	1.81	1.26	2.64
752A-13X-CC, 15	118.56	13.72	25.56	1.91	1.65	2.19
752B-2R-1, 78	120.78	28.16	51.45	1.94	1.39	2.74
752B-2R-2, 23	121.73	29.95	52.95	1.84	1.29	2.67
752A-14X-2, 80	124.90	29.13	51.05	1.86	1.32	2.57
752A-14X-4, 80	127.90	29.66	51.83	1.83	1.29	2.59
752B-3R-2, 79	131.99	28.75	51.44	1.91	1.36	2.66
752A-15X-2, 73	134.53	30.00	52.84	1.88	1.31	2.65
752B-3R-4, 140	135.60	24.89	47.28	1.99	1.49	2.75
752A-15X-4, 84	137.64	27.46	49.65	1.98	1.44	2.64
752B-3R-6, 87	138.07	24.55	46.57	1.99	1.50	2.72
752B-4W-2, 90	141.80	28.34	50.26	1.86	1.33	2.59
752A-16X-1, 120	143.20	30.08	53.74	1.84	1.29	2.74
752B-4W-4, 100	144.90	24.68	46.08	1.96	1.47	2.65
752A-16X-4, 85	147.35	26.75	48.50	1.90	1.39	2.62
752B-4W-6, 89	147.79	25.09	46.20	1.93	1.45	2.60
752A-17X-1, 35	152.05	27.52	49.76	1.91	1.38	2.64
752A-17X-3, 141	156.11	27.52	49.29	1.89	1.37	2.60
752A-18X-1, 90	162.30	28.35	50.12	1.86	1.33	2.57
752A-18X-CC, 19	163.97	29.28	51.73	1.87	1.32	2.62
752A-19X-1, 60	171.70	31.01	53.41	1.80	1.24	2.59
752A-19X-3, 63	174.73	36.07	59.89	1.76	1.12	2.68
752A-19X-4, 60	176.20	36.40	58.64	1.67	1.06	2.51
752A-20X-1, 60	181.30	26.54	47.86	1.89	1.39	2.58
752A-21X-1, 81	191.21	25.04	47.11	1.99	1.49	2.71
752A-21X-2, 57	192.47	31.85	54.73	1.81	1.24	2.62
752A-22X-1, 90	201.00	21.72	42.07	2.05	1.61	2.66
752A-22X-4, 40	205.00	22.12	42.49	2.02	1.58	2.64
752A-23X-1, 91	210.71	23.28	44.86	2.01	1.54	2.72
752A-23X-CC, 7	211.63	22.81	43.51	1.97	1.52	2.65
752A-24X-1, 30	219.80	12.01	25.91	1.83	1.61	2.60
752A-24X-2, 90	221.42	42.46	66.03	1.74	1.00	2.66
752A-25X-1, 142	230.52	38.51	61.69	1.83	1.13	2.60
752A-25X-2, 92	231.52	29.22	50.47	1.88	1.33	2.50
752A-26X-2, 38	240.68	38.72	60.68	1.66	1.02	2.47
752A-26X-4, 77	244.07	30.48	52.71	1.82	1.27	2.58
752A-26X-6, 77	247.07	38.01	60.14	1.67	1.03	2.49
752A-27X-1, 40	248.80	36.61	59.68	1.73	1.10	2.59
752A-27X-2, 40	250.30	30.18	52.88	1.86	1.30	2.63
752A-28X-3, 14	261.24	28.43	50.31	1.86	1.33	2.58
752A-28X-4, 12	262.72	25.88	46.97	1.89	1.40	2.57
752A-29X-2, 107	270.27	28.28	50.35	1.86	1.34	2.61
752A-29X-4, 11	272.31	30.34	52.98	1.81	1.26	2.62
752A-29X-6, 147	276.67	23.42	44.75	2.01	1.54	2.69
752A-30X-1, 122	278.62	24.71	45.99	1.95	1.47	2.63
752A-31X-2, 90	281.80	29.24	52.09	1.87	1.33	2.67
752A-31X-4, 2	283.92	34.36	57.36	1.74	1.14	2.60
752A-31X-6, 12	287.02	31.71	55.15	1.84	1.26	2.68

Table 11 (continued).

Sample (interval in cm)	Depth (mbsf)	Water content (%)	Porosity (%)	Density: Wet bulk (g/cm^3)	Density: Dry bulk (g/cm^3)	Density: Grain (g/cm^3)
752A-32X-2, 19	290.39	40.66	63.05	1.68	1.00	2.52
752A-32X-3, 105	292.75	32.22	55.23	1.78	1.21	2.63
752A-32X-6, 78	296.98	22.29	43.50	2.04	1.59	2.73
752B-5R-2, 79	299.29	22.74	43.61	2.04	1.57	2.67
752A-33X-1, 94	299.34	21.11	40.84	2.15	1.70	2.62
752A-33X-2, 37	300.27	21.84	42.83	2.07	1.62	2.72
752B-5R-4, 79	302.29	19.63	38.93	2.07	1.66	2.65
752A-33X-3, 94	302.34	29.20	51.95	1.81	1.28	2.66
752A-33X-4, 19	303.09	22.45	43.45	2.04	1.58	2.69
752B-6R-2, 89	308.99	11.27	24.64	2.30	2.04	2.61
752B-6R-4, 89	311.99	14.96	31.37	2.21	1.88	2.64
752B-7R-2, 89	318.49	13.92	30.22	2.25	1.94	2.72
752B-7R-4, 89	321.49	15.01	30.30	2.18	1.86	2.50
752B-7R-6, 89	324.49	16.28	33.61	2.19	1.84	2.64
752B-8R-2, 89	326.83	16.71	34.55	2.19	1.83	2.67
752B-8R-4, 89	329.79	8.26	16.07	2.30	2.11	2.16
752B-8R-6, 89	332.79	5.68	12.00	2.35	2.22	2.30
752B-9R-1, 100	336.40	12.71	27.17	2.26	1.98	2.60
752B-10R-2, 90	347.50	12.63	27.04	2.27	1.99	2.61
752B-10R-4, 69	350.29	10.44	23.20	2.37	2.12	2.63
752B-10R-6, 72	353.32	24.64	46.96	2.07	1.56	2.75
752B-11R-2, 88	357.18	22.60	42.21	1.99	1.54	2.54
752B-12R-3, 78	368.18	13.67	29.50	2.32	2.01	2.68
752B-12R-6, 87	372.77	17.76	36.21	2.17	1.79	2.67
752B-13R-1, 119	375.19	22.14	43.33	2.09	1.63	2.73
752B-13R-3, 100	378.00	12.13	27.03	2.34	2.06	2.72
752B-13R-5, 77	380.77	11.35	25.29	2.35	2.08	2.69
752B-14R-1, 91	384.51	11.42	25.32	2.32	2.06	2.67
752B-14R-3, 90	387.50	12.37	26.74	2.28	2.00	2.63
752B-14R-5, 82	390.42	14.00	30.08	2.27	1.95	2.68
752B-15R-2, 88	395.68	10.54	23.51	2.34	2.09	2.65
752B-15R-4, 89	398.69	12.40	26.80	2.28	2.00	2.63
752B-16R-2, 89	405.39	10.08	23.08	2.41	2.17	2.72
752B-17R-2, 89	414.99	14.12	30.34	2.28	1.96	2.69
752B-17R-4, 89	417.99	13.20	28.85	2.28	1.98	2.71
752B-19R-2, 89	433.99	12.09	26.99	2.34	2.06	2.73

Notes" chapter). Figure 31 is the downhole plot of estimated *in-situ* temperatures and the best-fit linear regression.

The records from Hole 752A (37.2 mbsf, Fig. 30A) and Hole 753A (53.43 mbsf, Fig. 30) and bottom water temperatures from all measurements yield a thermal gradient of 33.9°C/km. The best estimated *in-situ* temperatures for deployments 121-752A-8H (75.4 mbsf) and 121-753A-3H (24.2 mbsf) are shown in Figure 31, but were not used for the regression primarily because of their disrupted temperature logs. Run 121-752A-8H does not exhibit any form of decay following stab-in (measurement 30) of the tool; instead, the record appears to indicate that the probe was constantly moving in the formation. Pore water recovered from this particular run suggests that seawater contaminated the sample, confirming that during some part(s) of the test the probe was not firmly planted in the formation. Run 121-753A-3H indicates that the probe may have been inserted twice, possibly three times, at measurements 25, 52, and 60. Although the temperature decay following these stabs appears to tend toward an equilibrium value near 5.1°C, this interpretation is less substantial than the other measurements used for the depth-temperature regression. Pore-water chemical results for this later run suggest that the probe obtained a good sample; therefore, the temperature results from this test are probably better than those from the 75.4 mbsf test in Hole 752A. The linear temperature trend obtained for the upper 100-m section reflects the homogeneous character of this sediment cover. Using an average thermal conductivity of 1.32 W/m°C for the upper 60 m of the section, the heat flow for this northern part of Broken Ridge is

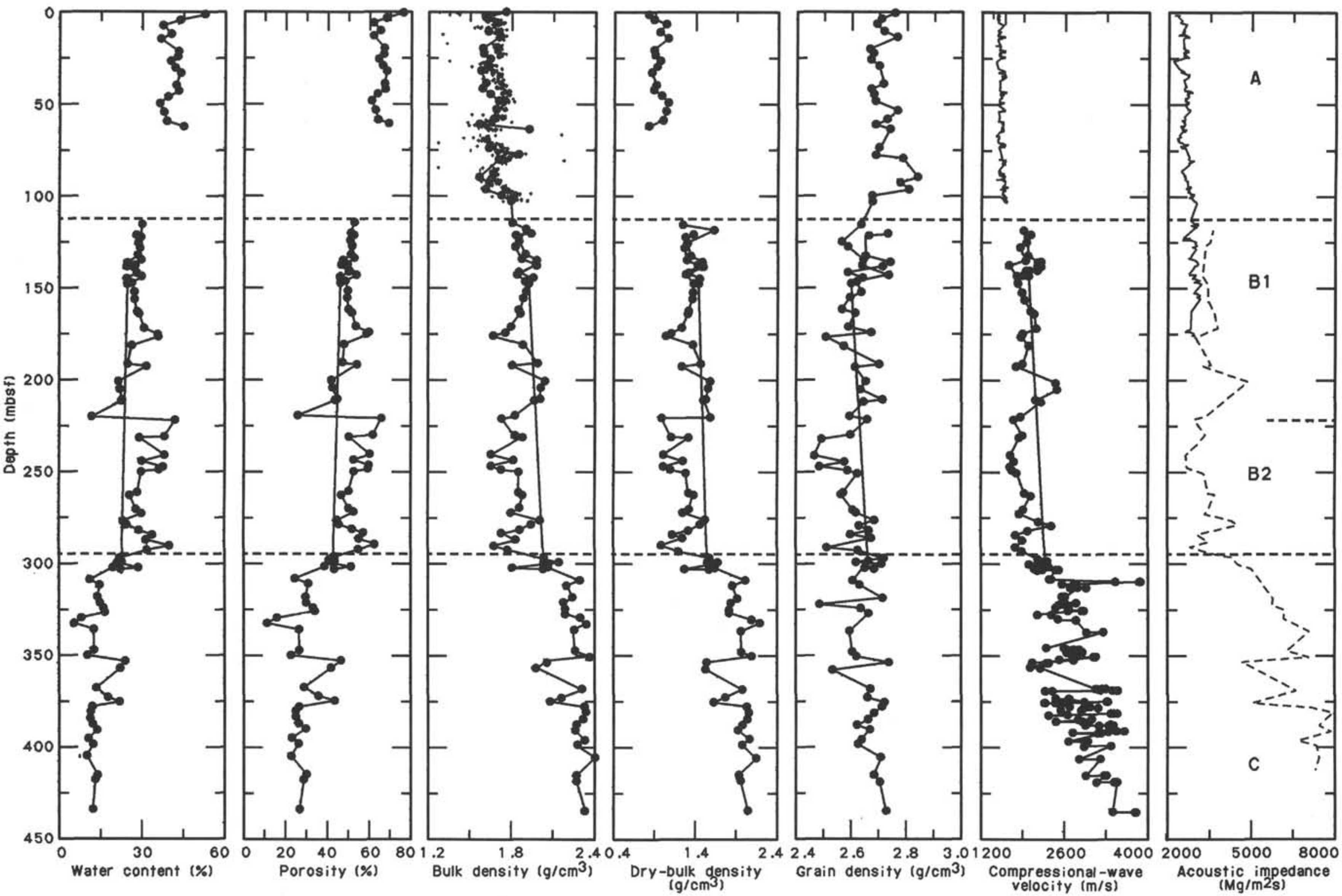

Figure 24. Water content, porosity, bulk density, dry-bulk density, bulk grain density, compressional-wave velocity, and acoustic impedance plots of Site 752 sediments. GRAPE densities and *P*-wave-logger velocities were collected in the upper 170-m section; however, these data are reliable only to 104 mbsf, where APC coring ended. Missing values from 65 to 110 mbsf are from laboratory error. Data from both Holes 752A and 752B are plotted such that the washed interval in Hole 752B between 145 and 297 mbsf appears as a straight line.

Table 12. Compressional-wave velocity of Site 752 sediments.

Sample (interval in cm)	Depth (mbsf)	Direction[a]	Compressional-wave velocity (m/s)
752A-13X-CC, 15	118.56	A	1921.2
752B-2R-1, 78	120.78	A	2048.5
752B-2R-2, 23	121.73	A	1995.4
752A-14X-2, 80	124.90	A	1980.0
752A-14X-4, 80	127.90	A	1872.4
752B-3R-2, 79	131.99	A	2003.7
752A-15X-2, 73	134.53	A	1948.6
752B-3R-4, 140	135.60	A	2156.2
752B-3R-4, 140	135.60	B	2201.8
752B-3R-4, 140	135.60	C	2198.6
752A-15X-4, 84	137.64	A	1688.7
752B-3R-6, 87	138.07	A	2156.7
752B-3R-6, 87	138.07	C	2168.7
752B-3R-6, 87	138.07	B	2200.6
752B-4W-1, 96	140.36	C	1961.2
752B-4W-1, 96	140.36	B	2152.2
752B-4W-1, 96	140.36	A	2018.7
752B-4W-2, 102	141.92	A	2000.0
752B-4W-2, 102	141.92	B	1974.4
752B-4W-2, 102	141.92	C	1977.2
752A-16X-1, 120	143.20	A	1803.5
752B-4W-3, 80	143.20	C	2007.4
752B-4W-3, 80	143.20	B	2005.6
752B-4W-3, 80	143.20	A	1909.6
752A-16X-4, 85	147.35	A	1830.2
752A-17X-1, 37	152.07	A	1895.4
752A-17X-3, 141	156.11	A	1940.4
752A-18X-1, 90	162.30	A	2040.9
752A-18X-CC, 19	163.97	A	2101.6
752A-19X-1, 60	171.70	A	2128.7
752A-19X-3, 63	174.73	A	1918.5
752A-19X-4, 60	176.20	A	1887.7
752A-20X-1, 60	181.30	A	2003.7
752A-21X-1, 81	191.21	A	1911.9
752A-21X-2, 57	192.47	A	1806.9
752A-22X-1, 90	201.00	A	2456.1
752A-22X-4, 40	205.00	B	2501.5
752A-23X-1, 91	210.71	A	2136.3
752A-23X-CC, 5	211.61	A	2208.6
752A-24X-1, 30	219.80	A	1882.1
752A-24X-2, 90	221.42	A	1751.4
752A-25X-1, 92	230.02	A	1904.0
752A-25X-2, 93	231.53	A	1849.3
752A-26X-2, 38	240.68	A	1709.7
752A-26X-4, 77	244.07	A	1778.7
752A-26X-6, 76	247.06	A	1704.5
752A-27X-1, 40	248.80	A	1746.5
752A-27X-2, 40	250.30	A	1822.3
752A-28X-3, 14	261.24	A	1943.5
752A-28X-4, 12	262.72	A	2051.1
752A-29X-2, 107	270.27	A	1929.7
752A-29X-4, 11	272.31	A	1862.5
752A-29X-6, 147	276.67	A	2181.5
752A-30X-1, 122	278.62	A	2405.8
752A-31X-2, 90	281.80	A	2001.9
752A-31X-4, 2	283.92	A	1810.4
752A-31X-6, 12	287.02	A	1923.8
752A-32X-2, 19	290.39	A	1798.0
752A-32X-3, 105	292.75	A	1900.2
752A-32X-6, 78	296.98	A	2172.7
752B-5R-1, 126	298.26	B	2287.4
752B-5R-1, 126	298.26	C	2321.9
752B-5R-1, 126	298.26	A	2296.8
752A-33X-1, 94	299.34	A	2161.6
752B-5R-2, 123	299.73	C	2208.5
752B-5R-2, 123	299.73	B	2165.8
752B-5R-2, 123	299.73	A	2022.5
752A-33X-2, 37	300.27	A	2157.2
752B-5R-3, 118	301.18	A	2187.8
752B-5R-3, 118	301.18	B	2362.4
752B-5R-3, 118	301.18	C	2365.5
752A-33X-3, 94	302.34	A	2115.2
752B-5R-4, 141	302.91	C	2476.0
752B-5R-4, 141	302.91	A	2252.6
752B-5R-4, 141	302.91	B	2522.1
752A-33X-4, 19	303.09	A	2157.5
752B-6R-1, 128	307.88	C	2389.8

Table 12 (continued).

Sample (interval in cm)	Depth (mbsf)	Direction[a]	Compressional-wave velocity (m/s)
752B-6R-1, 128	307.88	B	2383.4
752B-6R-1, 128	307.88	A	2359.6
752B-6R-2, 133	309.43	A	3462.3
752B-6R-2, 133	309.43	C	3873.0
752B-6R-2, 133	309.43	B	3888.7
752B-6R-3, 102	310.62	C	2773.7
752B-6R-3, 102	310.62	A	2582.8
752B-6R-3, 102	310.62	B	2815.6
752B-6R-4, 147	312.57	B	2973.9
752B-6R-4, 147	312.57	A	2719.1
752B-6R-4, 147	312.57	C	2837.0
752B-7R-1, 139	317.49	C	2570.2
752B-7R-1, 139	317.49	A	2629.0
752B-7R-1, 139	317.49	B	2572.6
752B-7R-2, 111	318.71	A	2600.2
752B-7R-2, 111	318.71	B	2576.4
752B-7R-2, 111	318.71	C	2601.2
752B-7R-3, 141	320.51	B	2807.5
752B-7R-3, 141	320.51	A	2621.2
752B-7R-3, 141	320.51	C	2814.4
752B-7R-4, 130	321.90	A	2529.9
752B-7R-4, 130	321.90	C	2740.8
752B-7R-4, 130	321.90	B	2746.8
752B-7R-5, 106	323.16	A	2467.9
752B-7R-5, 106	323.16	B	2681.1
752B-7R-5, 106	323.16	C	2682.0
752B-7R-6, 110	324.70	A	2669.1
752B-7R-6, 110	324.70	C	2903.5
752B-7R-6, 110	324.70	B	2928.0
752B-8R-2, 116	327.10	A	2161.8
752B-8R-2, 116	327.10	C	2392.3
752B-8R-2, 116	327.10	B	2397.6
752B-8R-4, 107	329.97	A	2500.0
752B-8R-4, 107	329.97	C	2804.6
752B-8R-4, 107	329.97	B	2802.3
752B-9R-1, 123	336.63	A	2972.4
752B-9R-1, 123	336.63	B	3259.0
752B-9R-1, 123	336.63	C	3263.5
752B-10R-1, 16	345.26	A	2320.4
752B-10R-1, 16	345.26	C	2604.5
752B-10R-1, 16	345.26	B	2606.2
752B-10R-1, 100	346.10	A	2657.7
752B-10R-1, 100	346.10	B	2776.5
752B-10R-1, 100	346.10	C	2860.1
752B-10R-2, 90	347.50	B	2915.0
752B-10R-2, 90	347.50	A	2647.3
752B-10R-3, 129	349.39	B	2765.9
752B-10R-3, 129	349.39	A	2743.1
752B-10R-3, 129	349.39	C	2845.9
752B-10R-4, 69	350.29	B	3142.2
752B-10R-4, 69	350.29	A	2785.7
752B-10R-4, 69	350.29	C	3104.3
752B-10R-5, 71	351.81	B	2767.9
752B-10R-5, 71	351.81	A	2532.2
752B-10R-6, 72	353.32	B	2362.4
752B-10R-6, 72	353.32	C	2315.9
752B-10R-6, 72	353.32	A	2079.6
752B-11R-1, 133	356.13	B	2208.3
752B-11R-1, 133	356.13	A	2038.6
752B-11R-1, 133	356.13	C	2217.3
752B-12R-3, 7	367.47	C	3304.8
752B-12R-3, 7	367.47	B	3250.0
752B-12R-3, 7	367.47	A	3136.1
752B-12R-3, 78	368.18	A	3218.3
752B-12R-3, 78	368.18	B	3420.3
752B-12R-3, 78	368.18	C	3504.0
752B-12R-3, 133	368.73	B	2411.4
752B-12R-3, 133	368.73	C	2410.3
752B-12R-3, 133	368.73	A	2287.9
752B-12R-6, 87	372.77	A	2461.8
752B-12R-6, 87	372.77	B	2703.6
752B-12R-6, 87	372.77	C	2683.4
752B-13R-1, 44	374.44	B	3315.6
752B-13R-1, 44	374.44	A	2937.8
752B-13R-1, 44	374.44	C	3332.3
752B-13R-1, 119	375.19	A	2297.6
752B-13R-1, 119	375.19	B	2590.8

Table 12 (continued).

Sample (interval in cm)	Depth (mbsf)	Direction[a]	Compressional-wave velocity (m/s)
752B-13R-1, 119	375.19	C	2574.3
752B-13R-1, 125	375.25	B	2504.4
752B-13R-1, 125	375.25	A	2284.4
752B-13R-1, 125	375.25	C	2470.0
752B-13R-2, 141	376.91	A	2693.1
752B-13R-2, 141	376.91	C	3015.2
752B-13R-2, 141	376.91	B	3029.2
752B-13R-3, 100	378.00	B	3175.9
752B-13R-3, 100	378.00	A	2928.8
752B-13R-3, 100	378.00	C	3181.4
752B-13R-4, 54	379.04	A	2557.7
752B-13R-4, 54	379.04	B	2904.0
752B-13R-4, 54	379.04	C	2900.0
752B-13R-5, 77	380.77	A	3375.2
752B-13R-5, 77	380.77	B	3439.4
752B-13R-5, 77	380.77	C	3489.6
752B-13R-6, 26	381.76	A	2349.7
752B-13R-6, 26	381.76	B	2661.0
752B-13R-6, 26	381.76	C	2660.6
752B-14R-1, 27	383.87	A	2846.5
752B-14R-1, 27	383.87	B	3060.7
752B-14R-1, 27	383.87	C	3072.2
752B-14R-2, 6	385.16	A	2478.9
752B-14R-2, 6	385.16	B	2915.7
752B-14R-2, 6	385.16	C	3019.4
752B-14R-3, 66	387.26	C	3370.5
752B-14R-3, 66	387.26	B	3372.7
752B-14R-3, 66	387.26	A	2963.1
752B-14R-3, 90	387.50	C	3348.2
752B-14R-3, 90	387.50	A	3188.2
752B-14R-3, 90	387.50	B	3407.5
752B-14R-5, 82	390.42	A	3352.9
752B-14R-5, 82	390.42	B	3489.5
752B-14R-5, 82	390.42	C	3610.7
752B-14R-6, 42	391.52	B	3171.3
752B-14R-6, 42	391.52	C	3227.7
752B-14R-6, 42	391.52	A	2761.5
752B-15R-2, 115	395.95	B	3005.5
752B-15R-2, 115	395.95	A	2683.2
752B-15R-2, 115	395.95	C	2932.4
752B-15R-4, 68	398.48	A	2934.8
752B-15R-4, 68	398.48	C	3399.4
752B-15R-4, 68	398.48	B	3391.2
752B-16R-2, 97	405.47	C	3218.6
752B-16R-2, 97	405.47	A	2858.1
752B-16R-2, 97	405.47	B	3210.6
752B-17R-2, 36	414.46	A	2975.2
752B-17R-2, 36	414.46	C	3311.0
752B-17R-2, 36	414.46	B	3285.3
752B-17R-4, 121	418.31	A	3151.8
752B-17R-4, 121	418.31	B	3447.5
752B-17R-4, 121	418.31	C	3492.8
752B-19R-2, 141	434.51	B	3806.3
752B-19R-2, 141	434.51	A	3421.6
752B-19R-2, 141	434.51	C	3798.2

[a] A = vertical propagation; B = propagation perpendicular to the split-core face; C = propagation parallel to the split-core face.

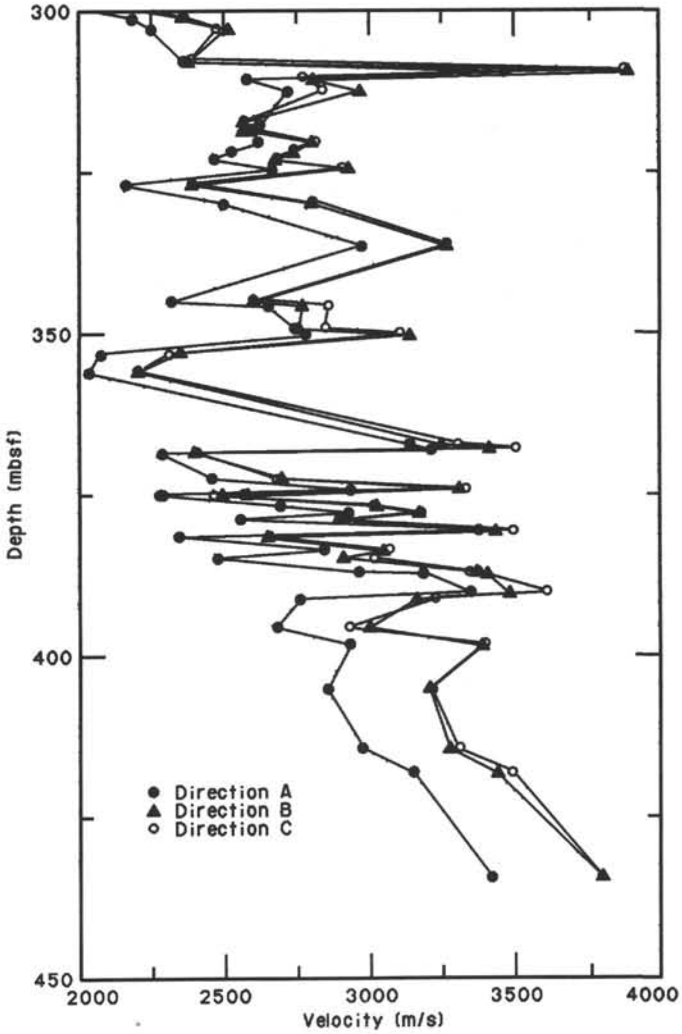

Figure 25. Velocity anisotropy in sediments from lithologic Subunit IIC in Hole 752B. The horizontal velocities are consistently higher.

44.8 mW/m^2, or 1.04 HFU. This value is intermediate to two heatflow measurements presented by Anderson et al. (1977) and approximates their regional Indian Ocean regression curve of age vs. heat flow for old oceanic basins formed at about 115 Ma.

Discussion

The nannofossil/foraminifer oozes capping the Eocene through Cretaceous section at Broken Ridge exhibit atypical properties for silty calcareous sediments. Hamilton (1976) described porosity and density downhole trends for several Pacific calcareous oozes that retained a higher water content than those recovered at Site 752. The index properties at this site define three major physical-properties units: unit A (0–104 mbsf), unit B (104–295 mbsf), and unit C (295–435.6 mbsf).

The upper unit A of unconsolidated oozes corresponds to lithologic Unit I. The slightly higher values of bulk density and thermal conductivity at about 60–80 mbsf may represent a winnowed sediment section correlated with an increase in grain size and a limited middle Miocene hiatus.

The top of unit B was not recovered and is marked by a disconformity between a thin middle Oligocene section and the upper Eocene chalks. High thermal-conductivity values in the 110–140 mbsf interval are not matched by lower water contents or higher bulk densities. These higher values may result from the occurrence of ash in this interval. Between 180 and 221 mbsf, physical-properties unit B exhibits higher bulk densities and velocities relative to the rest of the unit. This interval, which probably corresponds to a seismic reflector, is not clearly distinguished by lithologic changes. Mass accumulation rates for the Paleocene and Eocene section are quite high (3.6 to 6 $g/m^2/1000$ yr), but are slightly lower for the upper Paleocene (see "Broken Ridge Summary" chapter). A possible explanation for the highly consolidated nature of the sediments in this upper Paleocene zone may be current winnowing, which would tend to decrease accumulation rates and would contribute toward the formation of a lag deposit and possibly erosion of overburden. The occurrence of radiolarite and an increased silica contribution in the sediments at 221 mbsf marks the top of physical-properties subunit B2. Higher water contents are typical of biogenic silica in sediments.

Table 13. Velocity anisotropies calculated for physical-properties unit C, Hole 752B.

Core, section, interval (cm)	Depth (mbsf)	ANSI1[a] (%)	ANSI2[b] (%)
3R-4, 140	135.60	2.0	−0.1
3R-6, 87	138.07	1.3	−1.4
4W-1, 96	140.36	1.9	−8.9
4W-2, 102	141.92	−1.2	0.1
4W-3, 80	143.20	5.1	0.1
5R-1, 126	298.26	0.3	1.5
5R-2, 123	299.73	8.1	2.0
5R-3, 118	301.18	8.1	0.1
5R-4, 141	302.91	10.9	−1.8
6R-1, 128	307.88	1.1	0.3
6R-2, 133	309.43	12.1	−0.4
6R-3, 102	310.62	8.2	−1.5
6R-4, 147	312.57	6.9	−4.6
7R-1, 139	317.49	−2.2	−0.1
7R-2, 111	318.71	−0.4	1.0
7R-3, 141	320.51	7.2	0.2
7R-4, 130	321.90	8.5	−0.2
7R-5, 106	323.16	8.7	0.0
7R-6, 110	324.70	9.2	−0.8
8R-2, 116	327.10	10.8	−0.2
8R-4, 107	329.97	12.1	0.1
9R-1, 123	336.63	9.7	0.1
10R-1, 16	345.26	12.3	−0.1
10R-1, 100	346.10	6.0	3.0
10R-3, 129	349.39	2.3	2.9
10R-4, 69	350.29	12.1	−1.2
10R-6, 72	353.32	12.5	−2.0
11R-1, 133	356.13	8.5	0.4
12R-3, 7	367.47	4.5	1.7
12R-3, 78	368.18	7.6	2.4
12R-3, 133	368.73	5.4	0.0
12R-6, 87	372.77	9.4	−0.7
13R-1, 44	374.44	13.1	0.5
13R-1, 119	375.19	12.4	−0.6
13R-1, 125	375.25	8.9	−1.4
13R-2, 141	376.91	12.2	−0.5
13R-3, 100	378.00	8.5	0.2
13R-4, 54	379.04	13.5	−0.1
13R-5, 77	380.77	2.6	1.5
13R-6, 26	381.76	13.2	0.0
14R-1, 27	383.87	7.7	0.4
14R-2, 6	385.16	19.7	3.6
14R-3, 66	387.26	13.8	−0.1
14R-3, 90	387.50	5.9	−1.7
14R-5, 82	390.42	5.9	3.5
14R-6, 42	391.52	15.9	1.8
15R-2, 115	395.95	10.6	−2.4
15R-4, 68	398.48	15.7	0.2
16R-2, 97	405.47	12.5	0.2
17R-2, 36	414.46	10.9	0.8
17R-4, 121	418.31	10.1	1.3

[a] ANSI1 = ([Vb + Vc]/2 − Va)/Va, or ([Vb or Vc] − Va)/Va.
[b] ANSI2 = (Vc − Vb)/Vb.

The basal physical-properties unit C marks the transition from middle to lower Paleocene chalks. In the lower unit, calcareous cementation results in much higher densities and corresponding velocities. The thick ash layer overlying the Cretaceous/Tertiary boundary marks a low-velocity zone. The decrease in porosity and related increases in bulk density and thermal conductivity below 360 mbsf indicate a progressive stage in the calcareous lithification process.

The physical-properties units described for Site 752 can be correlated with similar units at all Broken Ridge sites. In addition, they closely match the results from downhole logging (see "Broken Ridge Summary" chapter).

Table 14. Vane shear strength and formation factor of Hole 752A sediments.

Core, section, interval (cm)	Depth (mbsf)	Undrained shear strength (kPa)	Formation factor
1H-1, 50	0.50	3.9	—
1H-1, 78	0.78	—	2.29
1H-3, 50	3.50	3.5	1.91
1H-5, 50	6.50	9.8	2.78
2H-2, 90	10.70	4.4	2.23
2H-4, 90	13.70	9.1	2.14
3H-2, 80	20.10	0.8	2.05
3H-4, 80	23.10	2.3	2.07
3H-6, 80	26.10	12.1	2.19
4H-2, 90	29.70	3.0	2.07
4H-4, 80	32.60	1.4	1.72
5H-2, 80	39.10	2.1	1.98
5H-4, 80	42.10	0.9	2.00
5H-6, 80	45.10	4.1	1.97
6H-2, 90	48.80	3.7	2.24
6H-5, 90	53.30	3.1	2.25
7H-2, 90	58.50	6.1	1.96
7H-4, 80	61.40	1.4	1.75
7H-6, 80	64.40	5.4	2.03
8H-2, 80	68.10	1.2	1.52
8H-6, 80	74.10	0.5	1.78
9H-2, 80	77.70	2.3	2.57
9H-4, 80	80.70	6.1	2.11
10H-2, 80	87.30	5.8	1.68
10H-4, 70	90.20	2.9	1.56
10H-6, 70	93.20	4.4	1.87
11H-2, 80	97.00	9.8	2.27
11H-4, 80	100.00	4.2	1.79
11H-6, 80	103.00	41.9	2.43

GEOPHYSICAL WELL LOGGING

The logging plan at Site 752 included three tool strings: the seismic stratigraphic, the lithoporosity, and the geochemical logging suites (see "Explanatory Notes" chapter). Hole 752B has a total depth of 435 mbsf in a water depth of 1098 m. The drill pipe was set at 60 mbsf for the first run, the seismic stratigraphic. Near the completion of this run, the tool caught in a chert gravel zone from 96 to 114 mbsf. As a result, the pipe was set lower to 129 mbsf for the lithoporosity and geochemical runs. Consequently, the open-hole logged interval varies for each of these tool strings, but overlaps for a significant part of the hole.

The seismic stratigraphic string made downhole and uphole recordings, from 0 to 435 mbsf (0–63 mbsf through pipe) and from 435 to 62 mbsf, respectively. At 114 mbsf in the uphole run, the tool was stopped by a constriction, and we ended logging with this tool. The interval of useful log data is 422–0 mbsf (60–0 mbsf is logged through pipe). The quality is good throughout the interval for the data, which includes natural gamma, resistivity, and velocity curves.

The lithoporosity string provided one uphole recording, from 339 to 97 mbsf (127–97 mbsf through pipe). The lithoporosity string was run with pipe at 127 mbsf to cover the chert gravel layer from 96 to 115 mbsf, but logging to total depth was prevented by a constriction at 320 mbsf. The quality of the data in the open hole is good, and the useful interval is 320–128 mbsf. Data include neutron porosity, natural gamma, and bulk density.

The geochemical string provided two uphole recordings, from 425 to 87 mbsf (127–87 mbsf through pipe) and 32–0 mbsf (entirely through pipe). Data quality is very good in open hole for the interval 129–422 mbsf, and the data include elemental yields of sulfur, iron, chlorine, hydrogen, aluminum, calcium, and sil-

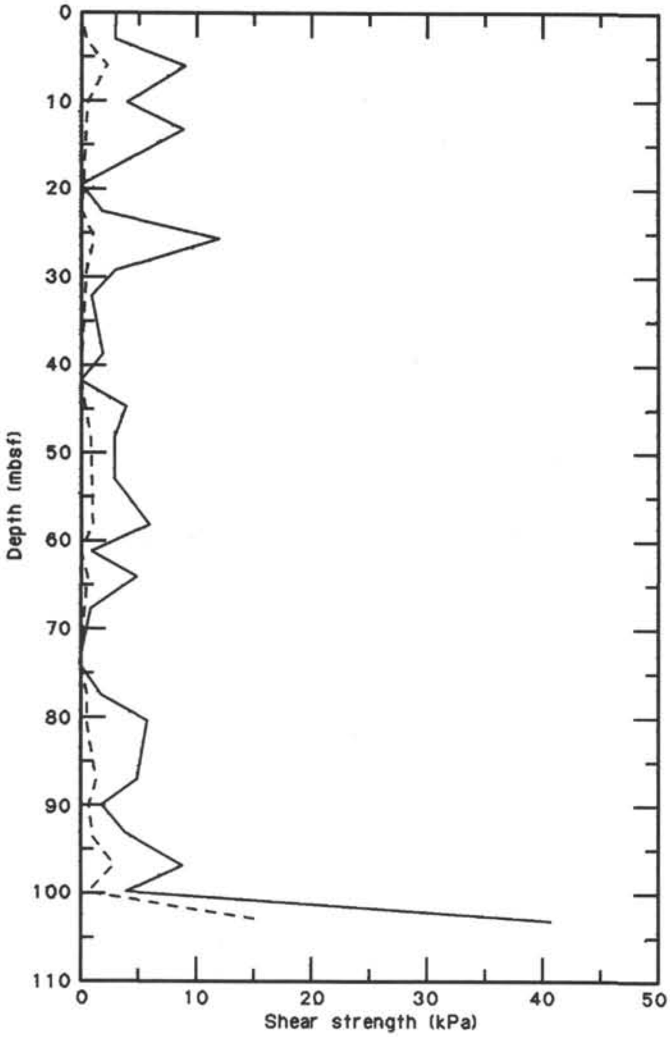

Figure 26. Vane shear strength (solid line) and residual strength (dashed line) of sediments from Hole 752A.

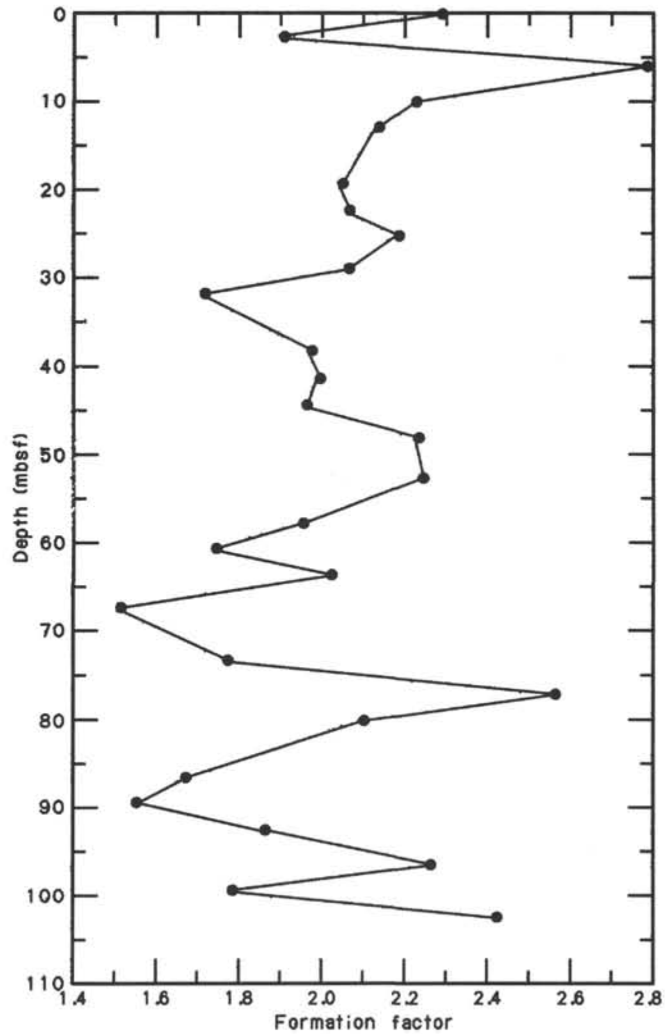

Figure 27. Formation factor profile for sediments from Hole 752A.

icon, as well as capture cross section, total gamma radiation, and uranium, potassium, and thorium percentages. Post-cruise processing will begin with a normalization procedure in order to obtain dry weight percentages for Ca, Si, Fe, S, Ti, K, Gd, Mg, and Al. This procedure allows for an estimate of the mineralogy.

Interpretation

The geochemical log across the seafloor indicates a transition from sediment to water at 5 mbsf. This suggests that either the process of washing down the hole or the use of the minicone created a depression or disturbed zone around the top of the hole. This effect is also seen in the logging data from Site 754, where a minicone was not used.

Figures 32 and 33 include plots of gamma ray, resistivity, sonic transit time, potassium, uranium, and thorium. A chert gravel layer from 96 to 115 mbsf (arrow 1, Fig. 32) reads high on the gamma and resistivity logs and shows a slight increase on the velocity log from the seismic stratigraphic string. The locations of the unconformities that bracket this gravel layer are clear from the gamma log. This interval was measured through pipe on subsequent runs and had no apparent effect on the other logs.

A chert layer in lithologic Subunit IIA at 177 mbsf (arrow 2, Fig. 32) shows high velocity and high resistivity. A decrease in resistivity and velocity marking the top of Subunit IIB at 215 mbsf (arrow 3, Fig. 32) corresponds to the observed increase in radiolarian and diatom content in these chalks (see "Lithostratigraphy and Sedimentology" section). The gamma log values are higher in this subunit relative to Subunit IIA, probably as a result of the presence of clay minerals from the alteration of ash, which is more common in this subunit.

The top of Subunit IIC is evidenced as a change to high resistivity and velocity from 290 to 310 mbsf (arrow 4, Fig. 32). This response is due to the common porcellanite and chert layers in this subunit. The ash layers above the Cretaceous/Tertiary boundary, which extends from 358.17 to 358.77 (arrow 5, Fig. 32), are evidenced by low resistivity, low velocity, and high gamma response. The high gamma response is due primarily to potassium, because uranium and thorium show little increase in this interval. A thin limestone bed between the thinner (2 m) upper ash layer at 353 mbsf and the thicker (4.5 m) lower ash layer is indicated by an increase in resistivity and velocity. The Cretaceous/Tertiary boundary zone (358.17–358.77 mbsf) is marked on the logs by a high-velocity spike resulting from the chalk, chert, and porcellanite in the uppermost Upper Cretaceous sediment.

A comparison of velocity and density data from laboratory measurements and from logging, respectively, shows good agreement between the two, even for minor peaks (Figs. 34 and 35).

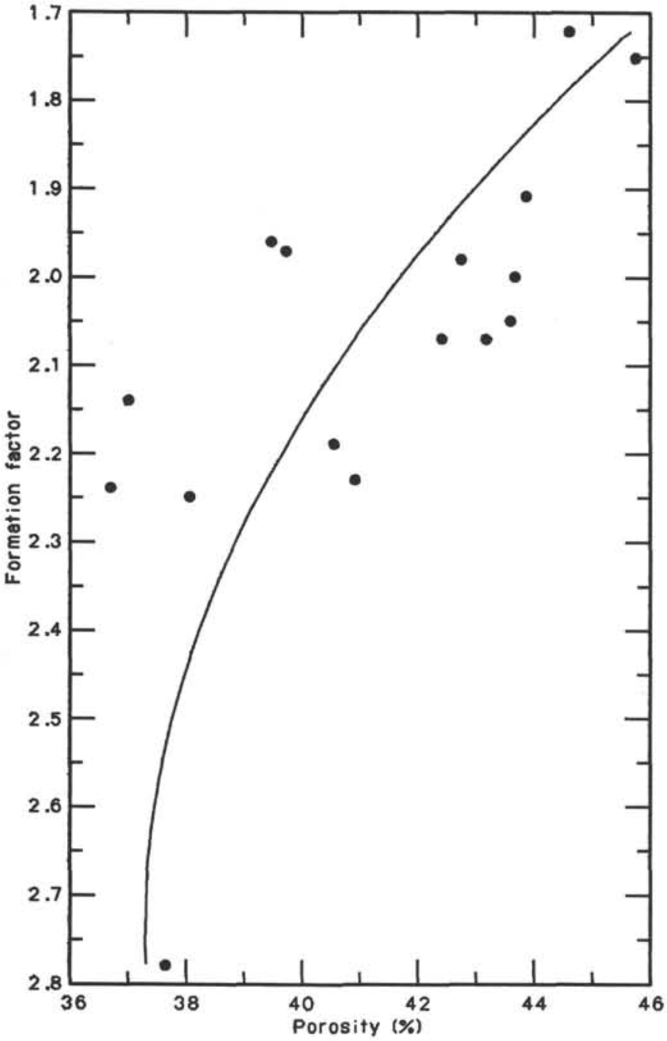

Figure 28. Formation factor vs. porosity of Hole 752A sediments. Although the porosity is relatively low, the formation factor of these calcareous silty to sandy sediments is also low.

The bulk-density and neutron porosity logs show a decrease in density and an increase in porosity from 215 to 293 mbsf (arrow 6, Fig. 33), which marks a zone of chalk with biogenic opal. The density high and porosity low at 281 mbsf reflect the porcellanite and chert recovered at that depth. The high density/low porosity spikes at 298, 300, and 306 mbsf (Fig. 33) are due to hard chalk layers. The density increases caused by the porcellanite in chalks are evident below 309 mbsf. No density logs are available below 334 mbsf.

Figure 36 is a synthetic seismogram generated from the velocity data assuming a constant bulk density of 1.8 g/cm^3, which is the average density over the logged interval, based on laboratory measurements. In this case, the assumption of constant density does not greatly impact the result. The velocity contrasts are the stronger impedance control. The synthetic calculation involves the convolution of the impedance (velocity × density) log with a zero-phase Ricker wavelet at a peak frequency of 60 Hz. A similar calculation using a 30-Hz wavelet produced a nearly identical positioning of major reflectors, but less resolution of the smaller ones. The logging data extend from 110 to 420 mbsf.

Figure 37 shows the excellent agreement between the synthetic seismogram and the seismic data, which contain seismic

Table 15. Thermal conductivity of Site 752 sediments.

Sample (interval in cm)	Depth (mbsf)	Thermal conductivity (W/m°C)
752A-1H-2, 80	2.30	1.248
752A-1H-6, 30	7.80	1.287
752A-2H-2, 45	10.25	1.453
752A-2H-4, 45	13.25	1.243
752A-2H-6, 45	16.25	1.668
752A-3H-2, 45	19.75	1.310
752A-3H-4, 45	22.75	1.537
752A-3H-6, 45	25.75	1.368
752A-4H-2, 80	29.60	1.297
752A-4H-4, 80	32.60	1.346
752A-4H-6, 80	35.60	1.300
752A-5H-2, 80	39.10	1.254
752A-5H-4, 80	42.10	1.352
752A-5H-6, 80	45.10	1.345
752A-6H-2, 80	48.70	1.320
752A-6H-4, 80	51.70	1.445
752A-6H-6, 10	54.00	1.270
752A-7H-2, 56	58.16	1.468
752A-7H-4, 56	61.16	1.293
752A-7H-6, 56	64.16	1.425
752A-8H-2, 70	68.00	1.130
752A-8H-4, 70	71.00	1.225
752A-8H-6, 70	74.00	1.336
752A-9H-2, 70	77.60	1.764
752A-9H-4, 70	80.60	1.553
752A-9H-6, 70	83.60	1.344
752A-10H-2, 70	87.20	1.203
752A-10H-4, 70	90.20	1.252
752A-10H-6, 70	93.20	1.378
752A-11H-2, 50	96.70	1.319
752A-11H-4, 50	99.70	1.505
752A-11H-6, 50	102.70	1.424
752A-13X-2, 70	115.10	2.014
752A-13X-4, 70	118.10	1.777
752B-2R-2, 0	121.50	1.650
752A-14X-2, 70	124.80	1.645
752A-14X-4, 70	127.80	1.408
752B-3R-2, 119	132.39	1.530
752A-15X-4, 70	137.50	2.217
752B-4W-2, 104	141.94	1.640
752A-16X-2, 70	144.20	1.439
752A-17X-1, 33	152.03	1.440
752A-18X-1, 88	162.28	1.590
752A-21X-1, 77	191.17	1.560
752A-22X-1, 82	200.92	1.690
752A-23X-1, 83	210.63	1.480
752A-24X-2, 92	221.44	1.400
752A-25X-2, 91	231.51	1.360
752A-26X-2, 35	240.65	1.300
752A-27X-1, 36	248.76	1.340
752A-28X-1, 38	258.48	1.520
752A-29X-3, 38	271.08	1.360
752A-30X-1, 0	277.40	1.490
752A-31X-1, 104	280.44	1.590
752A-32X-6, 75	296.95	1.710
752B-5R-1, 68	297.68	1.680
752A-33X-3, 97	302.37	1.310
752B-6R-1, 107	307.67	1.620
752B-7R-1, 56	316.66	1.520
752B-8R-2, 139	328.70	1.860
752B-9R-1, 109	336.49	1.550
752B-10R-1, 129	346.39	1.510
752B-12R-3, 82	368.22	2.280
752B-13R-2, 132	376.82	2.010
752B-14R-2, 126	386.36	2.070
752B-15R-5, 83	400.13	2.390
752B-16R-2, 13	404.63	2.300
752B-17R-2, 79	414.89	1.720

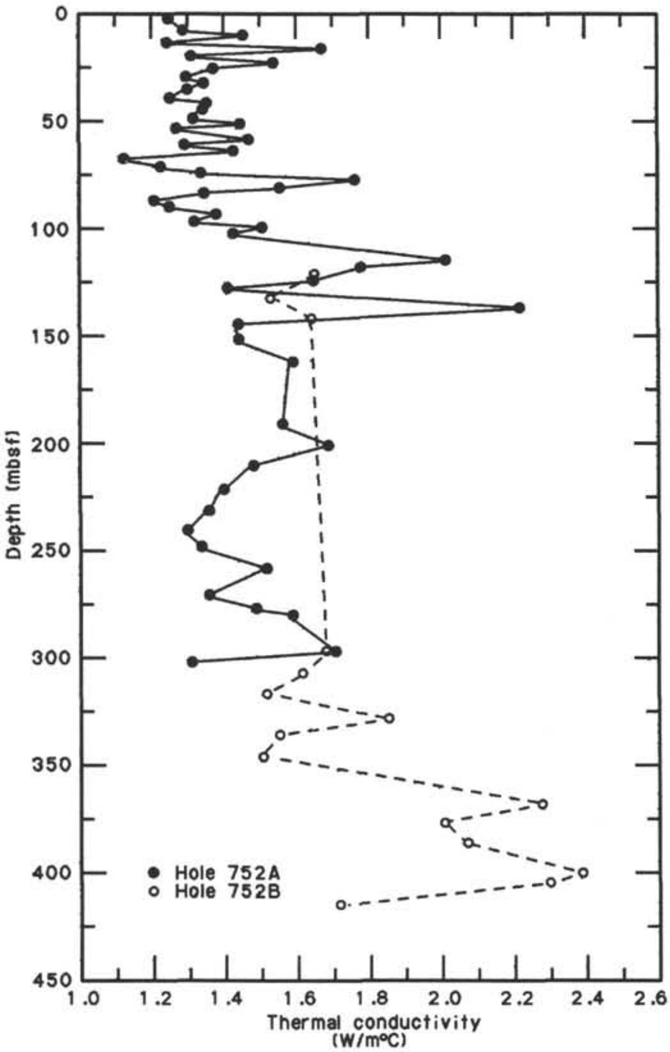

Figure 29. Thermal-conductivity profile for Site 752 sediments. The data from both Holes 752A and 752B are plotted such that the washed interval in Hole 752B between 145 and 297 mbsf appears as a straight line.

energy in the 25–103-Hz frequency range (see "Seismic Stratigraphy" section).

Summary

Geophysical well logging at Site 752 provides confirmation of lithostratigraphic boundaries, delineation of the properties of strata in poorly recovered intervals, and a time-depth tie by the generation of a synthetic seismogram.

SEISMIC STRATIGRAPHY

General Setting

Broken Ridge is an essentially continuous west-northwest–trending oceanic rise, greater than 1000 km long and approximately 100 km wide where it is shallower than 2000 m (Fig. 1). The ridge is markedly asymmetric in cross section, gently dipping toward the north (<1°–2°), in contrast to the steeply dipping south-facing escarpment (>10°). This asymmetry appears to have resulted from the rifting process, in which rift flank uplift is caused by mechanical unloading of the lithosphere during extension (Weissel and Karner, in press).

Approximately 4400 km of high-resolution water gun seismic-reflection data were collected during the RC2708 site survey for Leg 121 (see "Broken Ridge Underway Geophysics" chapter). In addition, over 50 sonobuoys were deployed to ascertain the velocity structure in the study region. These data were analyzed in conjunction with existing seismic-reflection profiles to investigate the nature of the rifting processes by identifying the pre-, syn- and post-rift stratigraphy. Predictable stratigraphic relationships should develop in response to relative sea-level changes (Vail et al., 1980; Vail, 1987) that are, in turn, associated with rifting and uplift at Broken Ridge. The unconformity-bounded stratal packages that developed on Broken Ridge record the interaction of tectonic uplift, thermal subsidence, sediment supply, and eustatic sea level (Vail et al., 1984). Although the Vail sea-level curve has been criticized (Pitman, 1978) in regard to the derivation of eustatic sea-level changes from seismic stratigraphic patterns, the technique of sequence analysis, upon which the curve is based, is a useful interpretative tool (Vail et al., 1980, 1984; Vail, 1987). Recognition of stratigraphic units bounded by unconformities has led to the identification of major seismic stratigraphic sequences on Broken Ridge (Fig. 4 in Driscoll et al., this volume).

Site 752

Site 752 is near the northern edge of Broken Ridge, approximately 15 km north of the prominent southward-dipping scarp (Figs. 1 and 2). Together with Sites 753, 754, and 755, Site 752 was drilled to ensure that the entire northward-dipping and truncated sequences would be sampled, with modest penetration (~450 m) at each site (Fig. 38). Site 752 sampled approximately 100 m of a subhorizontal foraminifer/nannofossil ooze, lithologic Unit I, above the prominent angular unconformity, and about 340 m of a northward-dipping and truncated chalk and chert sequence, lithologic Unit II, below the angular unconformity.

Correlation between Seismic Stratigraphy and Lithostratigraphy

Continuous downhole logging of sonic and density measurements was made only below 110 mbsf at Site 752 because of the hazardous hole conditions immediately above the prominent angular unconformity (limestone gravel layer). However, discrete *P*-wave-logger and density measurements on samples from Cores 121-752A-1H to 121-752A-12X (0–113.0 mbsf) were used to calculate the velocity and bulk density of Unit I (Fig. 39). The calculated velocities from laboratory and downhole measurements are in good agreement with velocities derived from sonobuoy solutions (Figs. 39 and 40). Sonobuoy velocity solutions and laboratory *P*-wave-logger measurements indicate average velocities of 1600 m/s for lithologic Unit I; for lithologic Unit II the sonobuoy velocity solutions, laboratory *P*-wave-logger measurements, and downhole sonic measurements indicate average velocities of 2200 m/s that increase to approximately 3000 m/s toward the base of Hole 752B.

Acoustic impedance (Mg/m^2s) is the product of velocity (m/s) and bulk density (g/cm^3). Seismic reflectors arise from changes in acoustic impedance with depth. Accordingly, downcore acoustic impedance calculations in conjunction with the seismic velocity allow correlation of the sampled lithostratigraphy at Site 752 with the seismic stratigraphy. Major changes in acoustic impedance are noted at 113, 140, 225, 275, and 360 mbsf (Fig. 39).

Synthetic Seismogram

A synthetic seismogram, for the interval of 113–420 mbsf, was calculated from downhole sonic and density measurements (Figs. 36 and 37, "Geophysical Well Logging" section). A zero-phase Ricker wavelet was convolved with the downhole acoustic impedance contrast to generate the synthetic seismogram. The lower 40 m of the synthetic seismogram is an artifact of the convolution program. The convolution generates a longer time se-

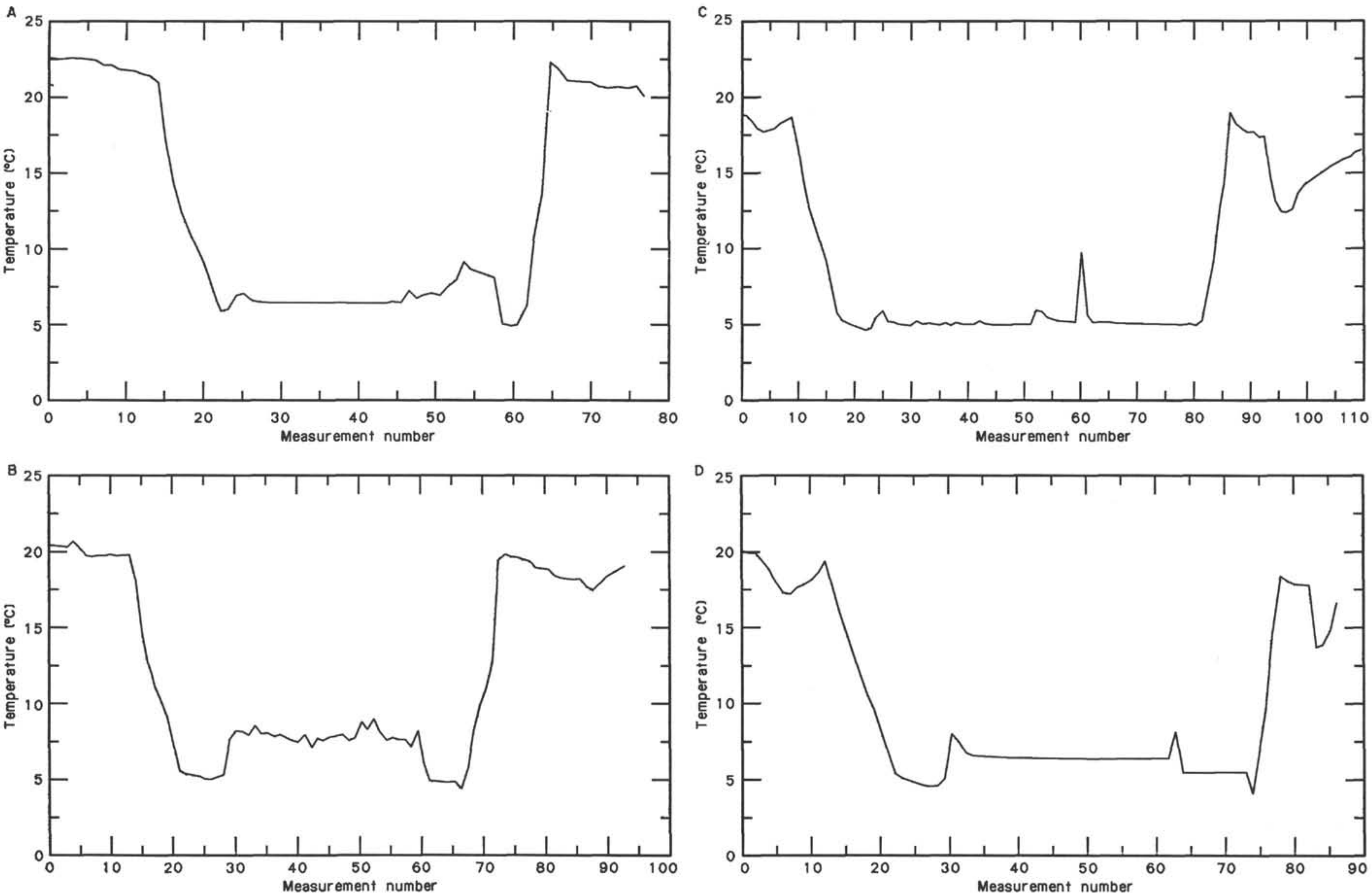

Figure 30. *In-situ* temperature measurements from Holes 752A and 753A. The entire converted Uyeda probe records shown are not fit to decay curves. **A.** Run 121-752A-4H, 37.2 mbsf. **B.** Run 121-752A-8H, 75.4 mbsf. **C.** Run 121-753A-3H, 24.2 mbsf. **D.** Run 121-753A-6H, 53.43 mbsf.

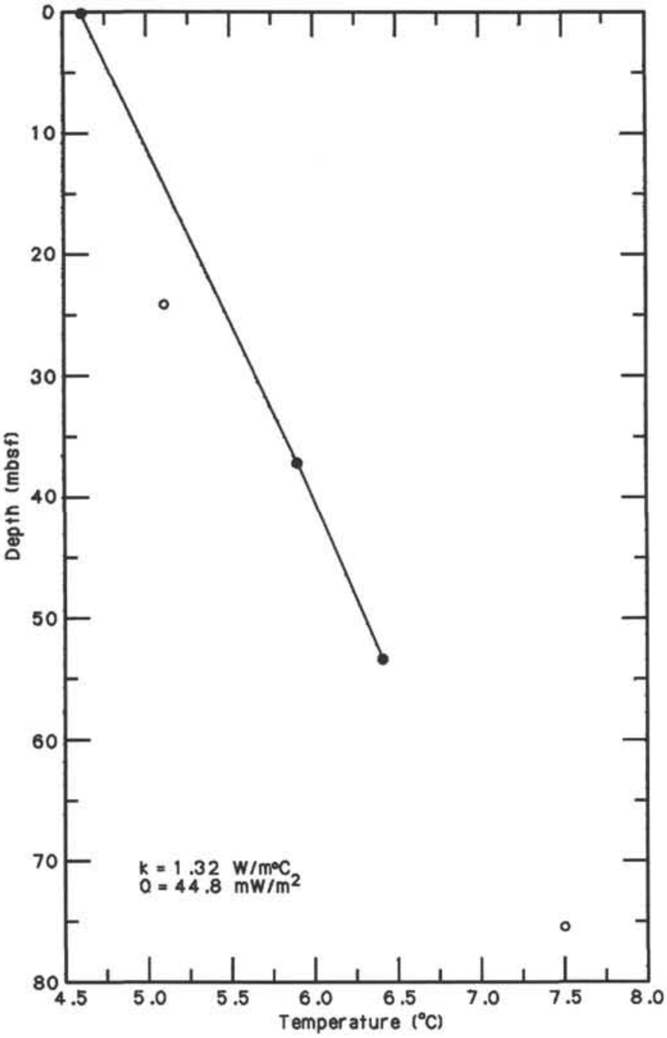

Figure 31. Composite downhole temperatures for Sites 752 and 753. Heat flow is calculated from the best-fit regression to the most reliable data and bottom-water temperature at the mud line.

ries than either of the input series because one of the input series has been padded with zeros and the 60-Hz Ricker wavelet has a wavelength of approximately 50 m.

Pelagic Cap

The horizontal pelagic cap (lithologic Unit I) rests unconformably on the dipping and truncated limestone, chert, and chalk sequence (Fig. 38). Unit I onlaps the northward-dipping truncated units and was probably deposited under the influence of both currents and relative sea-level changes. The depocenter for Unit I was sampled at Site 754. The following reflectors are observed within the horizontal cap:

1. A strong reflector is observed both in the seismic and the 3.5-kHz precision depth recorder (PDR) records at 0.047 s TWT bsf (Figs. 41 and 42). The reflector coincides with the base of an upper Miocene maximum in the mean grain size of the bulk sediment at 47 mbsf (Fig. 5). The coarser grain size may indicate a winnowed layer; this reflector can be traced between Sites 754, 753, and 752.

2. The second reflector is faint and fuzzy on the 3.5-kHz PDR record because of high-frequency attenuation, but it is a fairly strong event at 0.083 s TWT bsf on the water gun reflection records (Figs. 41 and 42) that coincides with an increase in the mean grain size of the middle Miocene bulk sediment (~15–16 Ma) (Fig. 5). This reflector can be traced between Sites 754, 753, and 752.

3. The third reflector, at 0.115 s TWT bsf (93 mbsf), coincides with a hiatus separating limestone pebbles in an upper Eocene ooze with ash from the overlying upper Oligocene brown ooze. Although this reflector is barely discernible on the 3.5-kHz PDR record (Figs. 41 and 42) because of attenuation, it can be observed on the seismic-reflection records.

4. The fourth reflector, at 0.133 s TWT bsf, corresponds to the earlier erosional hiatus separating lower Eocene nannofossil to calcareous chalk from overlying upper Eocene pebbles and brown ooze (Fig. 41). This prominent angular unconformity separates dipping and truncated lower Eocene chalks from horizontal upper Eocene oozes. An increase in acoustic impedance contrast in both the laboratory and downhole geophysical calculations correlates with this reflector; accordingly, the reflector on the synthetic seismogram at 113 mbsf is in good agreement with the observed seismic-reflection data (Figs. 36 and 37).

Dipping and Truncated Sequences

The dipping and truncated limestone, chert, and chalk sequences (downlapping prograding seismic stratigraphic sequence) underlying the angular unconformity thin toward the north (Fig. 38). The following reflectors are observed within this sequence:

1. A faint reflector (couplet) occurs at 0.160 s TWT bsf on the seismic-reflection profile (Fig. 41). A subtle change in acoustic impedance occurs at this depth (140 mbsf; Figs. 36 and 39) and coincides with the ash layers interspersed in the nannofossil chalk with an ash matrix (Cores 121-752A-13X to 121-752A-19X). Another fairly strong reflector (couplet) at 0.190 s TWT bsf is coincident with a subtle acoustic impedance contrast (180 mbsf; Figs. 36 and 37). This reflector also arises from the interspersed ash layers.

2. A strong reflector at 0.255 s TWT bsf on the water gun reflection profile (Fig. 41) correlates with a dramatic change in acoustic impedance in both the laboratory and downhole data (225 mbsf; Figs. 36 and 39). The synthetic seismogram is in good agreement with the seismic-reflection data in position (Fig. 37). A lithologic transition from a nannofossil calcareous chalk to a nannofossil calcareous chalk with radiolarians and diatoms in Subunit IIB (Core 121-752A-24X) correlates with this reflector. The porosity of lithologic Subunit IIB increases because siliceous biogenic material has a higher porosity than that of calcareous biogenic material. Accordingly, the velocity is lower for this interval in Subunit IIB in response to the higher porosity (Fig. 39). Although smear slide analysis indicates that the siliceous biogenic component increases in Core 121-752A-21X, it is only 10% of the material. Thus, an observable increase in porosity does not occur until a certain siliceous abundance threshold is reached downsection.

3. A high-amplitude reflector package (triplet) at 0.300 s TWT bsf on the water gun seismic-reflection profile coincides with a marked increase in acoustic impedance in both the laboratory and downhole data (275 mbsf) (Figs. 36 and 39). The synthetic seismogram generates three pronounced reflectors that correlate well with the observed seismic-reflection data in both amplitude and spacing (Figs. 37 and 41). The transition from a nannofossil calcareous chalk with radiolarians and diatoms to a nannofossil calcareous chalk occurs between Cores 121-752-28X and 121-752A-29X. This reflector marks the base of the low-velocity zone that extends from approximately 225 to 275 mbsf. Laboratory- and downhole-derived data indicate an average velocity of 2000 m/s for this zone in Subunit IIB (Fig. 39).

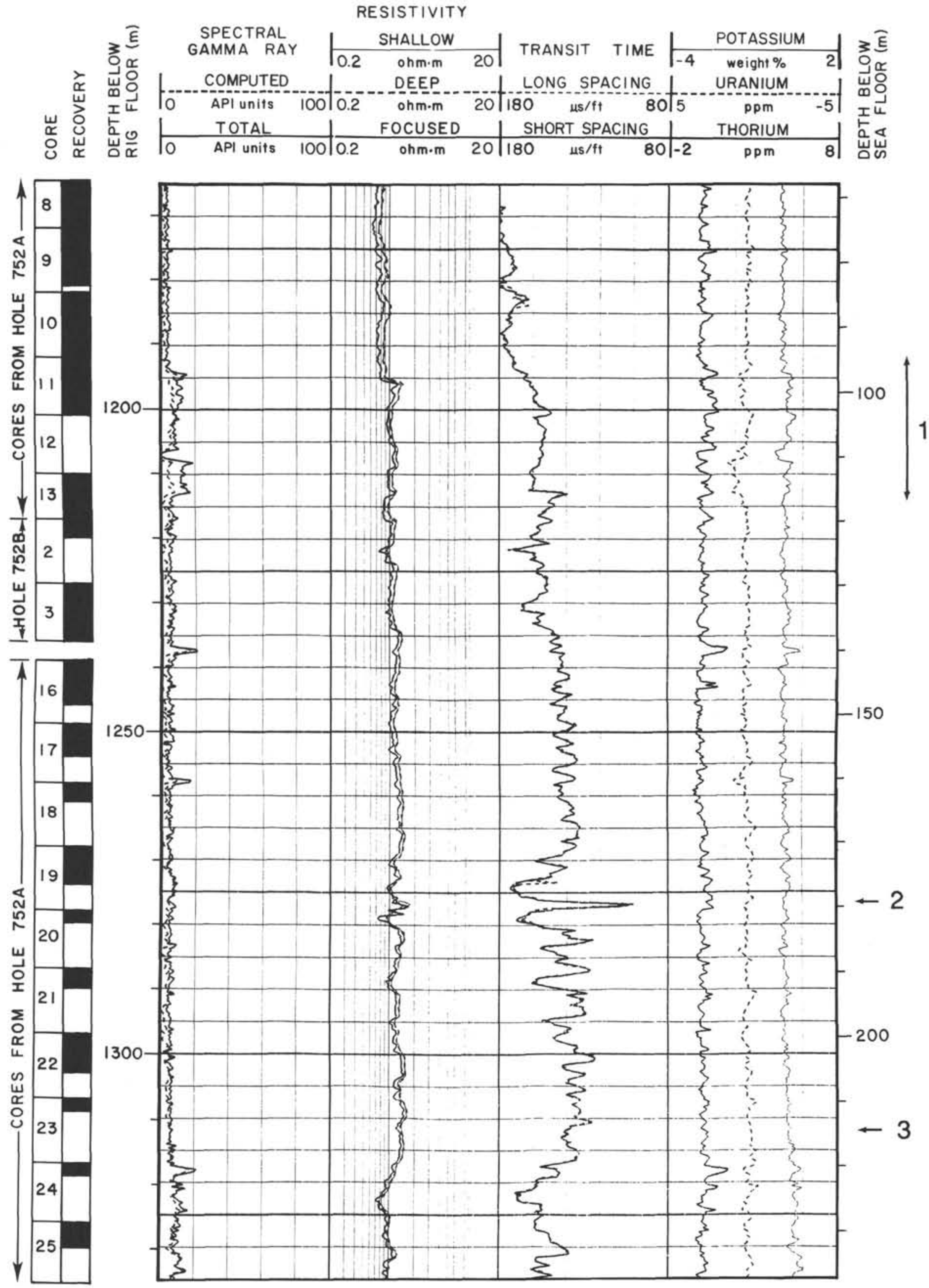

Figure 32. Core recovery; computed and total spectral gamma-ray; shallow, deep, and focused resistivity; long- and short-spacing transit time; and potassium, uranium, and thorium logs from Hole 752B, 68–407 mbsf. Numbered intervals at arrows are discussed in the text.

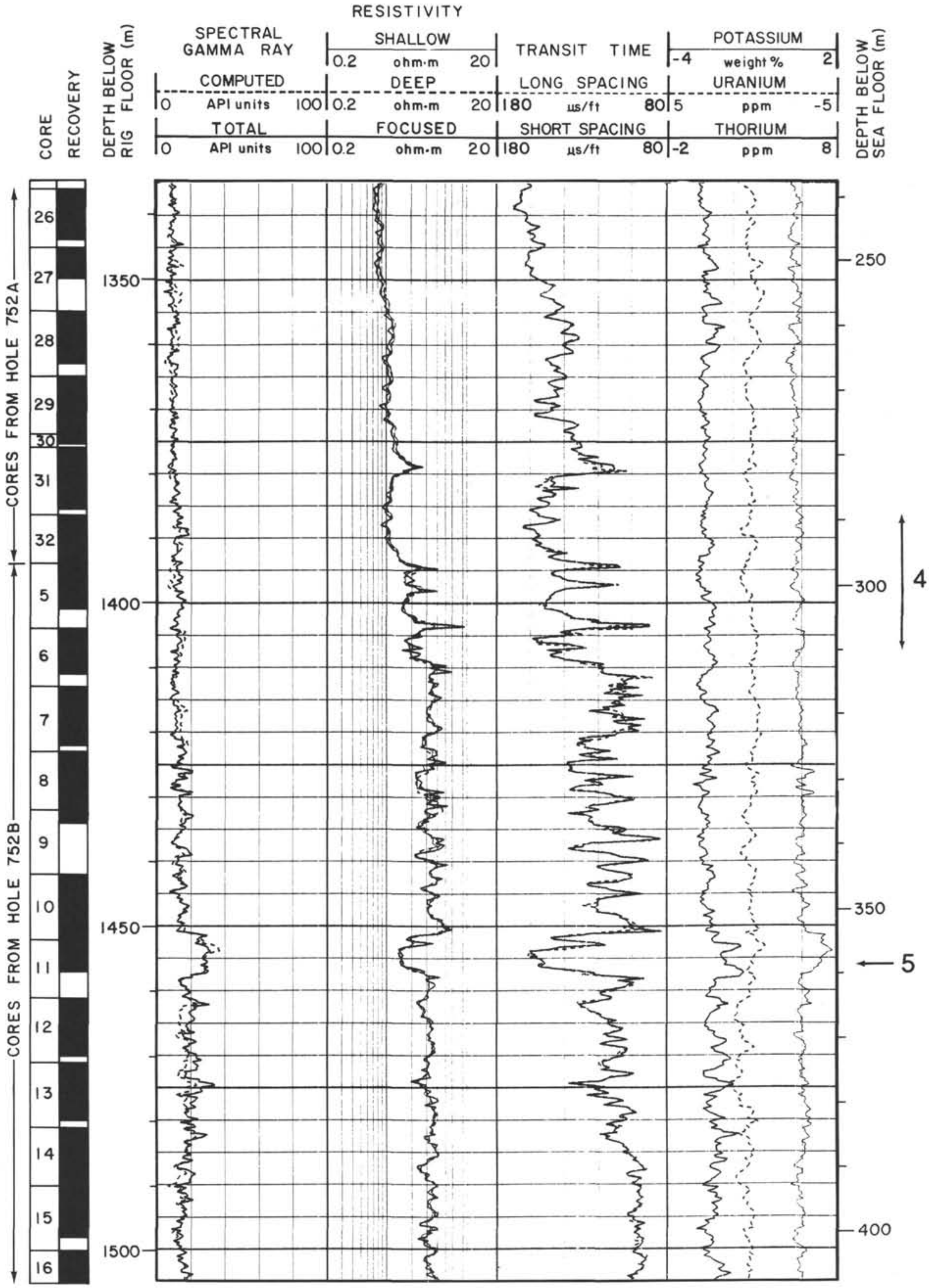

Figure 32 (continued).

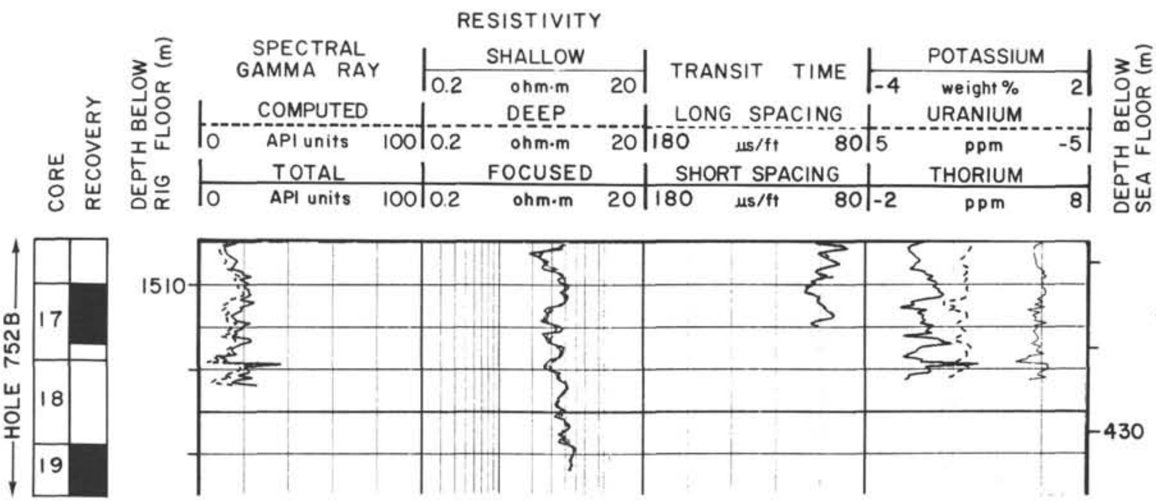

Figure 32 (continued).

A faint reflector (couplet) within the low-velocity zone results from interspersed ash layers at 240 mbsf (Figs. 36 and 37).

4. A faint reflector at 0.350 s TWT bsf on the water gun seismic-reflection record (Fig. 41) coincides with several abrupt fluctuations in acoustic impedance contrast in the downhole acoustic impedance data (~330 mbsf) (Fig. 36). Several distinct porcellanite layers in Cores 121-752B-6R through 121-752B-9R (~320-340 mbsf) correlate with the faint reflector.

5. A high-amplitude reflector at 0.380 s TWT bsf on the water gun seismic-reflection profile (Fig. 41) correlates with a dramatic decrease in acoustic impedance in both the laboratory and downhole data (360 mbsf) (Figs. 36 and 39). A sharp lithologic contact between the calcareous chalk and underlying volcanic ash with micrite occurs between Cores 121-752B-10R and 121-752B-11R. This contact coincides with the pronounced reflector that is immediately above the Cretaceous/Tertiary boundary.

We terminated drilling at Site 752 at 435.6 mbsf (0.410 s TWT bsf) when the biostratigraphic data indicated sufficient overlap with Site 754 to the south (see "Seismic Stratigraphy" section, "Site 754" chapter). Seismic stratigraphic and biostratigraphic data suggest a minimum overlap of 20 m between Sites 752 and 754.

REFERENCES

Anderson, R. N., Langseth, M. G., and Sclater, J. G., 1977. The mechanisms of heat transfer through the floor of the Indian Ocean. *J. Geophys. Res.*, 82:3391-3409.

Banner, F. T., and Blow, W. H., 1965. Progress in the planktonic foraminiferal biostratigraphy of the Neogene. *Nature*, 208:1164-1166.

Bé, A.W.H., and Tolderlund, D. S., 1971. Distribution and ecology of living planktonic foraminifera in surface waters of the Atlantic and Indian oceans. *In* Funnell, B. M., and Riedel, W. R. (Eds.), *Micropaleontology of Oceans*: Cambridge (Cambridge Univ. Press), 105-149.

Berggren, W. A., Kent, D. V., Flynn, J. J., and Van Couvering, J. A., 1985. Cenozoic geochronology. *Geol. Soc. Am. Bull.*, 96:1407-1408.

Blow, W. H., 1969. Late middle Eocene to Recent planktonic biostratigraphy. *In* Bronnimann, P., and Renz, H. H. (Eds.), *Proc. Int. Conf. Planktonic Microfossils, 1st, Geneva, 1967*, 1:199-421.

Bolli, H. M., Saunders, J. B., and Perch-Nielsen, K. (Eds.), 1985. *Plankton Stratigraphy*: Cambridge (Cambridge Univ. Press).

Bukry, D., 1974. Coccolith and silicoflagellate stratigraphy, eastern Indian Ocean, Deep Sea Drilling Project, Leg 122. *In* von der Borch, C. C., Sclater, J. G., et al., *Init. Repts. DSDP*, 22: Washington (U.S. Govt. Printing Office), 601-608.

Caron, M., 1985. Cretaceous planktic foraminifera. *In* Bolli, H. M., Saunders, J. B., and Perch-Nielsen, K. (Eds.), *Plankton Stratigraphy*: Cambridge (Cambridge Univ. Press), 713-762.

Corliss, B. C., 1979, Recent deep-sea benthonic foraminiferal distributions in the southeast Indian Ocean: inferred bottom-water routes and ecological implications. *Mar. Geol.*, 31:115-138.

Fenner, J., 1985. Late Cretaceous to Oligocene planktic diatoms. *In* Bolli, H. M., Saunders, J. B., and Perch-Nielsen, K. (Eds.), *Plankton Stratigraphy*: Cambridge (Cambridge Univ. Press), 713-762.

Geller, C. A., Weissel, J. K., and Anderson, R. N., 1983. Heat transfer and intraplate deformation in the central Indian Ocean. *J. Geophys. Res.*, 88:1018-1032.

Gieskes, J. M., 1975. Chemistry of interstitial waters of marine sediments. *Annu. Rev. Earth Planet. Sci.*, 3:433-453.

———, 1983. The chemistry of interstitial waters of deep sea sediments: interpretation of Deep Sea Drilling data. *Chem. Oceanogr.*, 8:221-269.

Gombos, A. M., 1977. Paleogene and Neogene diatoms from the Falkland Plateau and Malvinas Outer Basin, Leg 36, Deep Sea Drilling Project. *In* Barker, P. F., Dalziel, I.W.D., et al., *Init. Repts. DSDP*, 36: Washington (U.S. Govt. Printing Office), 575-687.

———, 1982. Early and middle Eocene diatom evolutionary events. *Bacillaria*, 5:225-242.

———, 1984. Late Paleocene diatoms in the Cape Basin. *In* Hsü, K. J., LaBrecque, J. L., et al., *Init. Repts. DSDP*, 73: Washington (U.S. Govt. Printing Office), 495-512.

Hamilton, E. L., 1976. Variations of density and porosity with depth in deep-sea sediments. *J. Sediment. Petrol.*, 46:280-300.

Herb, R., 1974. Cretaceous planktonic foraminifera from the eastern Indian Ocean. *In* Davies, T. A., Luyendyk, B. P., et al., *Init. Repts. DSDP*, 26: Washington (U.S. Govt. Printing Office), 745-771.

Jenkins, D. G., 1960. Planktonic foraminifera from the Lakes Entrance oil shaft, Victoria, Australia. *Micropaleontology*, 6:345-371.

———, 1967. Planktonic foraminiferal zones and new taxa from the lower Miocene to the Pleistocene of New Zealand. *N. Z. J. Geol. Geophys.*, 10:1064-1078.

———, 1971. New Zealand Cenozoic planktonic foraminifera. *N. Z. Geol. Surv. Paleontol. Bull.*, 42:1-278.

———, 1978. Neogene planktonic foraminifers from DSDP Leg 40 Sites 360 and 362 in the southeastern Atlantic. *In* Bolli, H. M., Ryan, W.B.F., et al., *Init. Repts. DSDP*, 40: Washington (U.S. Govt. Printing Office), 723-739.

———, 1985. Southern mid-latitude Paleocene to Holocene planktic Foraminifera. *In* Bolli, H. M., Saunders, J. B., and Perch-Nielsen, K. (Eds.), *Plankton Stratigraphy*: Cambridge (Cambridge Univ. Press), 263-283.

Kennett, J. P., 1973. Middle and late Cenozoic planktonic biostratigraphy of the southwest Pacific DSDP Leg 21. *In* Burns, R. E., Andrews, J. E., et al., *Init. Repts. DSDP*, 21: Washington (U.S. Govt. Printing Office), 575-640.

Kent, D. V., and Gradstein, F. M., 1985. A Cretaceous and Jurassic geochronology. *Geol. Soc. Am. Bull.*, 96:1419–1427.

Lawrence, J. R., and Gieskes, J. M., 1981. Constraints on water transport and alteration in the oceanic crust from the isotopic composition of pore water. *J. Geophys. Res.*, 86:7924–7934.

Liu, C. S., Curray, J. R., and MacDonald, J. M., 1983. New constraints on the tectonic evolution of the eastern Indian Ocean. *Earth Planet. Sci. Lett.*, 65:331–342.

Lowrie, W., Alvarez, W., Napoleone, G., Perch-Nielson, K., Premoli-Silva, I., and Toumarkine, M., 1982. Paleogene magnetic stratigraphy in Umbrian pelagic carbonate rocks: the Contessa sections, Gubbio. *Geol. Soc. Am. Bull.*, 93:414–432.

Martini, E., 1971. Standard Tertiary and Quaternary calcareous nannoplankton zonation. *In* Farinacci, A. (Ed.), *Proc. Planktonic Conf. II Rome 1970*: Rome (Technoscienze), 2:739–785.

Morkhoven, F.P.C.M. van, Berggren, W. A., and Edwards, A. S., 1986. Cenozoic cosmopolitan deep-water benthic foraminifera. *Bull. Cent. Rech. Explor. Prod. Elf-Aquitaine*, 11:1–421.

Mottl, M. J., Lawrence, J. R., and Keigwin, L. D., 1983. Elemental and stable-isotope composition of pore waters and carbonate sediments from Deep Sea Drilling Project Sites 501/504 and 505. *In* Cann, J. R., Langseth, M. L., et al., *Init. Repts. DSDP*, 69: Washington (U.S. Govt. Printing Office), 461–486.

Mukhina, V. P., 1974. The Paleocene diatom ooze in the eastern part of the Indian Ocean. *Okeanologiya*, 14:852–858.

———, 1976. Species composition of the late Paleocene diatoms and silicoflagellates in the Indian Ocean. *Micropaleontology*, 22:151–158.

Okada, H., and Bukry, D., 1980. Supplementary modification and introduction of code numbers to the low-latitude coccolith biostratigraphic zonation (Bukry, 1973; 1975). *Mar. Micropaleontol.*, 5:321–325.

Perch-Nielsen, K., 1985. Cenozoic calcareous nannofossils. *In* Bolli, H. M., Saunders, J. B., and Perch-Nielsen, K. (Eds.), *Plankton Stratigraphy*: Cambridge (Cambridge Univ. Press), 427–554.

Peterson, L. C., 1984. Recent abyssal benthic foraminiferal biofacies of the eastern equatorial Indian Ocean. *Mar. Micropaleontol.*, 8:479–519.

Pitman, W. C., 1978. Relationships between eustacy and stratigraphic sequences of passive margins. *Geol. Soc. Am. Bull.*, 89:1389–1403.

Shipboard Scientific Party, 1974. Site 255. *In* Davies, T. A., Luyendyk, B. P., et al., *Init. Repts. DSDP*, 26: Washington (U.S. Govt. Printing Office), 281–294.

Sissingh, W., 1977. Biostratigraphy of Cretaceous calcareous nannoplankton. *Geol. Mijnbouw*, 57:433–440.

Smit, J., 1982. Extinction and evolution of planktonic foraminifera at the Cretaceous/Tertiary boundary. *In* Silver, L. T., and Schultz, P. H. (Eds.), *Geological Implications of Impacts of Large Asteroids and Comets on the Earth*: Spec. Pap. Geol. Soc. Am., 190:329–353.

Smit, J., and Romein, A.J.T., 1985. A sequence of events across the Cretaceous/Tertiary boundary. *Earth Planet. Sci. Lett.*, 74:155–170.

Srinivasan, M. S., and Kennett, J. P., 1981. Neogene planktonic foraminiferal biostratigraphy: equatorial to subantarctic, South Pacific. *Mar. Micropaleontol.*, 6:499–534.

Strelnikova, N. I., 1987. Paleogene diatoms of the high latitudes of the Northern and Southern Hemispheres [Ph.D. dissert.]. Univ. of Leningrad.

Tjalsma, R. C., and Lohmann, G. P., 1983. Paleocene-Eocene bathyal and abyssal benthic foraminifera from the Atlantic Ocean. *Micropaleontology Spec. Publ.*, 4:1–90.

Toumarkine, M., and Luterbacher, H., 1985. Paleocene and Eocene planktic foraminifera. *In* Bolli, H. M., Saunders, J. B., Perch-Nielsen, K. (Eds.), *Plankton Stratigraphy*: Cambridge (Cambridge Univ. Press), 87–154.

Vail, P. R., 1987. Seismic stratigraphy interpretation utilizing sequence stratigraphy. *In* Bally, A. W. (Ed.), *Atlas of Seismic Stratigraphy*: AAPG Stud. Geol., 27:1–11.

Vail, P. R., Hardenbol, J., and Todd, R. G., 1984. Jurassic unconformities, chronostratigraphy and global sea-level changes from seismic stratigraphy and biostratigraphy. *In* Schlee, J. S. (Ed.), *Interregional Unconformities and Hydrocarbon Accumulation*: AAPG Memoir, 36:129–144.

Vail, P. R., Mitchum, R. M., Jr., Shipley, T. H., and Buffler, R. T., 1980. Unconformities of the North Atlantic. *Philos. Trans. R. Soc. London, A*, 294:137–155.

Walton, W. H., Sangrey, D. A., and Miller, S. A., 1983. Geotechnical engineering characterization of hydraulically piston-cored deep ocean sediments. *In* Barker, P. F., Carlson, R. L., Johnson, D. A., et al., *Init. Repts. DSDP*, 72: Washington (U.S. Govt. Printing Office), 537–550.

Weissel, J. K., and Karner, G. D., in press. Flexural uplift of rift flanks due to mechanical unloading of the lithosphere during extension. *J. Geophys. Res.*

Ms 121A-106

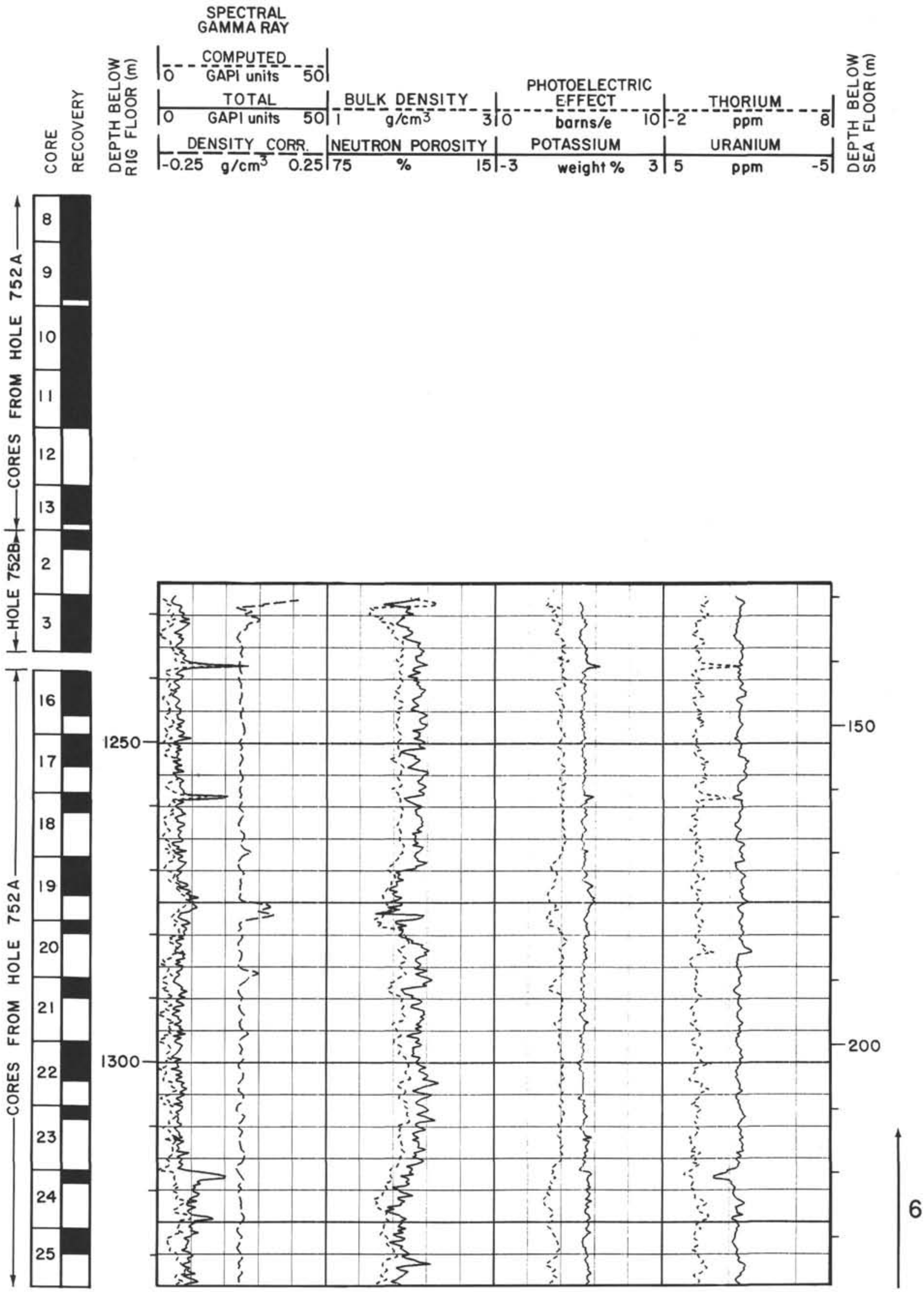

Figure 33. Core recovery, total and computed spectral gamma-ray, density correction, bulk density, neutron porosity, photoelectric effect, and potassium, thorium, and uranium logs from Hole 752B, 130–331 mbsf. Numbered interval (arrow) is discussed in the text.

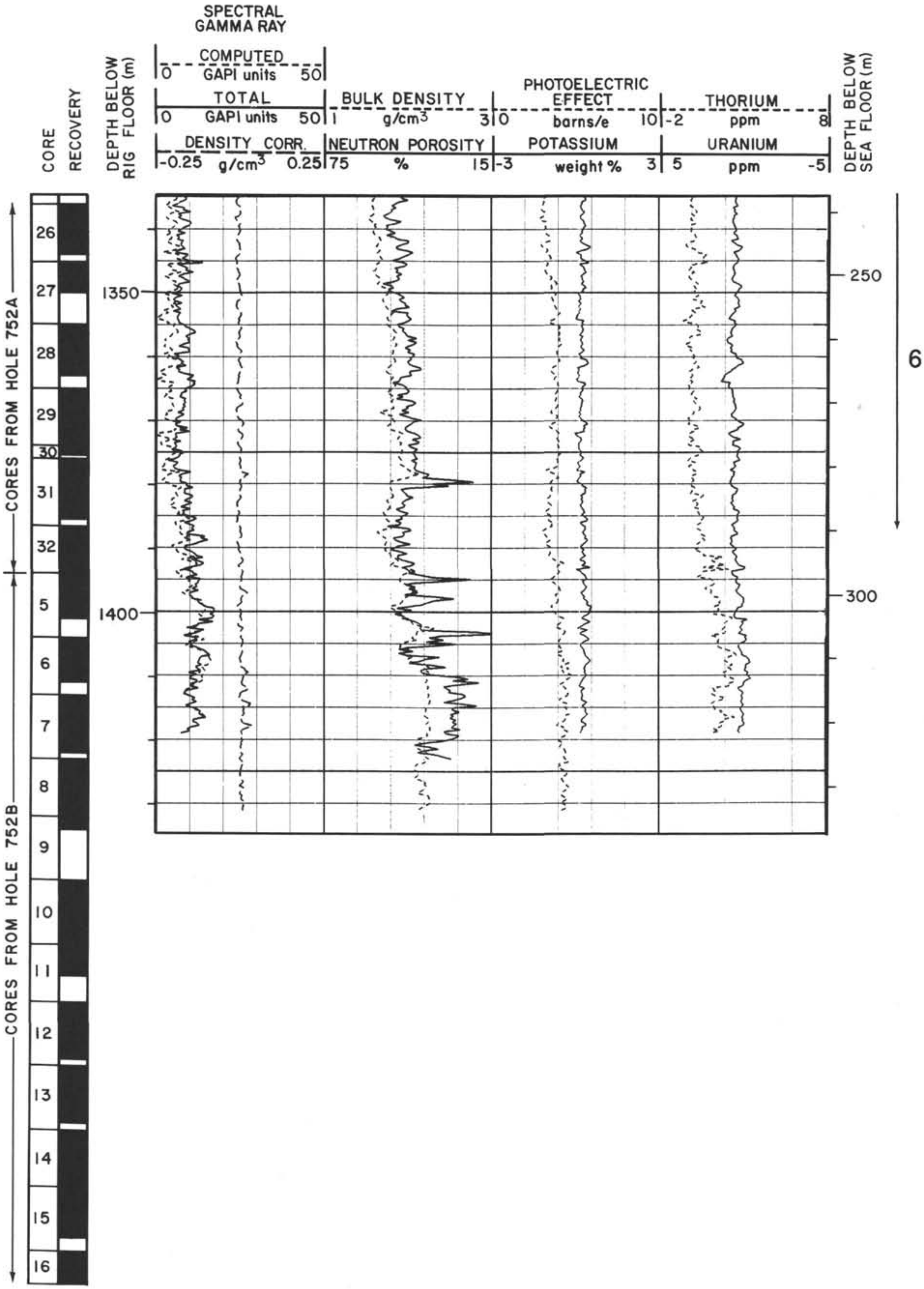

Figure 33 (continued).

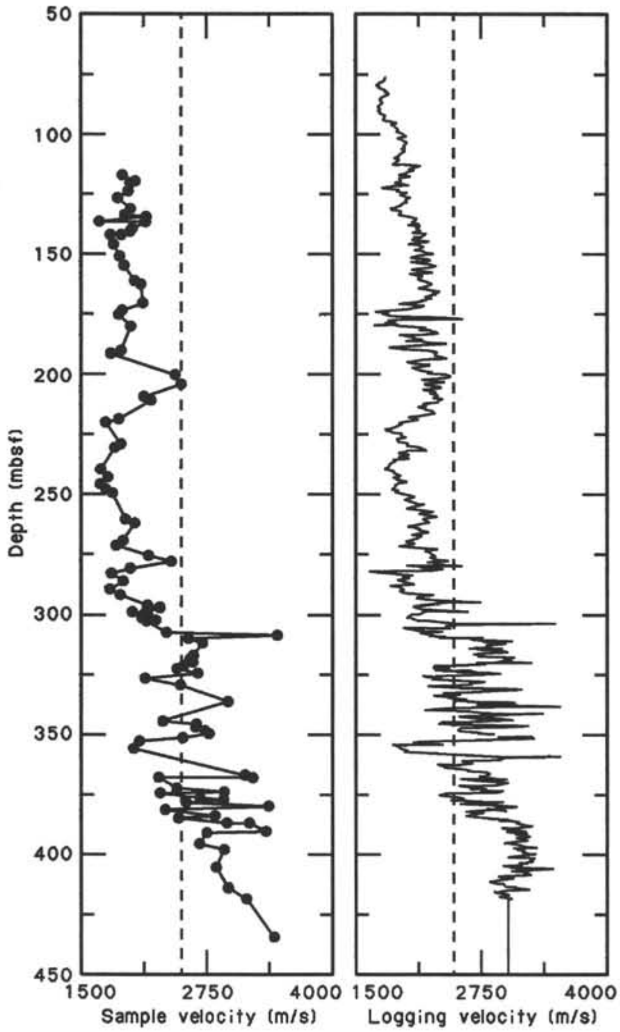

Figure 34. Velocity from laboratory and logging measurements.

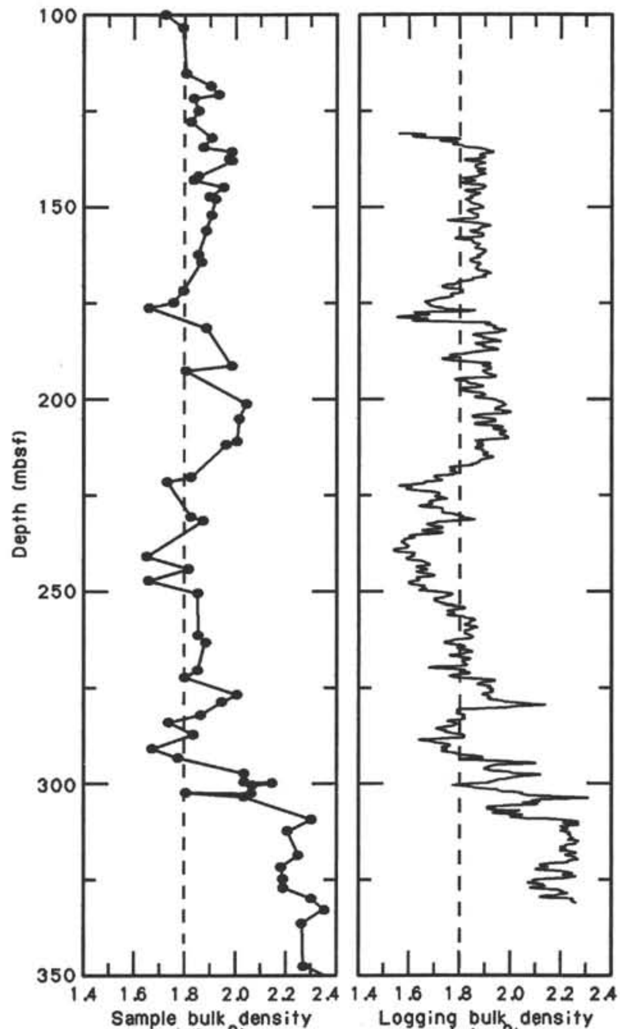

Figure 35. Bulk density from laboratory and logging measurements.

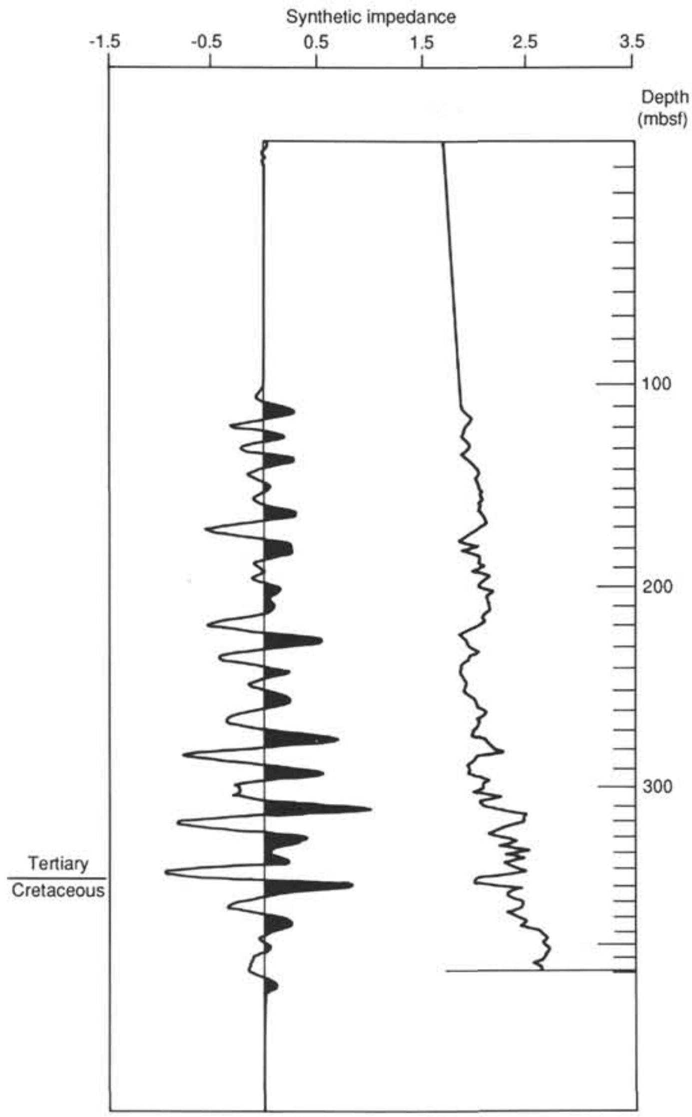

Figure 36. Synthetic seismogram using a zero-phase Ricker wavelet at a peak frequency of 60 Hz and a uniform density of 1.8 g/cm^3. Only the section below 110 mbsf was logged because of hazardous hole conditions. Vertical scale is nonlinear because of velocity variations.

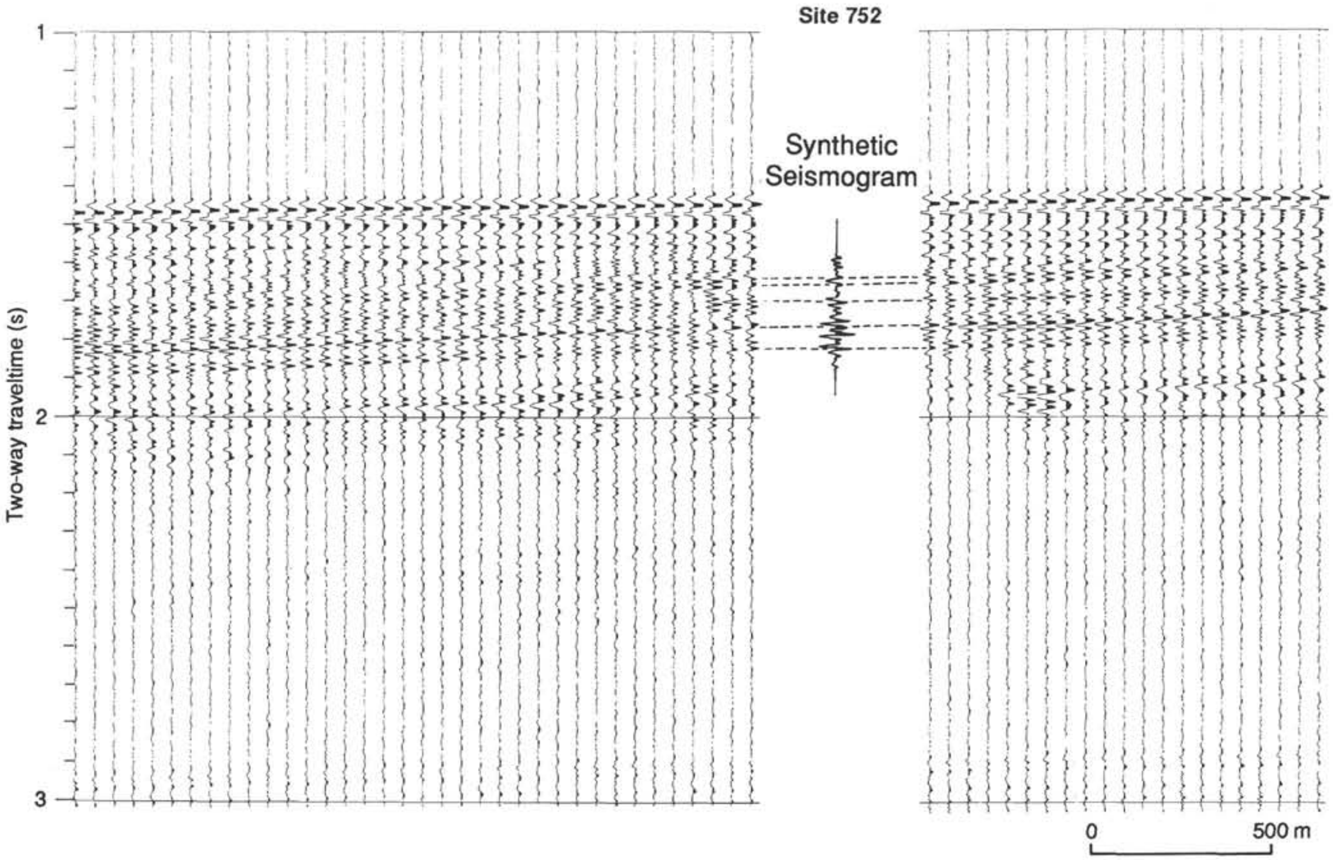

Figure 37. Comparison of the synthetic seismogram (Fig. 36) with RC2708 seismic-reflection data. The seismic profile is filtered with a 10–125-Hz filter.

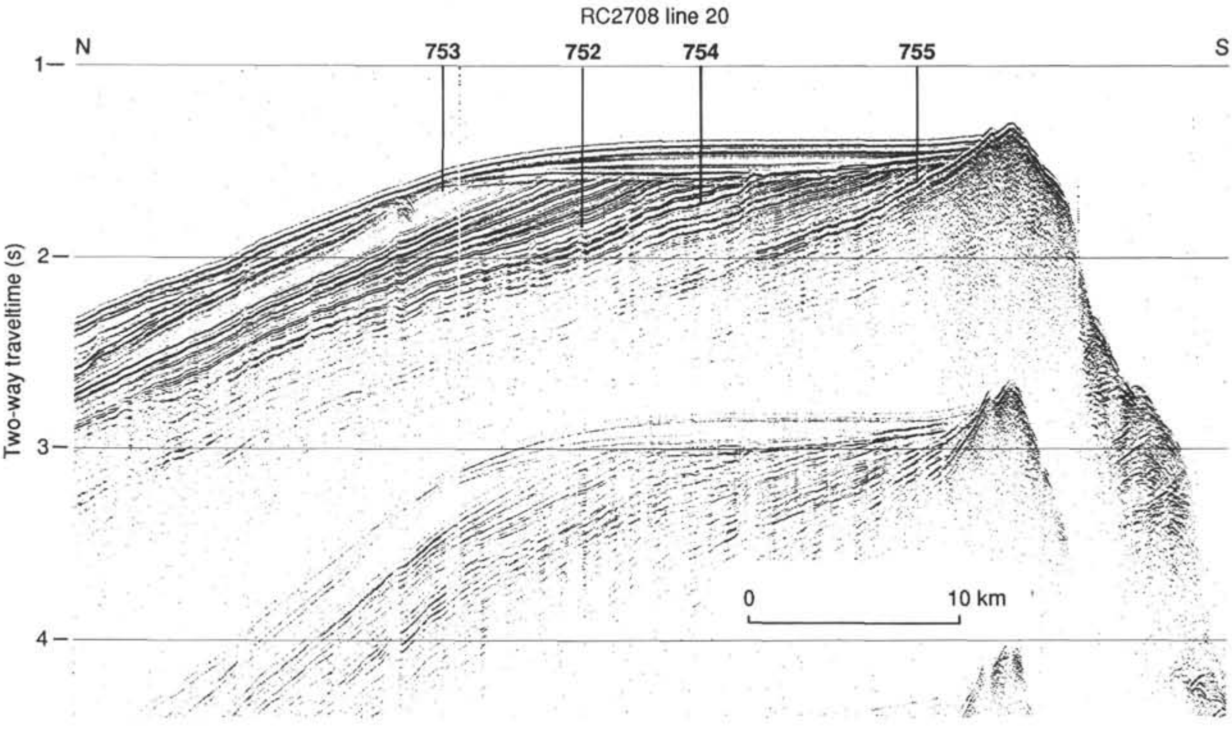

Figure 38. RC2708 single-channel seismic dip line 20 across Broken Ridge illustrates the stratigraphy observed on and surrounding the ridge. Site 752 penetrated the horizontal pelagic cap and bottomed in the prograding downlapping sequence.

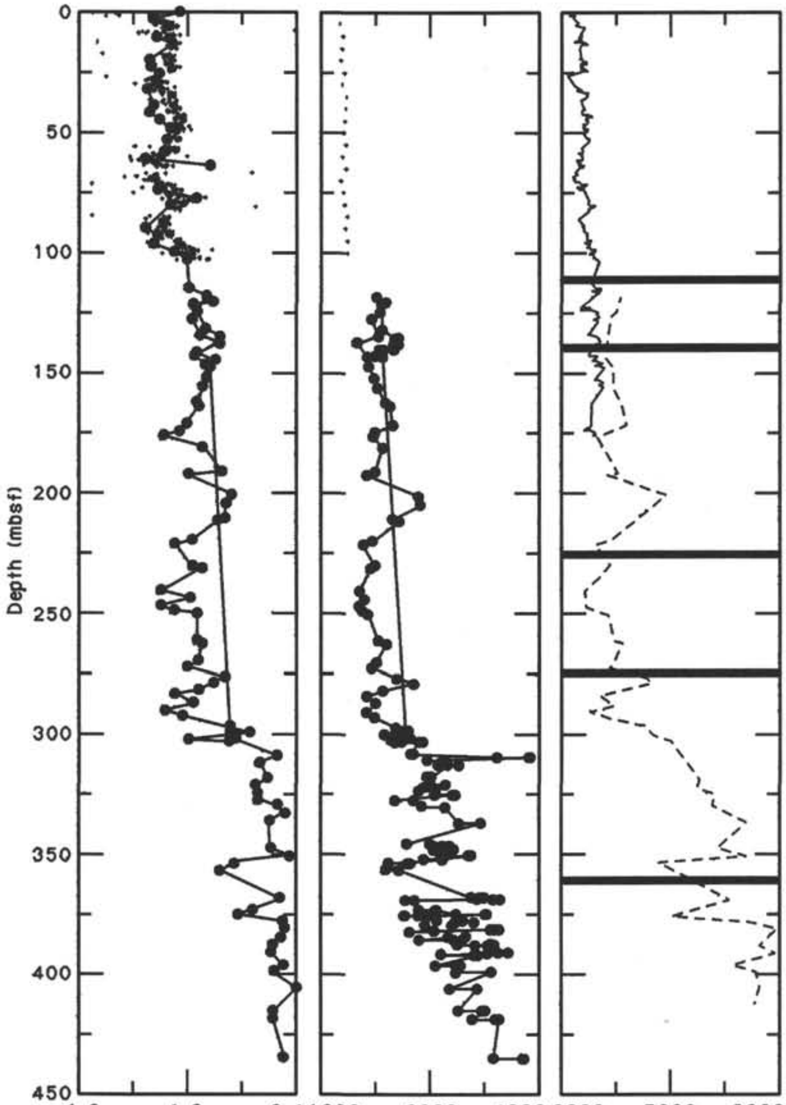

Figure 39. Acoustic impedance contrasts calculated from sonic and density measurements on sampled lithologies of Site 752. The black horizontal lines on the acoustic impedance plot indicate changes with depth that correlate with seismic reflectors.

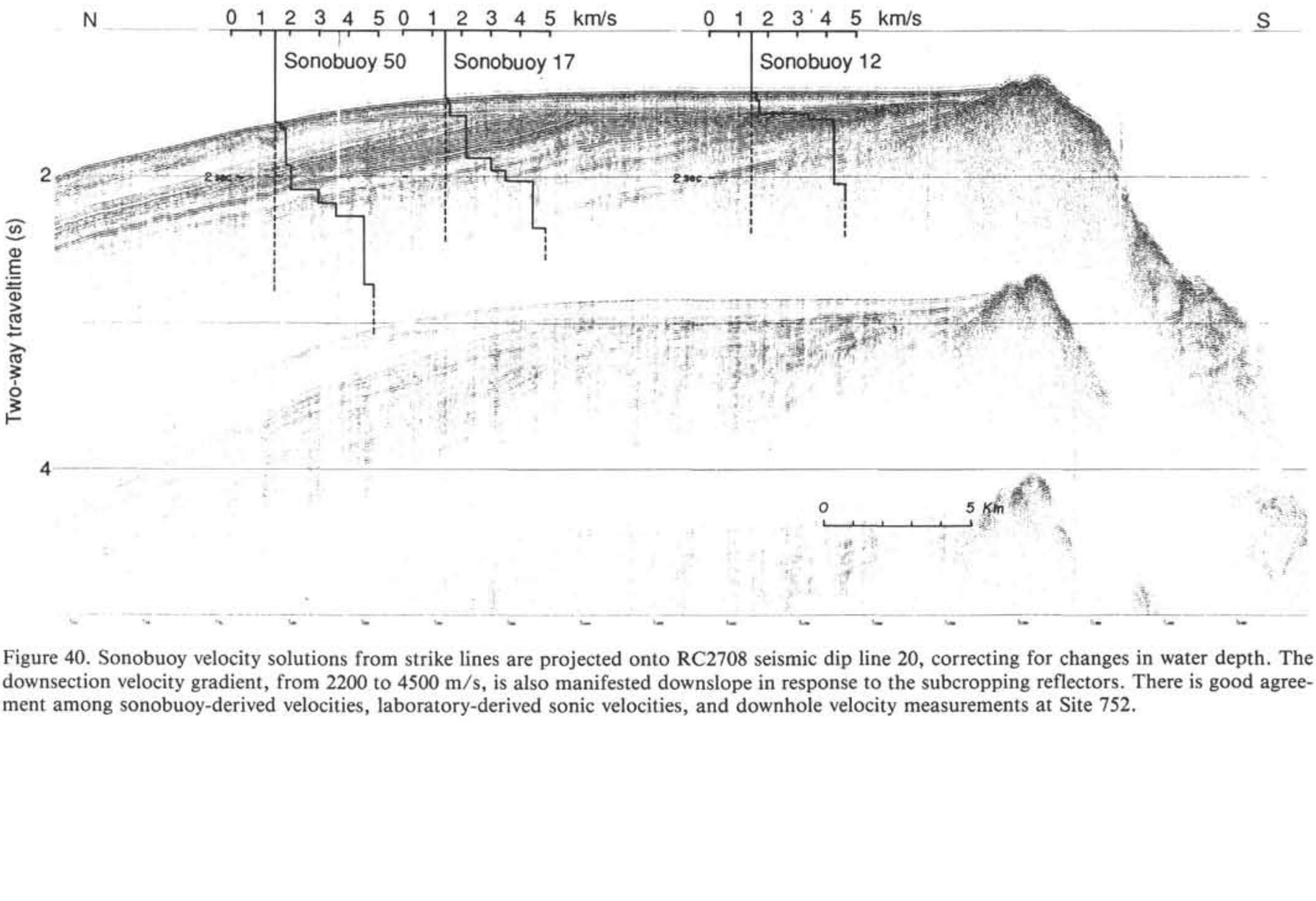

Figure 40. Sonobuoy velocity solutions from strike lines are projected onto RC2708 seismic dip line 20, correcting for changes in water depth. The downsection velocity gradient, from 2200 to 4500 m/s, is also manifested downslope in response to the subcropping reflectors. There is good agreement among sonobuoy-derived velocities, laboratory-derived sonic velocities, and downhole velocity measurements at Site 752.

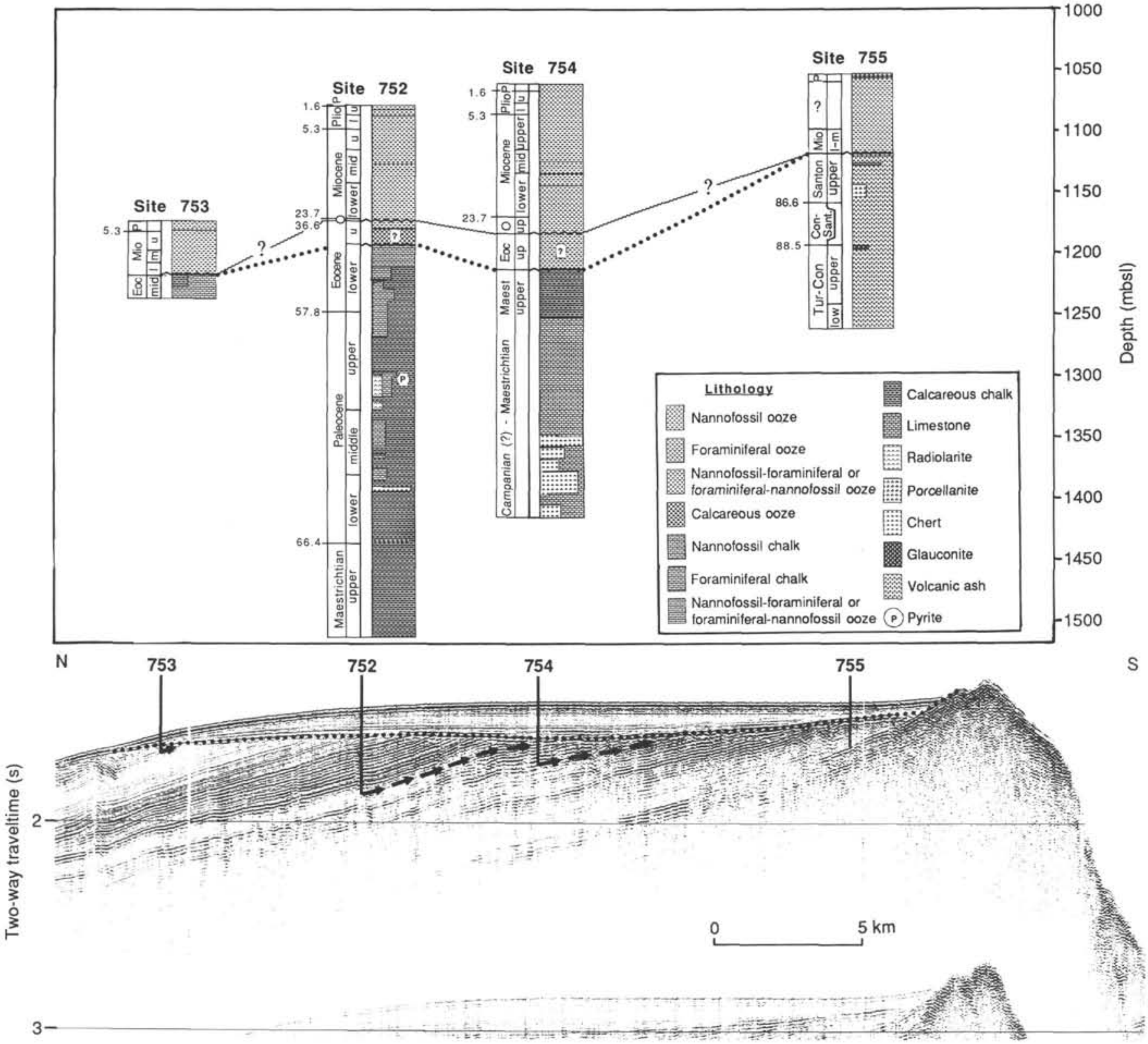

Figure 41. Correlation of seismic stratigraphy and lithostratigraphy sampled at Sites 752, 753, 754, and 755 on Broken Ridge. The arrows represent the upward continuation of the deepest horizon penetrated at Sites 752, 753, and 754 to the angular unconformity, illustrating the amount of stratigraphic section recovered and the stratigraphic overlap—if any—among the sites. The dotted line represents the middle Eocene hiatus and the wavy line denotes the Oligocene hiatus. The two hiatuses coalesce at Sites 753 and 755, but the question marks indicate that the position where they coalesce across Broken Ridge is not resolved.

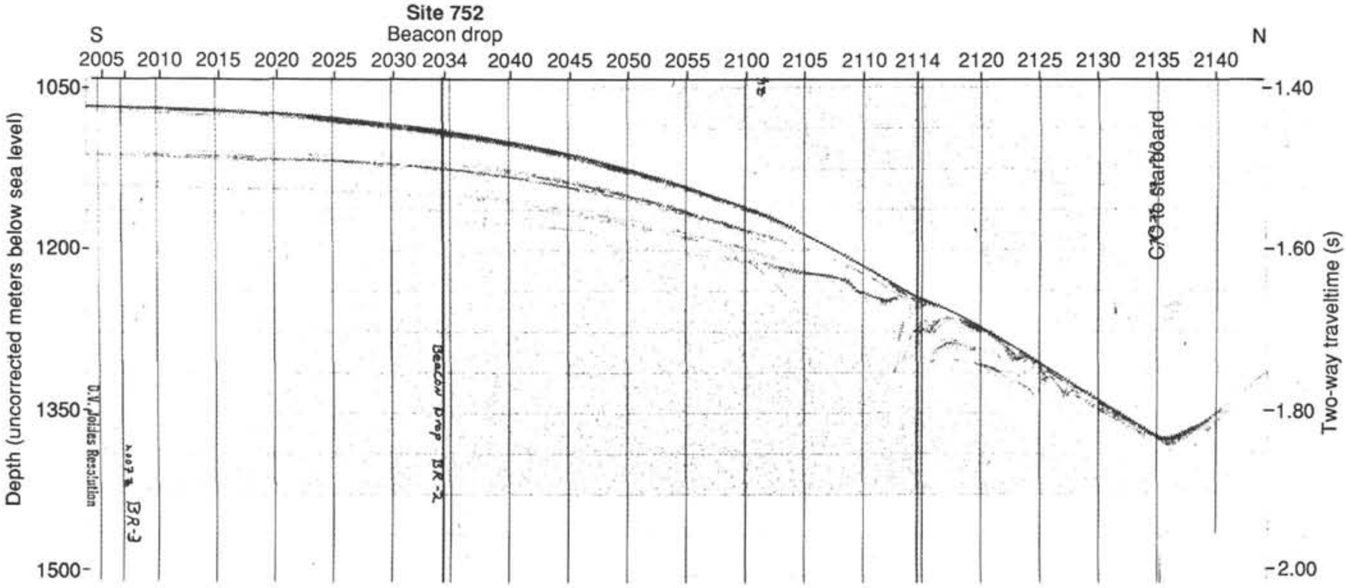

Figure 42. The 3.5-kHz PDR record over Site 752 that corresponds to part of the seismic section shown in Figure 41. The maximum acoustic penetration is approximately 100 mbsf because of the attenuation of the high-frequency signal. The 3.5-kHz profile augments the high-resolution seismic-reflection profile by providing a sonic character for shallow acoustic impedance contrasts that are at or below the vertical resolution of the water gun seismic system.

Summary Log for Hole 752B

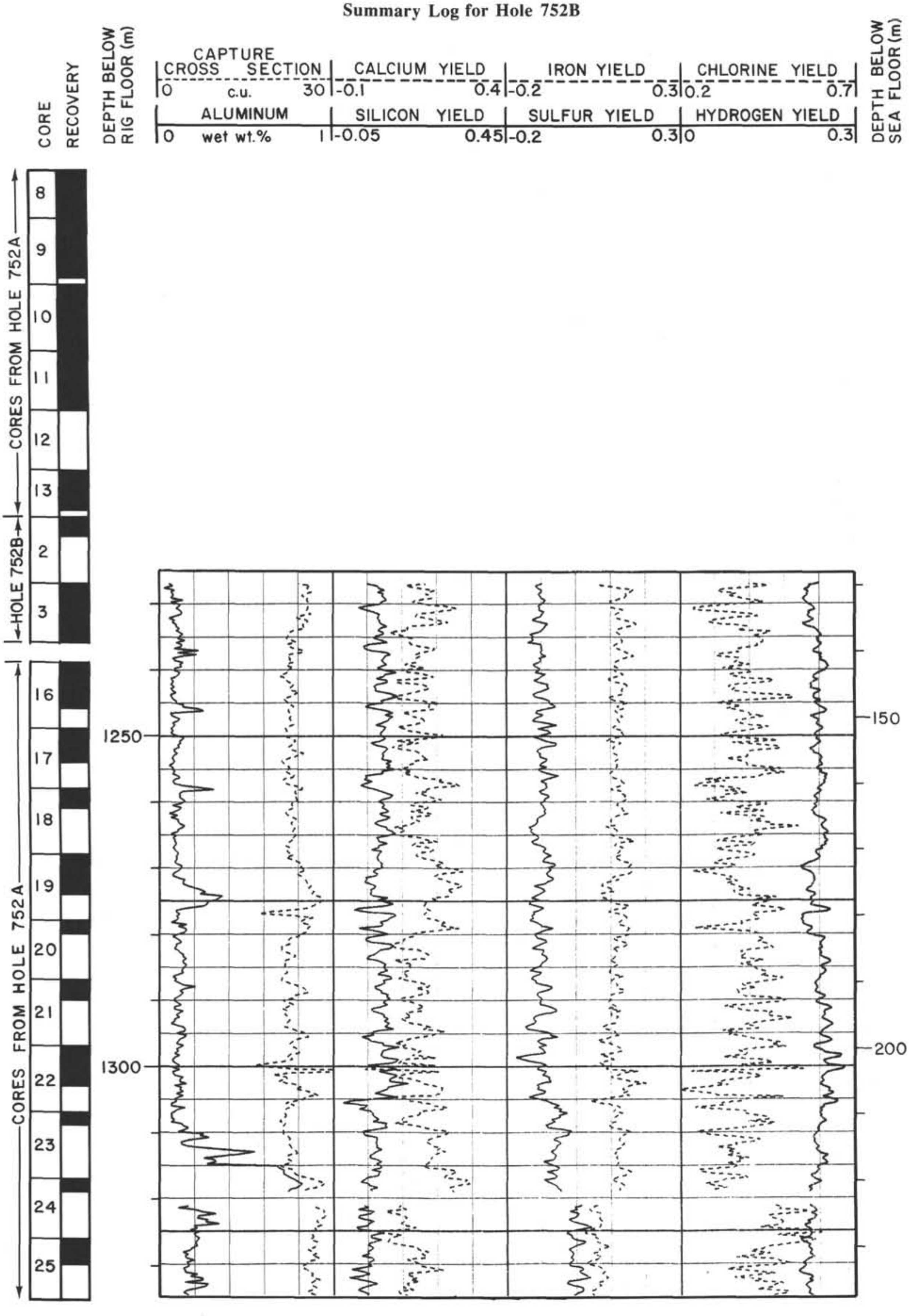

Summary Log for Hole 752B (continued)

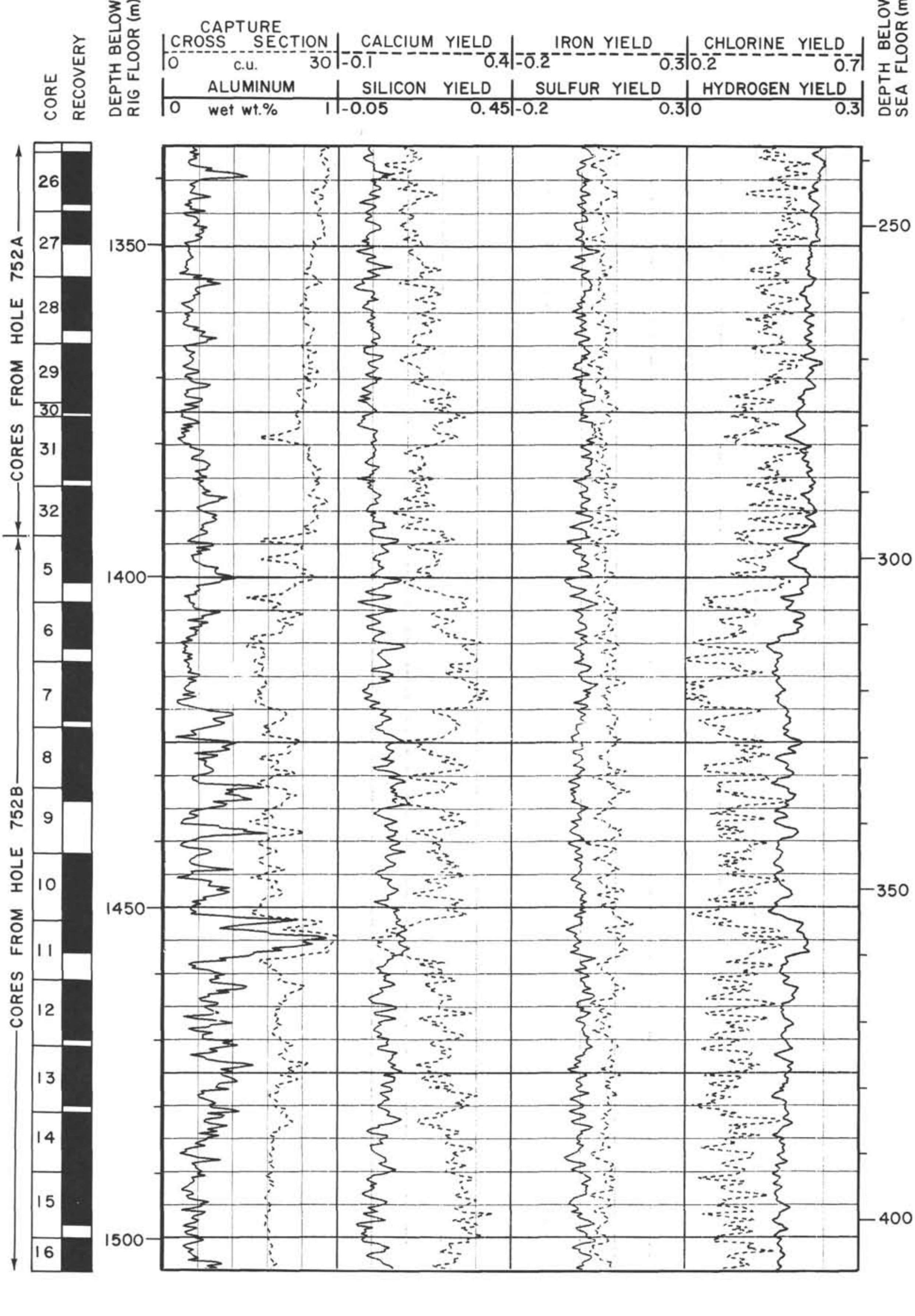

Summary Log for Hole 752B (continued)